CHEMICAL, PHYSICAL AND CELLULAR DELIVERY OF NITRIC OXIDE

By

MAHENDRA KAVDIA

Bachelor of Technology
Indian Institute of Technology
Delhi, India
1992

Master of Technology
Indian Institute of Technology
Madras, India
1995

Submitted to the Faculty of the
Graduate College of the
Oklahoma State University
in partial fulfillment of
the requirements for
the Degree of
DOCTOR OF PHILOSOPHY
July, 2000

CHEMICAL, PHYSICAL AND CELLULAR

DELIVERY OF NITRIC OXIDE

Thesis Approved:

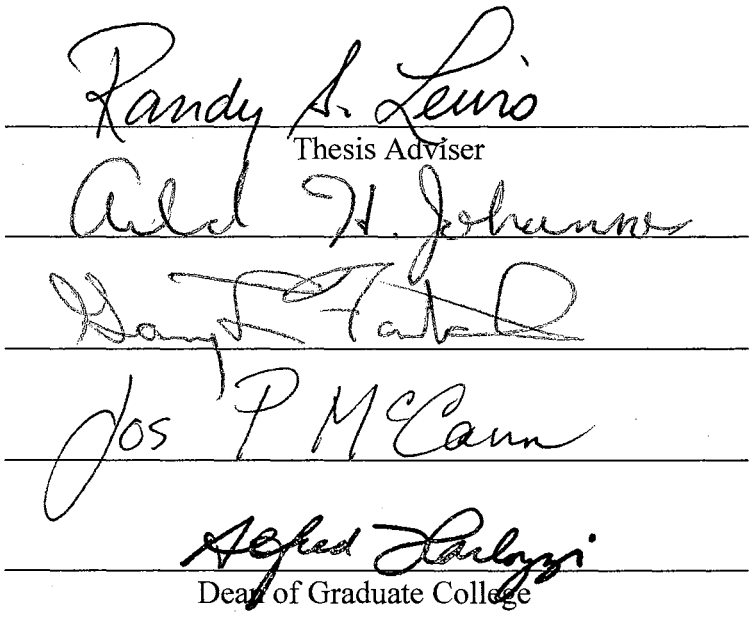

Thesis Adviser

Dean of Graduate College

Acknowledgments

I would like to express my sincere appreciation to my thesis advisor, Randy Lewis, for his thoughtful discussions, excellent guidance and helpful nature. Thanks also go to a great laboratory group consisting of Anand Ramamurthi, Chun Li, and Xun bao.

More over, my sincere appreciation extends to my parents, Tej and Jatan Kavdia, for supporting every decision of mine; my brothers, Sanjay and Sunil Kavdia, and my sister in-law, Seema Kavdia, for always being there; and to my nephew, Vickey Kavdia, for his love.

Finally, I would like to thank my friends Juntanee Uriyapongson and Patricia Rayas for their love and support during my stay at Stillwater.

Table of Contents

List of Tables

List of Figures

Nomenclature

C_b	Bulk NO concentration exiting delivery device (Chapter 3)
cGMP	Cyclic guanosine monophosphate
C_i	Concentration of species *i* (except for Chapter 2)
C_{NO}	Dimensionless concentration of NO ($=c_{NO}/E_{NO}C_{NOD}$; in Chapter 2)
c_i	Concentration of species *i* (Chapter 2)
C_{NOD}	Initial NO donor concentration, M
C_O	Aqueous NO concentration in equilibrium with the NO gas (Chapter 3)
CO_2	Carbon dioxide
C_{O_2}	Dimensionless concentration of O_2 ($=c_{O_2}/C_{O_2,S}$; in Chapter 2)
$C_{O_2,S}$	Saturation concentration of O_2 at 37 °C
DEA/NO	Diethylamine NONOate
D_i	Diffusivity of species *i*, m^2/s
DMEM	Dulbecco's modified Eagle's medium
E_{NO}	Moles of NO released per mole of NO donor
F	Factor accounts for oxygen uptake rate by cells (defined on page 18)
f	Fraction of total NO and O_2^- flux entering the film region
f_r	Fraction of outer radius to the total radius ($f_r=1-(r/R)$)
GSNO	S-nitrosoglutathione

H	Solubility of NO, μM/mmHg
H_2O_2	Hydrogen peroxide
IDDM	Insulin dependent diabetes mellitus
IL-1β	Interleukin-1β
k_i	Reaction rate constant of reaction *i*
k_{NOD}	Decomposition rate of NO donor
L	Depth of aqueous phase (Chapter 2), mm
L	Length of membrane through NO gas permeates (Chapter 3), cm
N_2O_3	Nitrous anhydride
N_i	Molar flux of species *i*
NO donor	Nitric oxide donor compound
NO	Nitric oxide
NO_2^-	Nitrite
NO_2	Nitrogen dioxide
NO_3^-	Nitrate
NONOate	Diazeniumdiolates class of NO donor compounds
O_2	Oxygen
O_2^-	Superoxide
$ONOO^-$	Peroxynitrite anion
ONOOH	Peroxynitrous acid
P	Permeability of NO, moles cm^{-1} s^{-1} $mmHg^{-1}$
PBS	Phosphate buffer saline
PER	Total peroxynitrite

R	Radius
r	Radius
R_i	Rate of formation of species *i*
SNAP	S-nitroso-n-acetylpenicillamine
S_{NO}	Maximum delivery rate of NO (Chapter 4), μM/min
SPER/NO	Spermine NONOate
T	Dimensionless time (=t*k_{NOD}; in Chapter 2)
t	Time
TNFα	Tumor necrosis factor α
XOD	Xanthine oxidase
Z	Dimensionless height (=z/L; in Chapter 2)
z	Liquid height coordinate
γIFN	Gamma interferon

Chapter 1. Nitric Oxide: An Introduction

Over the last two decades, nitric oxide (NO) has been the subject of intense interest in the scientific world with its wide range of biological activities. In the late 1980's, NO was recognized as a factor that mediates endothelium derived relaxation (Furchgott 1988; Ignarro et al., 1988). Now, NO is also known to be involved in many other physiological activities including acting as a neurotransmitter in the neuronal system and as a cytotoxic factor in the immune system.

1.1 Nitric oxide synthesis in biological systems

NO is synthesized from the amino acid L-arginine by NO synthase (NOS) enzymes, classified as constitutive NOS or inducible NOS. These NOS enzymes require tetrahydrobiopterin (BH_4), flavin adenine dinucleotide (FAD), flavin mononucleotide (FMN), nicotinamide adenine dinucleotide phosphate (NADPH) as well as calmodulin-calcium as cofactors (Moncada et al., 1991). The constitutive NOS (cNOS) includes the neuronal NOS (nNOS, found mainly in neuronal cells and skeletal muscle cells), and the endothelial NOS (eNOS, found mainly in endothelial cells). The cNOS is present in the catalytically active form and requires Ca^{2+} and in many cases calmodulin for activity. The cNOS generate low-levels of NO and produced NO mediates the glutamate linked cyclic guanosine monophosphate (cGMP) formation. Glutamate is the major excitatory

neurotransmitter in the brain and elicits effects on ion channels, inositol metabolism and cGMP formation (Lancaster, 1996).

Inducible NOS (iNOS) is expressed by many cells, such as mononuclear phagocytes, hepatocytes, and chondrocytes following activation by cytokines. The activity of iNOS is controlled by the regulation of mRNA transcription and translation and is independent of the intracellular Ca^{2+} level. The appropriate signal for induction of NO synthase is lipopolysaccharides and a variety of cytokines. The iNOS synthesizes NO for long periods and at high-levels relative to cNOS (Weinberg, 1998).

1.2 Nitric oxide reactions in biological systems

As a cell-signaling molecule, a cytotoxic agent, and an antioxidant, NO plays important roles in a biological system. NO is a highly reactive molecule because of its free radical nature. NO can react intracellularly as well as extracellularly with a wide range of molecules, such as molecular oxygen (O_2), superoxide (O_2^-), peroxynitrite ($ONOO^-$), thiols, and transition metals. The metabolic fate as well as the biological actions of NO depends on many factors including the release rate, biochemistry, and the presence of other free radicals. The intermediates and/or products of NO reactions posses their own unique characteristics and also have effects on the biological responses to NO. Some of the important intra and/or extra-cellular reactions of NO are shown in Figure 1.1. Although the figure does not present the gamut of NO reactions in biological systems, the shear diversity and range of NO and its metabolites with regards to

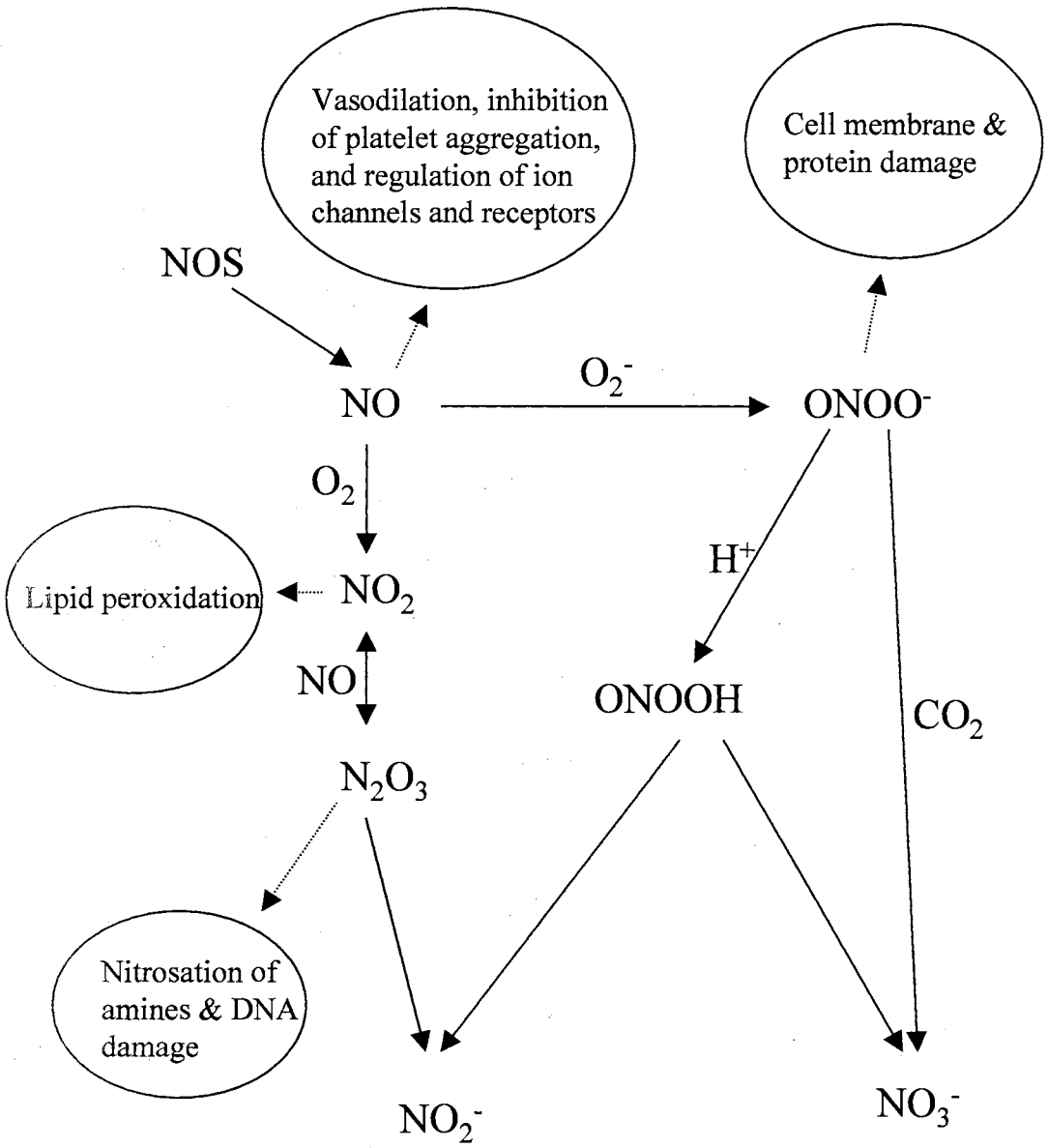

Figure 1.1. Reactions and bioactivities of NO related species.

involvement in biological environments are shown (for reviews, see Patel et al., 1999). Following is the description of some of the important reactions of NO.

1.2.1 Autoxidation of NO

The autoxidation of NO is one of the commonly occurring reactions. In aqueous solutions NO reacts with O_2 as

$$2NO + O_2 \xrightarrow{k_1} 2NO_2 \tag{1.1}$$

$$NO_2 + NO \underset{k_{-2}}{\overset{k_2}{\rightleftharpoons}} N_2O_3 \tag{1.2}$$

$$N_2O_3 + H_2O \xrightarrow{k_3} 2NO_2^- + 2H^+ \tag{1.3}$$

where k_i is the rate constant for reaction *i*. The value of rate constants are provided in subsequent Chapters. The rate controlling reaction (Equation 1.1) has a second-order dependence on the NO concentration (Lewis and Deen, 1994). At physiological low-concentrations of NO, the second-order dependence of the autoxidation on the NO concentration allows time for the diffusion of NO to various biological targets without significant depletion. The final product of the autoxidation of NO is nitrite (NO_2^-). Nitrogen dioxide (NO_2) and nitrous anhydride (N_2O_3) are intermediates between NO depletion and NO_2^- formation. In biological systems, NO_2 may initiate lipid peroxidation (Kappus, 1987). Being a strong oxidant, N_2O_3 can deaminate DNA causing damage to the DNA (Tannenbaum et al., 1993).

1.2.2 Reaction of NO with O_2^-

Nitric oxide reacts at a diffusion-controlled rate with O_2^- to form $ONOO^-$ (Huie and Padmaja, 1993).

$$NO + O_2^- \xrightarrow{k_4} ONOO^- \tag{1.4}$$

The reaction contributes significantly to NO reduction in the presence of O_2^-. The product $ONOO^-$, which reacts with all major classes of biomolecules including thiols, antioxidants, heamoglobin and lipids, has the potential to mediate cytotoxicty (Beckman et al., 1990). Under physiological conditions, $ONOO^-$ is chemically unstable and forms peroxynitrous acid (ONOOH),

$$ONOO^- + H^+ \xrightarrow{k_5} ONOOH \tag{1.5}$$

which decays rapidly to NO_2^- and nitrate (NO_3^-) according to (Koppenol et al., 1992; Huie and Padmaja, 1993; Pfeiffer et al., 1997).

$$ONOOH \xrightarrow{k_6} NO_3^- + H^+ \tag{1.6}$$

$$ONOOH \xrightarrow{k_7} NO_2^- + \frac{1}{2}O_2 + H^+ \tag{1.7}$$

One of the major depletion routes of $ONOO^-$ in biological systems is catalytic conversion to NO_3^- in the presence of CO_2 (Denicola et al., 1996; Uppu et al., 1996).

$$ONOO^- + CO_2 + H_2O \xrightarrow{k_8} NO_3^- + CO_3^{2-} + 2H^+ \quad (1.8)$$

The reaction with CO_2 modulates the chemical reactivity of $ONOO^-$ by decreasing the ability of $ONOO^-$ to oxidize glutathione and protecting the enzyme glutathione peroxidase (Padamaja et al., 1998).

In addition to the reaction with CO_2, NO can react with $ONOO^-$ as

$$ONOO^-(ONOOH) + NO \xrightarrow{k_9} NO_2 + NO_2^- \quad (1.9)$$

to form NO_2^- (Pfeiffer et al., 1997). However, the reactive form of peroxynitrite has not been identified. Recent studies have shown that N_2O_3, rather than NO, may be the reactive species with peroxynitrite (Goldstein et al., 1999).

1.3 Bioactivity of nitric oxide

Once formed, NO yields various nitrosated species, such as nitroxyl anion (NO^-) and nitrosonium ion (NO^+), in biological environments. Although the action of each nitrosated species has not yet been clarified, it may be similar to or different from the activity of NO alone. The wide range of action of NO includes controlling blood circulation, and regulating activities of the brain, lungs, liver, kidneys, stomach, genitals

and other organs (for a review see Moncada et al., 1991; Lancaster, 1996). The activity of NO can be divided into signal transduction roles and effector molecule roles.

As a signal transduction molecule, NO binds to the heme cofactor of guanylate cyclase to catalyze the conversion of GTP to produce intracellular signaling molecule cyclic guanosine monophosphate (cGMP) (Moncada et al., 1991). Endothelial cells (via cNOS route) forms NO when intracellular Ca^{2+} concentration increase by agonists like acetylcholine, thrombin, and bradykinin. NO is released to the neighboring smooth muscle cells causing vasodilation by increasing the cyclic GMP levels in the smooth muscle cells (Moncada et al., 1991). NO inhibits the platelet aggregation via cGMP dependent mechanism (Radomski et al., 1987). In addition, NO mediates transmission of signals across a synapse in cerebellum of brain (Garthwaite et al. 1988). The presynaptic neuron releases glutamate that binds to N-methyl-D-aspartate (NMDA) receptor on the postsynaptic neuron. In turn, the postsynaptic neuron releases NO (via cNOS route) as a messenger that acts on presynaptic neuron causing an increase in the levels of cGMP (Lancaster, 1992).

Immune cells, such as activated macrophages, monocytes, and Kupffer cells release a greater amount of NO, as compared to endothelium cells or nerve cells. Thus, NO can act as a cytotoxic agent to invading microorganisms or tumor cells. Several pathological conditions, including sepsis, ischemia/reperfusion, and atherosclerosis, are associated with accelerated NO production (Loskove and Frishman, 1995). Activated macrophages and natural killer cells have been reported in the vicinity of pancreatic islets during the development of insulin-dependent diabetes mellitus (IDDM) (Gepts and Lcompte, 1981).

Although intense investigations of the biological effects of NO, *in vivo* or *in vitro,* have been reported in the last decade, very little information about the required quantitative NO concentration is available. The lack of knowledge about the NO concentrations in studies can be overcome by applying fundamental engineering principles to obtain the NO concentrations in a system. Therefore, the major objective of this work was to quantitatively model the NO concentrations in biological systems resulting from the exposure to various types of NO delivery methods. The models could be useful for predicting NO concentration for studies in which NO effects on cell systems are determined.

1.4 Thesis objectives.

NO can be delivered to biological systems by chemical, physical, or cellular methods. The chemical, physical or cellular NO delivery methods were used in conjunction with reaction-diffusion models to achieve the overall objective of quantifying the NO concentrations in biological systems. An application of the physical delivery method to assess the impact of NO (and products) on pancreatic cell function was also demonstrated. The overall objective was accomplished by completion of the following Aims.

1.4.1 Aim 1: Chemical NO delivery

The chemical delivery of NO from NO donors is a widely used method to study the biological effects of NO. Despite extensive use of NO donors, very little quantitative information on spatial and time-dependent NO concentrations is available. Recently, Ramamurthi and Lewis (1997) and Schmidt et al. (1997) modeled the temporal NO concentrations from NO donors in a well-stirred system. However, many experimental systems are stagnant (not stirred). In a stagnant solution, diffusion rate of species become important and could lead to concentration gradient. Therefore, both temporal (time dependent) and spatial (position dependent) NO levels can be different in the system and can affect the experimental interpretations. The objective of this Aim was to model NO delivery using NO donor compounds in a stagnant system. The model results enable the quantitative predictions of NO concentrations that can be applied to study NO effects on biological systems using NO donor compounds. The model and results are described in Chapter 2.

1.4.2 Aim 2: Physical NO delivery with an application on pancreatic cell function

One method of physical NO delivery is permeation of gaseous NO via polymeric membranes. The physical delivery method overcomes some of the shortcomings, such as non-constant release of NO and release of other species that may occur from chemical and cellular NO delivery methods. In addition, physical NO delivery can achieve constant NO delivery over long periods. Therefore, the concept of permeation of gaseous

NO to a biological solution was exploited to achieve constant NO delivery rates. One device was designed to deliver constant NO to flowing solutions. The NO concentrations in solution were predicted from reaction-diffusion models. Chapter 3 describes the design of the delivery device and presents the experimental results of NO delivery with the model predictions. In addition, an experimental system was designed to deliver NO to a stirred solution using gaseous NO. In some pathophysiological conditions, O_2^- is also released by the immune cells along with NO. Extremely rapid reaction between NO and O_2^- leads to the generation of $ONOO^-$, which has many detrimental effects on biological systems. Therefore, the combined delivery of NO and O_2^- was also assessed. Chapter 4 describes the design of the experimental system and shows the predictions of the NO concentration in the system using physical NO delivery.

As an application of physical delivery on cellular systems, pancreatic β cells were used to assess the effect of NO on cell function. Contradictory results reported in the literature for the effects of NO on the function of pancreatic β cells for insulin secretion and cell viability using different NO donors and/or cells led to this study (Cunningham et al., 1994; Eizirik et al., 1996; Green et al., 1994). The contradictions may be a result of shortcomings of chemical or cellular NO delivery methods. The results and conclusions of the application of physical NO delivery are given in Chapter 4. The effects of O_2^- and $ONOO^-$ on the pancreatic cell function were also studied and the results are reported in Chapter 4.

1.4.3 Aim 3: Cellular NO delivery

Many cells, such as activated macrophages, synthesize NO and other species, which then diffuse towards neighboring cells and tissues. Therefore, it is important to assess the effects of NO-generating cells on the neighboring cells and tissues. The third objective of this Aim was the development of a model for the estimation of spatial concentrations of NO and other species (from NO reaction with O_2^-) in a matrix of target cells surrounded by activated macrophages. The target cells were assumed to be pancreatic cells. The infiltration of pancreatic cells by immune cells, such as macrophages, is one of the potential causes of the onset of insulin dependent diabetes mellitus (IDDM). As mentioned previously, activated macrophages release cytokines and free radicals (NO and O_2^-). Chapter 5 describes the model and the results. The predicted concentrations of species (NO, O_2^-, and $ONOO^-$) were compared with the results of the application of physical NO delivery described in Aim 2.

Finally, an expanded model was also developed for an *in vitro* experimental study using encapsulated pancreatic cells. The model predicts the spatial concentration of NO and other species in the matrix and in the surrounding liquid region of the matrix. Thus, measured extracellular concentrations can be used to validate the model to provide credibility to the predictions. Chapter 6 provides the details of the extended model.

Chapter 2. Quantitative Chemical NO Delivery

2.1 Introduction

NO, a small biological molecule, plays a key role in diverse cellular functions. The involvement of NO in physiological actions is extensively studied using nitric oxide donor compounds (NO donors), which release NO and other NO related redox species at physiological conditions. In addition, NO donors hold great potential as a therapeutic agent for many conditions, such as vasospasm, restenosis and impotence, in which physiological NO levels are diminished (Keefer, 1998). A wide range of NO donors is available. NO donors are categorized based on their chemical structure, such as organic nitrates/nitrites, diazeniumdiolates (NONOates), sydnonimines and s-nitrosothiols (Feelisch and Stamler, 1996).

The mechanisms leading to NO formation differ significantly among individual classes of NO donors. In addition, the kinetics of NO release are often more important than the total NO released by the NO donors since the kinetics affect the temporal exposure levels. The same total amounts of NO released over different time ranges may lead to different NO concentrations in a system due to the autoxidation of NO. Thus, it is difficult to assess the exact physiological effects of NO using different NO donors unless the NO concentration to which biological systems are exposed is known.

Wink et al. (1996) reported the effects of NO donors on hydrogen peroxide (H_2O_2) mediated cytotoxicity in V79 Chinese hamster lung fibroblasts. The NO donors used

were s-nitrosoglutathione (GSNO), s-nitroso-n-acetylpenicillamine (SNAP), diethylamine NONOate (DEA/NO), sodium nitroprusside (SNP), and sulfite NONOate (Sulfi/NO). The measured release rates of NO were first order for many of these NO donors in a well-stirred solution and the reported well-stirred NO concentrations, electrochemically measured, ranged between 0.3-12.0 μM.

Wink et al. (1996) reported that DEA/NO, SNAP and GSNO at concentrations of 0.1, 1.0, 1.0 mM, respectively, protected cells against H_2O_2 cytotoxicity, but 1.0 mM SNP enhanced H_2O_2 cytotoxicity. In addition, Sulfi/NO had no effects on the protection against H_2O_2 mediated toxicity. The contradictory results among NO-donors have limited the use of this study as authors (Wink et al., 1996) state that caution should be exercised when using the NO donor agents and correlating their effects. The reasons for different conclusions may be varying time-dependent release rates of NO donors, and release of additional species, such as cyanide (CN^-) in the case of SNP. In addition, the experiments were conducted in a stagnant solution contained in a petri dish leading to a potential NO concentration gradient in the experimental system.

Many other studies assessed the effects of NO on biological systems, such as pancreatic cells or islets, using NO donors (Cunningham et al., 1994; Eizirik et al., 1996; Kroncke et al., 1993). Results of these studies were confounded by the inability to control NO release rates, release of other species, and stagnant systems.

In view of the importance of knowing the NO concentration in an experimental system, Schmidt et al. (1997) developed a mathematical model to estimate the NO concentration in a well stirred system following the addition of an NO donor. The model successfully predicted the experimental NO concentration incorporating the first order

decomposition rate of an NO donor together with the autoxidation of NO. However, the model assumed a constant O_2 concentration in a well-stirred solution, which is not applicable to *in vitro* studies usually performed in stagnant solutions, especially when O_2 consuming cells are present. The loss of NO to the head-space was also not considered. Ramamurthi and Lewis (1997) successfully modeled the loss of NO to the head-space to predict the temporal NO concentration in a well-stirred system containing NO donor diethylamine NONOate and spermine NONOate.

Many of the experimental systems used to assess the role of NO were stagnant (i.e. culture plate). Therefore, a mathematical model was developed to quantify the spatial and temporal NO concentration in stagnant systems, such as culture plates or micro-wells, following the addition of an NO donor characterized with first order release kinetics. The model takes into account the diffusion of NO and O_2 in the culture medium, the kinetics of NO autoxidation in aqueous solutions, and the O_2 consumption by cells, thus eliminating the assumptions of constant O_2 and well-stirred solution of the Schmidt et al. (1997) and Ramamurthi and Lewis (1997) studies. The results showed that under widely used *in vitro* experimental conditions, the spatial and temporal NO concentration range can vary significantly. In addition, hypoxic conditions may occur in the vicinity of cells in some situations.

2.2 Mathematical Model

2.2.1 Model description

The modeled system is a petri dish or micro-well containing adherent cells at the bottom as shown in Figure 2.1. Dimensionless values for the height, time and concentrations are utilized as described below. NO is uniformly released into the media after the addition of an NO donor. The released NO can diffuse through the media and react with O_2 to form nitrite (NO_2^-) according to the following reaction scheme

$$2NO + O_2 \xrightarrow{k_1} 2NO_2 \tag{2.1}$$

$$NO_2 + NO \underset{k_{-2}}{\overset{k_2}{\rightleftharpoons}} N_2O_3 \tag{2.2}$$

$$N_2O_3 + H_2O \xrightarrow{k_3} 2NO_2^- + 2H^+ \tag{2.3}$$

The NO donor decomposition kinetics are assumed to have first order NO-release kinetics and can be described via a batch system (since the NO donor is uniformly distributed) such that

$$-\frac{dc_{NOD}}{dt} = k_{NOD}c_{NOD} \tag{2.4a}$$

$$NO_{released} = E_{NOD}k_{NOD}C_{NOD}e^{-k_{NOD}t} \tag{2.4b}$$

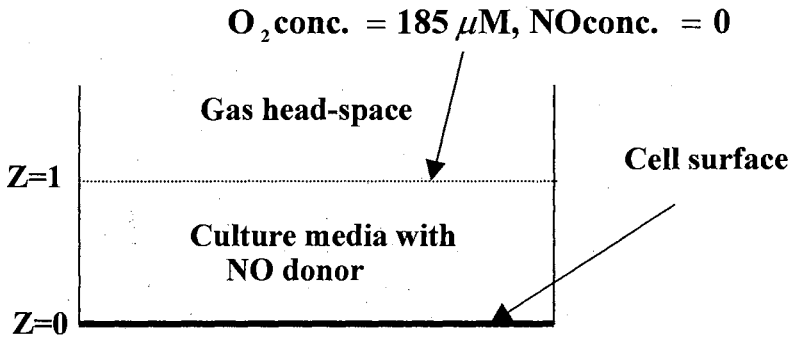

Figure 2.1. Stagnant experimental system. The cells are at Z=0. At T=0, the O_2 concentration is 185 μM and NO concentration is 0 in the aqueous phase (culture media). At all time, the concentration of O_2 is 185 μM and NO is 0, at the interface of gas and culture media.

where c_{NOD} is the concentration of the NO donor at time *t*. The first order decomposition rate constant of the NO donor is represented as k_{NOD}. The initial concentration of the NO donor is represented as C_{NOD}. Integration of Equation 2.4 gives the amount of NO released as shown in Equation 2.4b, where the moles of NO released per mole of NO donor decomposed is represented as E_{NO} (Ramamurthi and Lewis, 1997). Therefore, the total NO delivered to the media following complete decomposition of the NO donor is $E_{NOD}C_{NOD}$. However, some of the NO may be lost to the gas space as described later.

The simultaneous solution of the following dimensionless continuity equations provides the spatio-temporal distribution of NO and O_2 in the media.

$$\frac{\partial C_{NO}}{\partial T} = \frac{D_{NO}}{k_{NOD}L^2}\frac{\partial^2 C_{NO}}{\partial Z^2} - \frac{4k_1 E_{NO} C_{NOD} C_{O_2,S}}{k_{NOD}} C_{NO}^2 C_{O_2} + e^{-T} \tag{2.5}$$

$$\frac{\partial C_{O_2}}{\partial T} = \frac{D_{O_2}}{k_{NOD}L^2}\frac{\partial^2 C_{O_2}}{\partial Z^2} - \frac{4k_1 E_{NO}^2 C_{NOD}^2}{k_{NOD}} C_{NO}^2 C_{O_2} \tag{2.6}$$

The dimensionless concentration of NO (C_{NO}) is $c_{NO}/(E_{NO}C_{NOD})$ where c_{NO} is the concentration of NO at time *t*. For O_2, the dimensionless concentration (C_{O_2}) is $c_{O_2} / C_{O_2,S}$ where c_{O_2} is the concentration at time *t* and $C_{O_2,S}$ is the saturated O_2 concentration. The value of $C_{O_2,S}$ is 185.0 μM at 37 °C (Schmidt et al., 1997). The dimensionless time T is t^*k_{NOD}. The dimensionless height Z is z/L where the z coordinate represents the liquid height (z = 0 at the bottom) and L is the total depth of the aqueous phase. The diffusivity values of NO (D_{NO}) and O_2 (D_{O_2}) in the aqueous phase are assumed similar to that in water which are 5.1 x 10^{-9} and 3.0 x 10^{-9} m^2/s, respectively

at 37 °C (Chen et al., 1998; Tziampazis and Sambanis, 1995). The value of the autoxidation rate constant of NO (k_1) is 2.4 x 10^6 $M^{-2}s^{-1}$ at 37 °C (Lewis and Deen, 1994).

For Equations 2.5 and 2.6, the term on the left represents the dimensionless temporal change in concentration. The first term on the right represents the diffusion of the species. The reaction of NO with O_2 is represented by the 2nd term on the right. The last term on in Equation 2.5 represents the NO release by the NO donor.

2.2.2 Boundary Conditions

The solution to Equations 2.5 and 2.6 requires one initial and two boundary conditions for each equation or species (NO and O_2). Assuming at T=0 that NO is not present and the medium is saturated with O_2 (O_2 concentration=185 μM), the initial conditions at T=0 are C_{NO}=0, and C_{O_2}=1 for all Z.

Assuming the head-space contains air and does not contain NO and the head-space is in equilibrium with the aqueous phase interface, the boundary conditions at Z=1 for NO and O_2 are C_{NO}=0, and C_{O_2}=1, respectively, for all T. The boundary condition for NO at the bottom (Z=0) is zero flux for NO. For the O_2 boundary condition, the gradient at Z=0 is calculated from the O_2 consumption flux by adherent cells and is represented by

$$\left.\frac{dC_{O_2}}{dZ}\right|_{Z=0} = F\left[\frac{C_{O_2}}{(k_m/C_{O_2,S})+C_{O_2}}\right]_{Z=0}$$
$$\text{where } F = \left(\frac{L * N_{cell} v_{\max}}{C_{O_2,S} D_{O_2}}\right) \qquad (2.7)$$

where k_m and v_{max} are the half-maximum oxygen uptake concentration and the maximum cellular oxygen uptake rate, respectively. The half-maximum oxygen uptake concentration (k_m) is assumed to be 0.01 mM as the oxygen uptake rate does not depend on the dissolved O_2 concentration as low as 0.015 mM (Miller et al., 1987). The number of cells per unit cross-sectional area of the system is N_{cell}. The unitless parameter F accounts for cumulative effect of changes in cell density, liquid height and the maximum oxygen uptake rate.

2.2.3 Adjustable parameters

The effects of change in adjustable experimental parameters on spatial and temporal profiles of NO and O_2 were simulated by varying the NO donor decomposition kinetics (k_{NOD}) and initial concentrations (C_{NOD}), the aqueous phase height (L), and F.

NO donors DEA/NO and SPER/NO were used for the simulations since DEA/NO and SPER/NO are commonly used NO donors of the NONOate class and have widely differing first order decomposition rates (Maragos et al., 1991; Ramamurthi and Lewis, 1997; Schmidt et al., 1997). The decomposition rate constants (k_{NOD}) are 5.4×10^{-3} and 0.30×10^{-3} s^{-1}, and the E_{NO} values are 1.5 and 1.9, respectively for DEA/NO and SPER/NO at 37 °C and pH 7.4 (Maragos et al. 1991). In addition to the NO donor release rates, the amount of NO donor used in reported experiments varied from nM to mM concentrations (Homer and Wanstall, 1998). Thus, two different initial NO donor concentrations (C_{NOD}) of 10 and 100 μM were used.

The height L was assumed to be either 3 or 6 mm based on typical petri dishes (d=35 mm) containing 2.5 ml culture media (L=3 mm) or micro-wells containing 0.2 ml culture media (L=6 mm).

The range of the dimensionless parameter F was obtained from typical values as follows. The maximum oxygen uptake rate (v_{max}) for mammalian cells varies between 0.001-0.02 μmol/10^6 cells/min. The typical number of cells per unit area (N_{cell}) varies between 11-280 x 10^6 cells/m^2 (based on 1-10 x 10^4 cells). As stated before, L ranges between 3 and 6 mm. $C_{O_2,S}$ is 185 x 10^3 μmol/m^3 and D_{O_2} is 1.8 x 10^{-7} m^2/min. Based on these typical values, F varies between 0.001 and 1.0. These bounds for F were used for simulations.

2.2.4 Numerical solution

The coupled system of time-dependent partial differential Equations 2.5 and 2.6 were solved using PDETWO software, which uses the methods of lines (Melgaard and Sincovec, 1981). The height L was divided into 51 equal grids. The time integration error tolerance was 1 x 10^{-7}. Main program and sub-routines used to run PDETWO are given in Appendix 1. The PDETWO software can be obtained from the web site www.netlib.org.

2.3 Results

2.3.1 Spatial and temporal distribution of NO and O_2

The predicted dimensionless spatial and temporal distributions of NO and O_2 are shown in Figures 2.2 and 2.3, respectively, for an initial concentration of 100 μM DEA/NO or SPER/NO for L=3 mm and F=1.0. Since the NO concentrations were non-dimensionlized with total NO delivered ($E_{NO}C_{NOD}$) to the system (see Section 2.2.1), the dimensionless NO concentration C_{NO}=1 corresponds to 150 and 190 μM, respectively, for DEA/NO and SPER/NO. In addition, T=1 corresponds to 3.1 and 55.6 min, respectively, for DEA/NO and SPER/NO (see Section 2.2.3).

As shown, the spatial distribution of NO and O_2 varies significantly with time for both NO donors. Note that DEA/NO has a larger gradient at Z=1 as compared to the SPER/NO. Thus DEA/NO results in a more uniform concentration between Z=0 and 0.75 as compared to SPER/NO. The reason is discussed in Section 2.4. At Z=0, the C_{NO} values were 0.14 and 0.04, respectively at T=0.5 for DEA/NO and SPER/NO. With increasing time (T>0.5), C_{NO} decreased at all Z for both NO donors. Furthermore for the same initial NO donor concentration, C_{NO} was always higher for DEA/NO than SPER/NO at the same time and height. This is due to the higher NO release rate for DEA/NO than SPER/NO.

As shown in Figure 2.3, C_{O_2} reduced over time for both NO donors. There was a significant variation in C_{O_2} at all Z for both NO donors. For both NO donors, the system

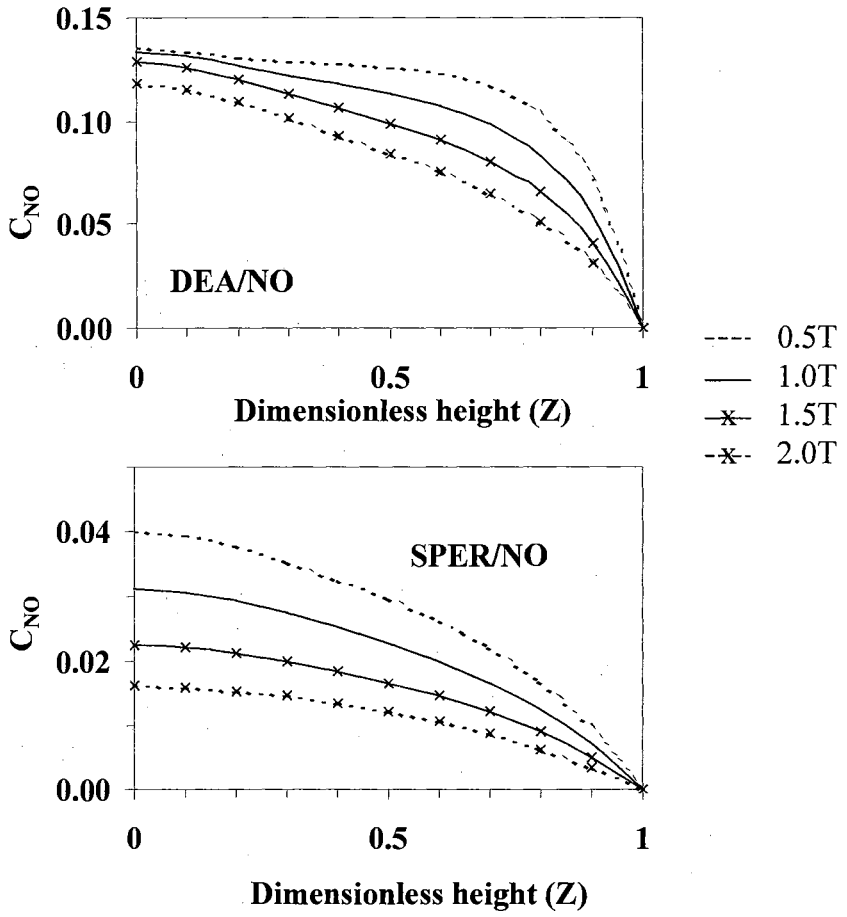

Figure 2.2. Dimensionless NO concentration predictions for NO donors. At T=0, C_{NO} is zero. The parameter values are L=3 mm (represents Z=1), F=1, and C_{NOD}=100 μM. The cells are at Z=0 and the gas-liquid interface is at Z=1. For DEA/NO: T=1 is 3.1 min; C_{NO}=1 is 150 μM NO. For SPER/NO: T=1 is 55.6 min; C_{NO}=1 is 190 μM NO.

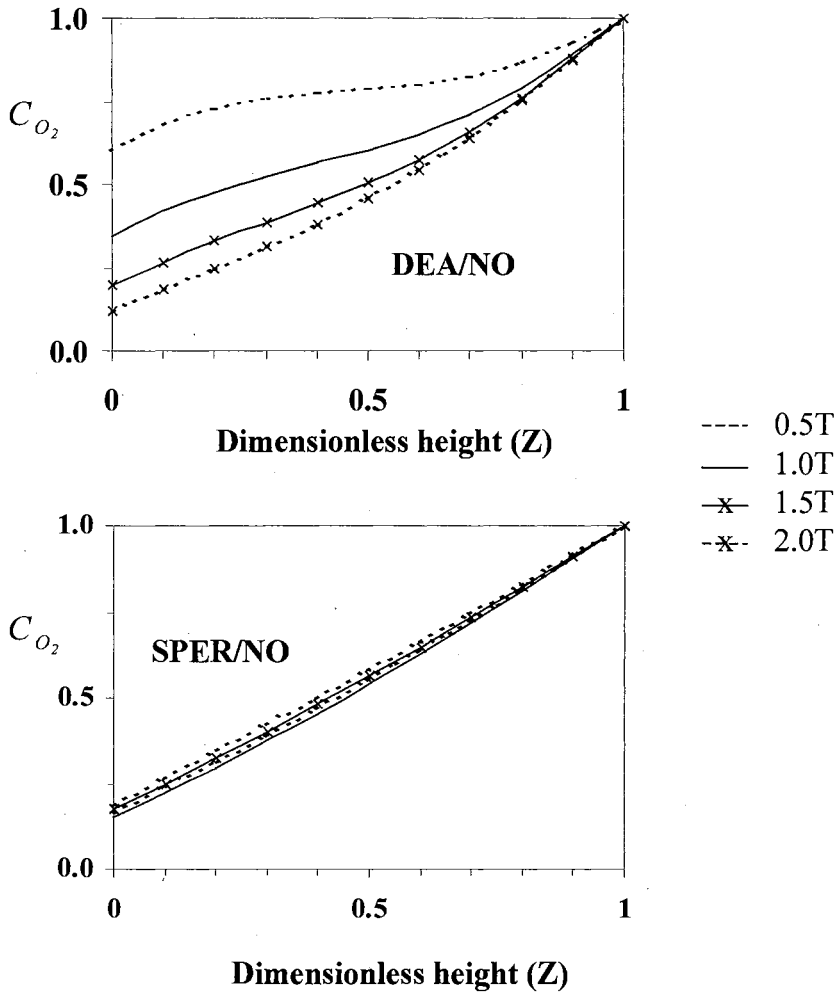

Figure 2.3. Dimensionless O_2 concentration predictions for NO donors. At T=0, C_{O2} is 1.0. The parameter values are L=3 mm (represents Z=1), F=1, and C_{NOD}=100 μM. The cells are at Z=0 and the gas-liquid interface is at Z=1. C_{O2}=1 is 185 μM O_2. T=1 is 3.1 min for DEA/NO and 55.6 min for SPER/NO.

O_2 levels reached steady-state value when no significant NO was present in the system (data not shown). The steady state value of 0.22 for C_{O_2} at Z=0 was achieved at T=29.5 (91 min) and 5.7 (317 min) for DEA/NO and SPER/NO, respectively. Thus, cells observed O_2 concentrations much lower than the saturated conditions.

2.3.2 Effect of aqueous phase height

The spatial and temporal (position and time dependent, respectively) profiles of NO and O_2 for L=6 mm (F=1.0, C_{NOD}=100 μM) were also predicted for both NO donors, since the height of the aqueous phase can vary depending on the experimental system. The effect of height (6 mm) on the spatial distribution of NO (generated from DEA/NO) and O_2, respectively, at T=1 is shown in Figures 2.4 and 2.5 relative to the base-case (L=3 mm). For L=6 mm, NO was more evenly distributed as compared to L=3 mm. However, C_{NO} was similar at Z=0 for both heights. Thus, the cells would be exposed to a similar NO concentration irrespective of the depth of the aqueous phase. For Z between 0.4 and 1.0, a higher C_{NO} was predicted for L=6 mm compared to L=3 mm, as shown in Figure 2.4. This agrees with the lower C_{O_2} observed in the same region (Figure 2.5) for L=6 mm since more NO could react with O_2. The converse was true for Z between 0 and 0.4. As shown in Figure 2.5, C_{O_2} at Z=0 was higher with L=6 mm due to less NO available for reaction.

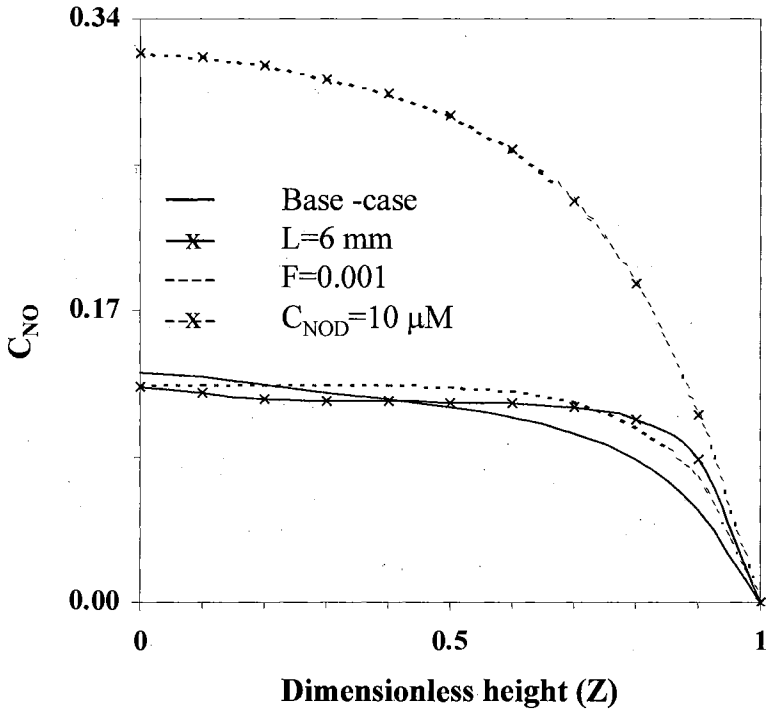

Figure 2.4. Dimensionless NO concentration predictions for DEA/NO at T=1. The base-case adjustable parameters are L=3 mm, F=1.0, and C_{NOD}=100 μM. Profiles based on changes in one adjustable parameter are also shown. The cells are at Z=0 and the gas-liquid interface is at Z=1. T=1 is 3.1 min. C_{NO}=1 represents NO concentrations of 150 and 15 μM for C_{NOD} of 100 and 10 μM, respectively.

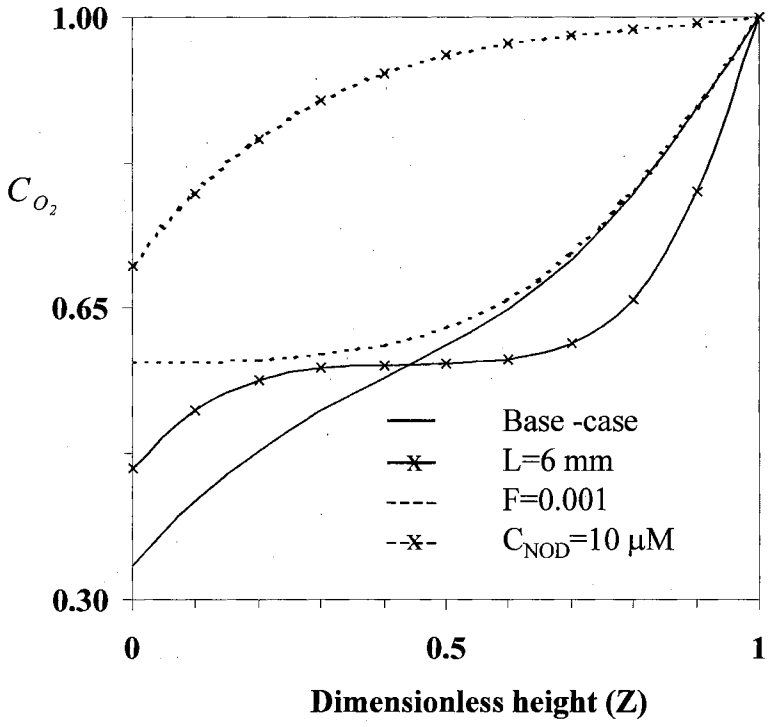

Figure 2.5. Dimensionless O_2 concentration predictions for DEA/NO at T=1. The base-case adjustable parameters are L=3 mm, F=1.0, and C_{NOD}=100 μM. Profiles based on changes in one adjustable parameter are also shown. The cells are at Z=0 and the gas-liquid interface is at Z=1. T=1 is 3.1 min. C_{O2}=1 is 185 μM O_2.

Since the NO generation is much slower for the SPER/NO than DEA/NO, the spatial distribution profiles of NO and O_2 were different for both heights as shown in Figure 2.6 and 2.7, respectively. As compared to L=3 mm, C_{NO} was higher and C_{O_2} was lower for all Z with L=6 mm because of the slow diffusion of O_2 in a large system and subsequent smaller consumption of the NO through autoxidation.

2.3.3 Effect of O_2 consumption

The cell numbers, cellular O_2 consumption rate and the height of the system varies largely among experiment studies. Thus, F can vary significantly. The NO and O_2 spatial and temporal profiles were simulated for a lower F of 0.001 and compared with those of F=1.0 for both NO donors (L=3 mm, C_{NOD}=100 μM). In the case of DEA/NO for F=0.001, C_{NO} and C_{O_2} were constant (0.13 and 0.59, respectively) between Z values of 0 and 0.3, as shown in Figures 2.4 and 2.5, respectively. C_{O_2} at Z=0 was higher for F=0.001 since cells consumed less O_2. NO was not affected drastically by varying F.

For SPER/NO, C_{O_2} increased (see Figure 2.7), thus C_{NO} decreased (see Figure 2.7) at all Z for a lower F. This is a result of less O_2 consumption by the cells.

2.3.4 Effect of NO donor concentration

The amount of NO donor used in experiments can vary. Thus, a lower value of C_{NOD} (10 μM) was used for simulation for both NO donors with L=3 mm and F=1.0.

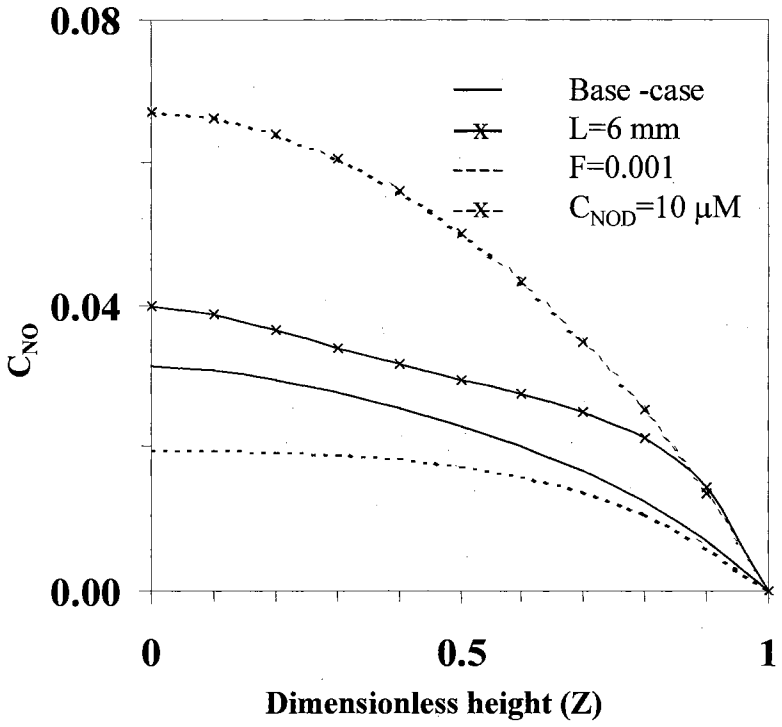

Figure 2.6. Dimensionless NO concentration predictions for SPER/NO at T=1. The base-case adjustable parameters are L=3 mm, F=1.0, and C_{NOD}=100 μM. Profiles based on changes in one adjustable parameter are also shown. The cells are at Z=0 and the gas-liquid interface is at Z=1. T=1 is 55.6 min. C_{NO}=1 represents NO concentrations of 190 and 19 μM for C_{NOD} of 100 and 10 μM, respectively.

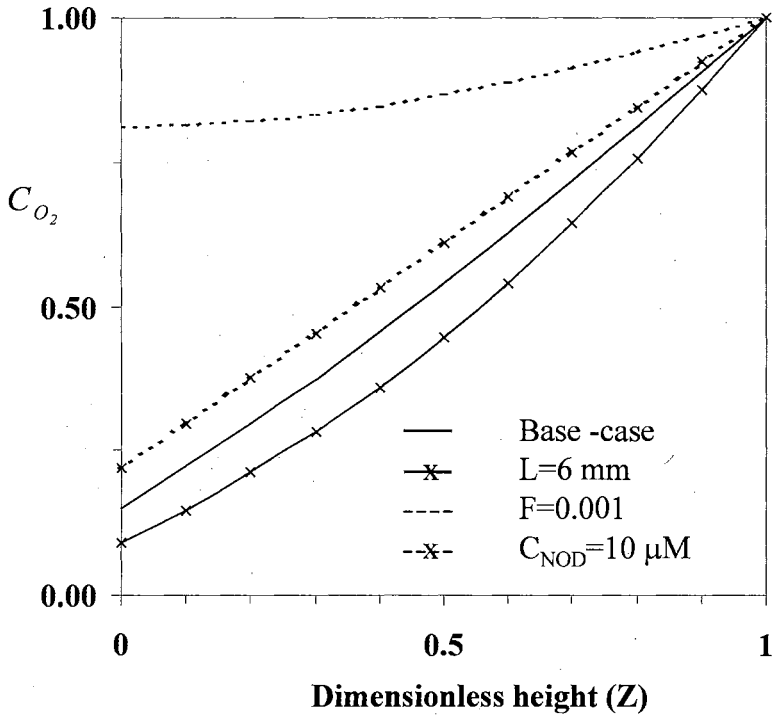

Figure 2.7. Dimensionless O_2 concentration predictions for SPER/NO at T=1. The base-case adjustable parameters are L=3 mm, F=1.0, and C_{NOD}=100 μM. Profiles based on changes in one adjustable parameter are also shown. The cells are at Z=0 and the gas-liquid interface is at Z=1. T=1 is 55.6 min. C_{O2}=1 is 185 μM O_2.

The dimensionless spatial profiles relative to the base-case for NO and O_2 at T=1 are shown in Figures 2.4-2.7. It should be noted that for C_{NOD} values of 10 and 100 μM, the C_{NO}=1 corresponds to 15 and 150 μM, respectively for DEA/NO, and 19 and 190 μM, respectively for SPER/NO. The lower concentration of NO donors released NO at the lower rates, thus achieved the lower c_{NO}. However, C_{NO} was much higher since the rate of NO reacting with O_2 is less than for the higher C_{NOD}. The low NO concentrations due to C_{NOD}=10 μM increased the amount of available O_2 in the media for both NO donors (see Figure 2.5 and 2.7). However, the change in O_2 profile for DEA/NO was more pronounced than SPER/NO due to a faster NO release rate for DEA/NO.

2.4 Discussion

This study estimates the spatial and temporal distributions of NO and O_2 following the addition of an NO donor to a stagnant media. The model presented here incorporates the diffusion and autoxidation of NO, as well as the O_2 consumption of the adherent cells. The results show that the spatial and temporal profiles of the NO and O_2 can be affected based on the experimental conditions. There can be a variation in the NO and O_2 concentration in different regions of the stagnant media at a given time. A fast releasing NO donor distributes NO more evenly in the media at a given time as seen for DEA/NO (see Figure 2.4) than a slow releasing NO donor as seen for SPER/NO (see Figure 2.6). The assumption of constant O_2 concentration also requires careful study of media conditions as in some cases the O_2 concentration dropped as low as 15 μM within three

hr. Thus, the NO concentration can be significantly different from that of obtained from well-stirred model and constant O_2 concentration.

Based on the well-stirred model with a constant O_2 concentration (Schmidt et al., 1997), C_{NO} was 0.12 and 0.057 for DEA/NO and 0.02 and 0.01 for SPER/NO, at T=0.5 and 2.0, respectively. However, the stagnant model predictions for C_{NO} were 0.14 and 0.12 for DEA/NO and 0.04 and 0.016 for SPER/NO, at T=0.5 and 2.0, respectively at Z=0. This shows that the NO concentrations obtained from a well-stirred model give approximate, but not accurate predictions. The difference between the two models is especially apparent for slow releasing NO donors (SPER/NO) at all times and for the fast releasing NO donors (DEA/NO) at later times.

An order-of-magnitude analysis was applied to understand the extent of various parameters affecting the spatial and temporal profiles of NO. In Equation 2.5, the term $D_{NO}/k_{NOD}L^2$ represents the ratio of NO diffusion to NO release rate in the system. This term also provides the information whether the media appears well-mixed over the majority of the height ($<<1$) or the media is stagnant ($>>1$). In the case of DEA/NO, the values of $D_{NO}/k_{NOD}L^2$ are 0.1 and 0.03, respectively for the L=3 and 6 mm. Thus, the concentration profiles of NO should be essentially the same over a majority of the height (except near Z=1). This result is shown in Figure 2.4. However for the SPER/NO, $D_{NO}/k_{NOD}L^2$ is 1.9 and 0.5, respectively for the L=3 and 6 mm, providing information that there would be a significant variation in the NO concentration across most of the media height. The observation is shown in Figures 2.3 and 2.6. Another method for the order of magnitude analysis would involve a height scale equal to $(D_{NO}/k_{NOD})^{0.5}$ which would provide the approximate distance to which concentration change would primarily occur

in the media. Based on $(D_{NO}/k_{NOD})^{0.5}$, concentration changes would mostly occur in 1 and 4 mm for DEA/NO and SPER/NO, respectively. These predictions are evident in Figures 2.4 and 2.6.

The extent of the autoxidation reaction rate to the NO release rate ($R_r=4k_1E_{NO}C_{NOD}C_{O_2,S}/k_{NOD}$, from Equation 2.5) provides information about the NO concentration build up in the system. A large value of R_r means a higher consumption of NO from the autoxidation than the release of NO by an NO donor, hence a faster depletion of NO in the system. For DEA/NO and SPER/NO, R_r is 49 and 745, respectively for C_{NOD}=100 μM. Thus, the NO reaction with O_2 is significant and SPER/NO should have a lower NO concentration than DEA/NO for a given T (see Section 2.3.1). This is evident in Figures 2.4 and 2.6.

Another important consideration in assessing the effects of NO on biological systems is the amount of total NO delivered to the system. Mainly, the total NO delivered is calculated from the NO donor decomposition rate given in Equation 2.4b. However, for many experimental systems there would be a loss of NO to the head-space, which would reduce the amount of NO delivered to the biological system. Based on the calculated flux of NO at the gas-liquid interface, the fraction of NO leaving the system to the total NO delivered is calculated by

$$\frac{NO_{removed}}{NO_{delivered}} = \frac{D_{NO}}{k_{NOD}L^2} \frac{\int_0^T \left.\frac{dC_{NO}}{dZ}\right|_{Z=1} dT}{\int_0^T e^{-T} dT} \tag{2.8}$$

The fraction values at T=0.5 and 2.0 were 0.0009 and 0.0013 for DEA/NO, and 0.041 and 0.054 for SPER/NO, respectively, for parameter values of C_{NOD}=100 μM, L=3 mm, and F=1.0. Since only ~0.1 and 5 % of the total NO delivered leaves the system for DEA/NO and SPER/NO, the loss of NO is not significant to the head-space.

2.5 Conclusions

Even though the present model was applied to NONOates, the spatial and temporal (position and time dependent, respectively) profiles can be estimated for other NO donor classes if the decomposition kinetics of NO donors are known. However, care must be taken as the decomposition kinetics of NO donors may vary depending on the experimental conditions, such as pH and temperature (Keefer et al., 1996). The presented model is expected to overestimate the NO concentrations in systems where the consumption of NO is not solely due to its reaction with O_2. Example of these conditions include the presence of heme proteins and superoxide, the latter which is released by SIN-1 a widely used NO donor compound.

In addition, biological systems may not be completely stagnant which could lead to a more homogeneous concentration of NO and O_2 in the system than the estimated concentrations in this study. As demonstrated, however, the potential exists for the concentration gradients in many experimental studies involving NO donors and stagnant solutions.

In summary, the presented mathematical model can estimate the NO concentrations in various regions of a system and thus eliminated the need of complex *in situ*

measurements of the NO concentration. However, chemical compounds that release NO result in non-constant concentration profiles. Interpretation of NO effect would be difficult. The controlled and constant delivery of NO through the chemical methods using NO donors is a difficult process and requires the consideration of many factors including pH, media preparation, temperature, and system parameters. Thus, a more appropriate method to maintain steady state NO concentrations for experimental studies is needed.

Chapter 3. Physical NO Delivery

3.1 Introduction

The non-constant release rate of NO, the release of other species, and the reactivity and/or toxicity of the NO donor compound in biological systems are some of the problems associated with NO delivery through the chemical method of NO donors as discussed in Chapter 2. In light of both the physiological and pathophysiological actions of NO, controlled and quantitative delivery of NO would be beneficial for studying the effects of NO and its reactive products on biological systems.

Physical NO delivery (i.e. the delivery of gaseous NO) to a biological system can eliminate some of the shortcomings of other NO delivery methods, such as release of other species. The physical delivery of NO includes the addition of NO saturated solutions, the administration of gaseous NO by gas tight syringes, or the permeation of NO through polymeric membranes (Feelisch and Stamler, 1996; Kavdia et al., 2000; Tamir et al., 1993). A drawback of using gas tight syringes (with either saturated solutions or gaseous NO) to deliver NO is the inability to maintain steady state concentrations of NO, especially in a reactive environment.

Permeation of gaseous NO through polymeric membranes enables a constant NO delivery rate that leads to steady state NO concentrations, even in the presence of species which react with NO. A previous study incorporating NO permeation through a membrane resulted in constant formation of NO_2^- in the presence of O_2, suggesting that

the NO concentration achieved steady state (Tamir et al., 1993). However, the delivery rate was only semi-quantifiable and the aqueous NO concentrations were not predictable or measured. In all methods of NO delivery, it is often advantageous to deliver NO at a constant and controlled rate to maintain a desired and predictable NO concentration in a biological environment. Knowledge of the concentration is beneficial for assessing the effects of NO on biological systems, especially when assessing the physiological relevance of the NO exposure level.

In view of the advantages of a constant NO delivery method in which predictable and steady state NO concentrations can be maintained, one device for delivering NO through permeable membrane and into a flowing solution has been developed and modeled. The advantages of the device are that 1) a controlled amount of NO is delivered to maintain a steady state NO concentration, 2) the NO concentrations are predictable from models, 3) the pH and light effects on the delivery rate are avoided, and 4) the addition of undesired species is eliminated to avoid undesired reactions.

3.2 Materials and Methods

3.2.1 Precautions

It was critical to handle NO gas only with stainless steel tubing and high quality stainless steel fittings because NO is a strong oxidizing agent. In addition, due to the potential toxicity of NO, all NO gas was vented to a hood.

3.2.2 Reagents

Ultra-high pure nitrogen, after passage through an O_2 trap, was mixed with a mixture of 10 % NO, balance N_2 using controlled gas flow meters (Porter Instrument Co. Hatfield, PA) to obtain the desired NO gas concentration. Phosphate-buffered saline (PBS, 0.01 M) was obtained from Life Technologies (Grand Island, NY). Potassium iodide and glacial acetic acid were obtained from Sigma (St. Louis, MO).

3.2.3 Delivery device

A device composed of a permeable tube was designed for physical delivery of NO to a flowing solution. Advantages of the devices are that the physical dimensions can easily be modified to vary the NO delivery rate and it is simple to fabricate.

The tube delivery device is shown in Figure 3.1. The device consists of Silastic tubing (VWR Products, 0.147 cm i.d., 0.196 cm o.d.) placed inside a stainless steel Swagelock® cross attached to Teflon tubing (0.132 cm i.d., 0.193 cm o.d.). Heat shrink tubing (made of polyolefins), which is significantly less permeable to gas as compared to Silastic, is utilized to attach the Teflon tubing to the Silastic tubing. A section (3.0 cm) of the Silastic tubing is left exposed such that gas flowing across the tube permeates through the exposed Silastic tube and into a flowing solution. The exposed section or the NO gas

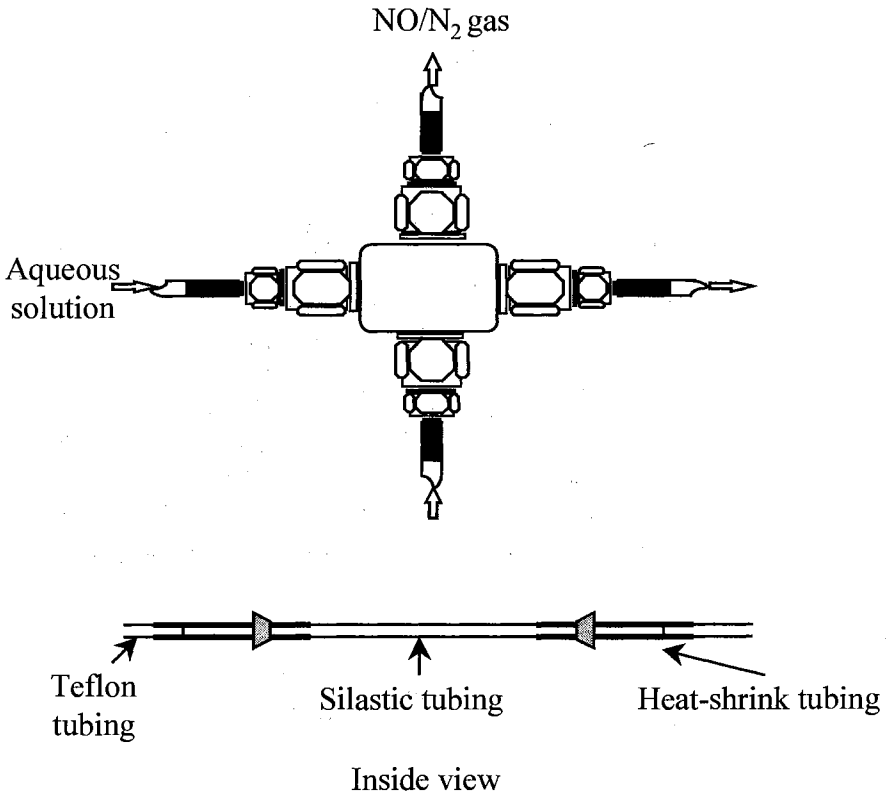

Figure 3.1. Tube delivery device. The device is composed of Silastic tubing (0.147 cm i.d., 0.196 cm o.d.) attached to Teflon tubing (0.132 cm i.d., 0.193 cm o.d.) and placed inside a Swagelok® cross. Heat shrink tubing covers all but 3.0 cm of the Silastic tubing to allow for NO permeation into solution following exposure of the tubing exterior to NO gas.

concentration can easily be adjusted to permit more or less gas from permeating into the solution.

3.2.4 Delivery device experiments

PBS was continuously pumped through the tube delivery device at a flow rate of 3 mL/min using a peristaltic pump (Masterflex R, Model 77390-00, Cole-Palmer Instrument Co., Vernon Hills, IL). Thus, the residence time (volume divided by volumetric flow rate) in the region of gas exposure was 1.0 second. A gaseous mixture of NO and N_2 of a specified concentration continuously flowed across the exterior of the Silastic tubing. The NO concentration was measured at the delivery device outlet and compared to model predictions. Experiments were performed at 37 °C. For the 37 °C experiments, the delivery device was autoclaved for 25 minutes at 250 °F prior to each experiment. The device was autoclaved to assess the predictability of NO delivery for applications in which sterile delivery devices are desired.

3.2.5 Nitric oxide analysis

The aqueous NO concentration, following exposure to NO gas, was measured using either a chemiluminescence analyzer (Model NOA 270B, Seivers Corporation, Boulder, CO) or an amperometric probe (ISO-NOP, World Precision Instrument, Sarasota, FL).

For the chemiluminescence method, aqueous samples were drawn using a gas-tight syringe (Hamilton Company, Reno, NV) and 0.1 or 0.25mL was injected into 10 mL of nitrite reducing solution composed of 0.2 M potassium iodide and glacial acetic acid mixed in a 1:3 volumetric ratio. The solution was contained in a glass vial and was continuously stirred and bubbled with N_2 at 200 sccm to purge NO from the solution and transport the NO into the chemiluminescence detector. The concentration of NO in the sample was obtained by comparison with NO_2^- standards since NO_2^- is instantaneously converted to NO in the solution (Cox, 1980). The calibration curve was linear over the range of concentrations studied. The minimum detection limit is 25 pmoles.

For the amperometric probe measurements, the probe was inserted into a tee at the point of measurement. As experiments were at 37 °C, the probe was located in an incubator since the probe response is sensitive to temperature. The probe was calibrated at 37 °C. The calibration consisted of bubbling known concentrations of NO gas into deoxygenated PBS. The saturated NO aqueous concentrations were obtained from NO solubility data which is 2.14 μM/mmHg for NO at 37 °C (Lange, 1967). The saturated solution was pumped at 3.0 mL/min through the tee containing the probe to obtain the calibration curve. The solution was re-circulated through the tee. The calibration curve was linear over the range of concentrations studied.

Although the amperometric probe measures NO and not NO_2^-, the sensitive nature of the probe response to normal disturbances in the experimental set-up renders it difficult to use for the measurement of NO. On the contrary for the chemiluminescence method, the NO measurement is independent of the experimental set-up, therefore it is easier to use. The measurement of NO concentrations using both methods were similar

as discussed in Section 3.3.1. Thus, most of the NO concentration measurements in this chapter and all the results in Chapter 4 are based on the chemiluminescence method.

3.2.6 Model for prediction of the NO concentration

The bulk (or mixing-cup) NO concentration exiting the delivery device (C_b) was modeled and compared with experiments. The aqueous NO concentration (C) in the delivery device is obtained from the steady state dimensionless continuity equation for NO which is

$$(1-\eta^2)\frac{\partial\theta}{\partial\xi} = \mathrm{A}\left[\frac{\partial^2\theta}{\partial\eta^2} + \mathrm{B}\frac{\partial\theta}{\partial\eta}\right] \tag{3.1}$$

The dimensionless concentration (θ) is $(C\text{-}C_o)/(C_i\text{-}C_o)$ where C_o is the aqueous NO concentration in equilibrium with the gaseous NO to which the delivery device is exposed and C_i is the aqueous NO concentration at the inlet. For this study, C_i=0. The value of C_o is the product of the NO solubility (H) and the gas partial pressure of NO. The dimensionless parameter ξ is z/L where the z coordinate represents the direction of flow (z = 0 at the flow inlet) and L is the length of the membrane through which NO gas permeates. Equation 3.1 is based on fully developed laminar flow with a homogenous fluid. The reaction of NO with aqueous O_2 was not included in Equation 3.1 since the reaction is slow for the NO concentrations of this study compared to the residence time of the solution the device.

For a tube device, η is r/R where the r coordinate represents the radial direction (r = 0 at tube center) with a tube inner radius of R. The parameter A is $DL/(U_mR^2)$, where D is the aqueous NO diffusivity and U_m is the maximum velocity. The value of U_m is twice the average velocity. The parameter B is $1/\eta$.

The initial and boundary conditions to solve Equation 3.1 are

ξ=0	All η	θ=1	(3.2)
All ξ	η=0	$\partial\theta/\partial\eta$=0	(3.3)
All ξ	η=1	$\partial\theta/\partial\eta$= -$N_{Shw}\theta$	(3.4)

The Sherwood number (N_{Shw}) at the wall is k_wR/D. The mass transfer coefficient characterizing the transport of NO through the permeable membrane is k_w.

The solution to Equation 3.1 yields $\theta = f(\xi,\eta)$. The solution can be obtained using a numerical package such as Matlab®. Thus, the NO concentration profile within the delivery device is obtained. The predicted value of the bulk (mixing-cup or velocity-weighted) NO concentration (C_b) exiting the NO delivery device (at ξ=1) is

$$\theta_b = \frac{\int_0^1 (1-\eta^2)\theta_{\xi=1}\, d\eta}{\int_0^1 (1-\eta^2) d\eta} = \frac{C_b - C_o}{C_i - C_o} \tag{3.5}$$

Analytical solutions for C_b for tube devices have previously been solved (Colton and Lowrie, 1981; Davis and Parkinson, 1971).

For the model, the average velocity was obtained from the geometric dimensions and the volumetric flow rate. The value of D in PBS was assumed similar to that in water which is 5.1 x 10^{-5} cm^2/sec at 37 °C (Wise and Houghton, 1968). The value of k_w was obtained from the NO permeability (P) of polydimethylsiloxane membranes (i.e. Silastic) according to $k_w = P/[HRln(R_o/R)]$ for flow in a tube. The tube outer radius is R_o. The value of P for NO is 2.3 x 10^{-13} moles cm^{-1} s^{-1} $mmHg^{-1}$ at 25 °C (Rob, 1968). The permeability at 37 °C is approximately twice the reported value at 25 °C in order to account for the effect of heating the membrane during autoclaving (Lewis et al., 1992). The value of H for NO is 2.14 μM/mmHg at 37 °C, respectively (Lange, 1967).

3.3 Results and Discussion

3.3.1 Aqueous NO concentration in exiting perfusate

The bulk or mixing-cup NO concentration (C_b) in the perfusate at the exit of the delivery device was measured as a function of the NO gas concentration to which the semi-permeable membrane was exposed. Figure 3.2 shows the measured aqueous NO concentrations at steady state exiting the delivery device. The steady state aqueous NO concentrations were obtained within two minutes of changing the NO gas concentration, of which part of the time was due to the time required for the NO gas concentration to obtain steady state. The measured aqueous NO concentrations are

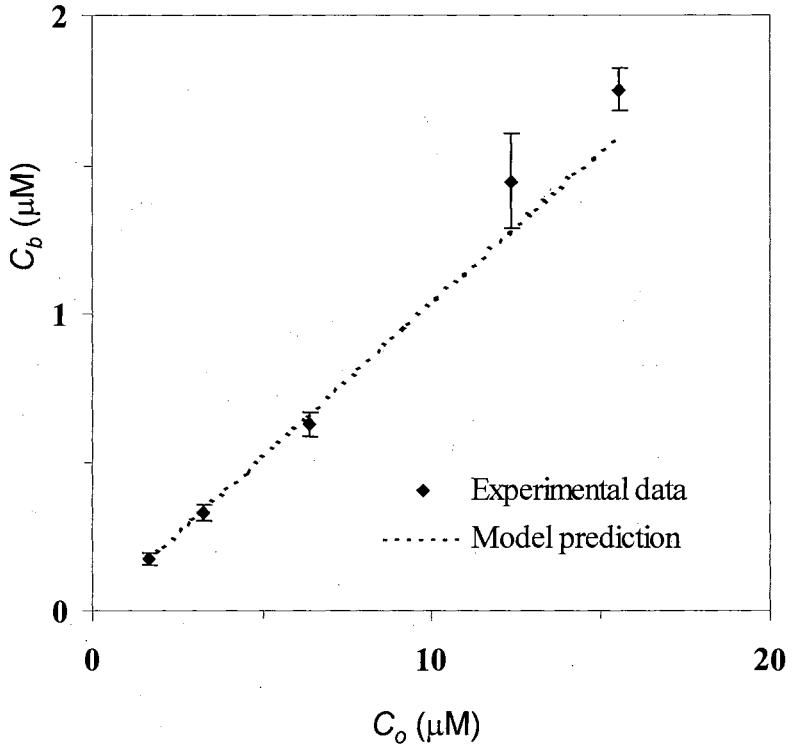

Figure 3.2. The delivery device NO concentrations at the outlet (C_b) are shown relative to NO concentrations (C_o) that would be in equilibrium with the NO gas exposed to the delivery device. Experimental measured values of C_b (mean $\pm$ sd) at the exit of the delivery device are shown as discrete symbols for the tube delivery device at 37 °C. The dashed lines represent model predictions as described in the text.

shown relative to the NO concentrations (C_o) which would be in equilibrium with the NO gas. The equilibrium NO gas concentrations were obtained using NO solubility data as previously given. Model predictions are also shown which are described later.

The average value of C_b/C_o at all NO gas exposure levels was 0.107 ± 0.011 (n=15) for tube flow at 37 °C. The measured values were obtained using chemiluminescence. In addition, the NO concentration exiting the tube device at 37 °C was also measured using the amperometric probe, with an average value of C_b/C_o of 0.120 ± 0.019 (n=8) over a similar range of C_o. This shows that the NO concentrations as measured using the amperometric probe or chemiluminescence are similar. Thus, bioavailable NO is exiting the delivery device. As shown, C_b/C_o is not a function of C_o as expected from model predictions explained later. It is also evident that the aqueous NO concentration is not saturated at any of the gas exposure levels, with only a maximum of 10% saturation achieved. By increasing the membrane exposure area and/or decreasing the flow rate, the NO concentration relative to equilibrium can be increased. Although at the highest gas exposure level the aqueous NO concentration approached 2 μM, higher concentrations are obtainable by increasing the NO gas exposure level, adjusting the flow rate, or modifying the delivery device dimensions.

3.3.2 Model predictions of exiting NO concentration

Although the bulk aqueous NO concentrations were measured in the exiting perfusate, it is useful to predict the NO concentrations. Predictions would be beneficial for selecting a desired NO concentration without experimental measurements based on

adjustments in the flow rate or device dimensions (i.e. membrane exposure area). The value of C_b at the delivery device exit was predicted using the model for a tube geometry. The values of C_b/C_o predicted by the model are shown in Figure 3.2. The models show good agreement with experiments, irrespective of the size and geometry of the delivery device. It is notable that the model parameters were obtained independent of the experiments. The general agreement of the model predictions with experimental results suggests that the models can be utilized to effectively predict the outlet NO concentrations of the delivery devices. If desired, the model can also be used to obtain the spatial concentration profiles within the tube.

3.4 Conclusions

In view of the importance of delivering predictable quantities of NO to biological systems for investigating the biological effects of NO, a simple delivery device was designed. For applications of the delivery device to study the effects of NO exposure to biological systems, several methods can be utilized which incorporate the delivery devices. Cell adhesion (such as platelets) to various proteins coated on the permeable membrane can be studied in the presence or absence of NO delivery to assess the effects of NO on the adhesion process. The delivery device can be included in a circulating or non-circulating loop connected to a stirred chamber to expose cells in the chamber to steady state NO conditions.

In all designs, it is important to assess the effects of reacting species with NO in order to predict the NO concentrations to which biological systems are exposed. NO is a

highly reactive molecule and can react with species such as superoxide, metal-containing proteins, or oxygen. Previous studies have shown that NO concentrations resulting from the delivery of NO to oxygenated culture medium containing serum were predictable while only accounting for the reaction with O_2 (Ramamurthi and Lewis, 1997). However, if other unknown but significant reactions with NO exist, the models described in this work can be used to provide an upper estimate of the NO concentration.

Chapter 4. Physical NO Delivery: An Application to Pancreatic Cell System

4.1 Introduction

Due to the advantages of achieving controlled and quantitative NO delivery via physical NO delivery for long periods to biological systems, as presented in Chapter 3, the concept of physical NO delivery was applied to assess the effects of NO on a cellular system of pancreatic cells. Initially, a well-stirred chamber (Kavdia et al., 1998) downstream of the delivery device was used to expose the pancreatic cells HIT-T15 to a controlled delivery of NO achieved with the cross-flow delivery device designed in Section 3.2.3. However, the flowing solution resulted in cell detachment within the chamber. An additional problem was the difficulty in measuring the low levels of insulin concentrations exiting the well-mixed chamber. To eliminate these problems, an experimental system was developed to maintain steady state concentration exposures of NO and/or O_2^- during the experiment. In addition, the prediction of NO following the physical delivery of NO was investigated in the presence O_2^- and other related species.

The onset of Insulin Dependent Diabetes Mellitus (IDDM, type1) has been associated with the infiltration of pancreatic islets by macrophages and lymphocytes leading to an attenuation of the insulin secreting capacity (Mandrup-Poulsen et al., 1990). T-lymphocyte mediated pancreatic cell destruction and/or macrophage and lymphocyte production of cytokines are involved with the insidious development of IDDM (Campbell

et al., 1988; Mandrup-poulsen et al., 1987). The cytokines include interleukin 1-β (IL-1β), tumor necrosis factor (TNFα) and gamma interferon (γIFN). The effects of cytokines on pancreatic cell dysfunction may be a consequence of cytokine-induced generation of free radicals such as O_2^- and/or NO (Denicola et al., 1996; Kolb and Kolb-Bachofen, 1992). These free radicals are produced intracellularly by pancreatic cells on consumption of cytokines as well as extracellularly by cytokine-activated macrophages and pancreatic endothelial cells.

Studies assessing the effects of NO on the function and viability of pancreatic β-cells have focused on both intracellularly- and extracellularly- generated NO. NO is synthesized intracellularly by β-cells following the addition of TNFα, γIFN, and/or IL-1β (Green et al., 1994; Janjic and Asfari, 1992). NO donor compounds (i.e. sodium nitroprusside, 3-morpholinosydnonimine (SIN-1), S-nitrosoglutathione) or macrophages have been used extensively for extracellular NO generation studies. The studies involving extracellularly-generated NO have reported contradictory NO-dependent effects on insulin secretion and cell lysis using different NO donor sources and/or cells (Cunningham et al., 1994; Eizirik et al., 1996; Green et al., 1994; Kroncke et al., 1993). For example, NO donors SIN-1 and GSNO lowered insulin secretion of human and rat islets (Eizirik et al., 1996), whereas SNAP had no effects and SIN-1 stimulated the insulin secretion of RINm5f cells (Green et al., 1994).

The contradictions in the NO effects on the insulin secretion ability of pancreatic cells may be a result of several aspects. First, some NO donor compounds release additional species that may be harmful, such as O_2^- and the by-products $ONOO^-$ and hydrogen peroxide (H_2O_2) from SIN-1 (Green et al., 1994). Second, the non-constant

release rate of NO results in unsteady state and potentially high concentration exposures to NO that may last from minutes to days depending on the NO donor (Green et al., 1994). Third, the reactivity, toxicity, and/or cellular metabolism of NO donor compounds following the release of NO are generally unknown and such compounds may affect the β-cells. Fourth, several experiments were performed in stagnant micro-well or tissue culture plates that may lead to a non-uniform exposure of NO to cells (see Chapter 2). But these problems occur in all *in vitro* systems to some extent, yet many useful results and conclusions are obtained. Finally, studies using macrophages as the NO donor source lead to the release of other constituents such as IL-1β and O_2^-. The IL-1β can lead to intracellular generation of NO in the β-cells. In many NO donor studies, the NO (or other species) concentrations to which the cells were exposed were not quantified.

In this chapter, the effects of extracellularly generated NO, O_2^-, and/or $ONOO^-$ on the insulin secretion rate and viability of βTC3 pancreatic cells (β-cells) are presented. An experimental system was developed to maintain steady state concentration exposures of NO and/or O_2^- during the experiment. The NO was delivered to the cells using a modified membrane delivery system (Tamir et al., 1993). An enzymatic method was utilized to deliver O_2^- to the cells. The combined delivery of NO and O_2^- resulted in the formation of $ONOO^-$. Using these controlled delivery methods, several of the previously described experimental problems associated with NO delivery were eliminated and the steady state concentrations of NO, O_2^-, and $ONOO^-$ to which cells were exposed were predictable.

4.2 Materials and Methods

4.2.1 Materials

Ultra-high pure nitrogen, after passage through an oxygen trap (VWR, Sugarland,TX), was mixed with pure NO (Matheson, Twinsburg, OH) using controlled gas flow meters (Porter Instrument Co. Hatfield, PA) to obtain the desired NO gas concentration. Nitrite reducing solution consisted of glacial acetic acid and 0.2 M potassium iodide (Sigma, St. Louis, MO) mixed in a 1:3 volumetric ratio, as described in Section 3.2.5. Due to the potential toxicity of NO, all NO gas was vented to a hood.

Dulbecco's modified Eagle's medium (DMEM) containing 25 mM glucose, penicillin-streptomycin (pen-strep, 10,000 U/ml), and phosphate-buffered saline (PBS) were obtained from Gibco-BRL (Grand Island, NY). Rat insulin was purchased from Linco Research (St.Louis, MO). Fetal calf serum was purchased from Hyclone (Logan, UT). Low glucose DMEM and horse serum were purchased from Sigma (St.Louis, MO). Growth media of βTC3 cells consisted of high glucose DMEM supplemented with 2.5% fetal calf serum, 12.5% horse serum, and 1% pen-strep (vol/vol). The supplements for the low glucose DMEM were the same as the growth media. For experiments, high glucose DMEM was supplemented only with 1% pen-strep.

For experiments with O_2^-, catalase and hypoxanthine were purchased from Sigma (St.Louis, MO) and xanthine oxidase (XOD) was purchased from Boehringer Mannheim (Indianapolis, IN). Stock solutions of hypoxanthine (25.0 mM), catalase (10000 U/ml), and xanthine oxidase (0.15 U/ml) were made in DMEM.

4.2.2 Cell culture preparation

βTC3 cells obtained from transgenic mice (Efrat et al., 1988) were a kind gift from S. Efrat (Albert Einstein College of Medicine, Bronx, NY). The cells were obtained at passage 29 and subsequently passaged in Falcon® (100 mm x 20 mm) tissue culture plates at 37 °C in growth media. For the experiments, confluent cultures at passage 35 to 40 were used. Two days prior to the experiment, 30 million freshly trypsinized βTC3 cells were seeded on a small Falcon® (60 mm x 15 mm) plate, which was placed in a larger culture plate. The cells were grown in growth media until 12 hours prior to the experiment, at which time the cells were incubated in low glucose DMEM. At the beginning of the experiment, the cells were washed with 10 ml of PBS. The cells appeared confluent prior to each experiment.

4.2.3 Experimental system and protocol

The experimental system consisted of a Teflon container (model E-06103-50, Cole-Parmer, Vernon Hills, IL) as shown in Figure 4.1. The container lid was modified to include a modified CYTOSTIR® stirrer (Kontes, Vineland, NJ), a septum port for sample collection, two ports for air/CO_2 gas inlet and outlet, and two ports for delivering NO to the solution via a gas-permeable membrane. Silastic tubing (VWR Products, 0.147 cm i.d., 0.196 cm o.d., and 5 cm exposed length) was attached to 0.159 cm o.d. stainless steel tubing which was connected to the two ports for NO delivery. A thin stainless steel wire was inserted in the Silastic tubing to enhance the stability of the tubing.

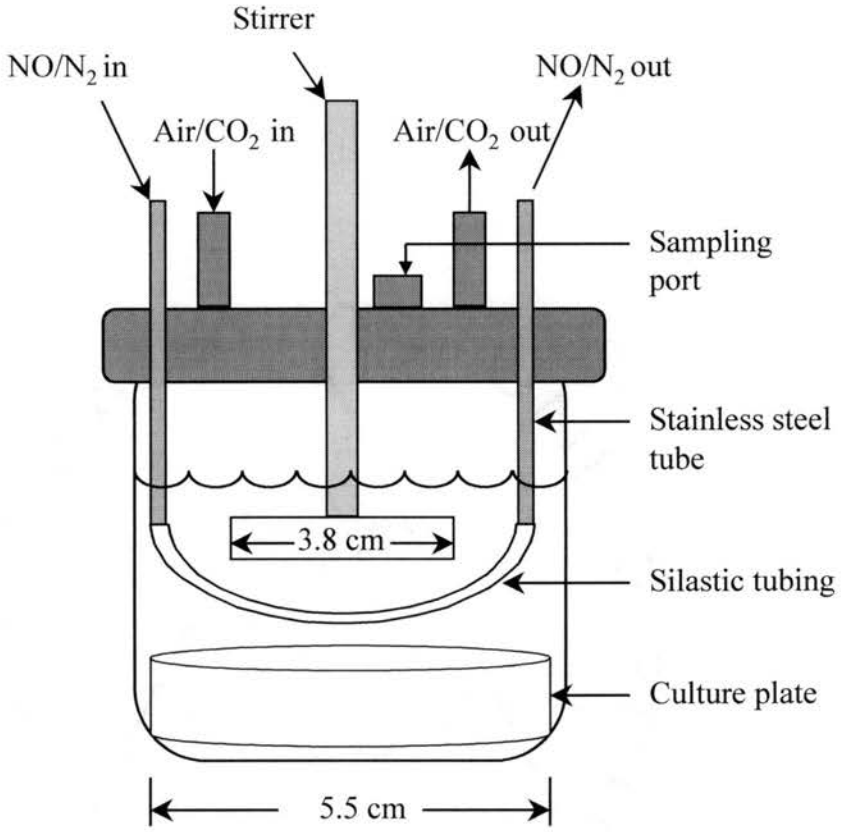

Figure 4.1. Experimental set-up for the study of the NO & O_2^- effects on pancreatic cells. Silastic tubing (5 cm) was attached to stainless steel tubing. Culture medium was stirred with a stir-bar (3.8 cm length and 0.9 cm diameter) to minimize diffusional limitations. The culture plate containing the βTC3 cells was secured to the bottom. Stirring speed was 10 rpm. Aqueous samples (1-1.5 ml) were collected by inserting a needle into the sampling port every 30 minutes. A gas mixture of NO/N_2 at a NO gas partial pressure of 6.9 cmHg was perfused through the gas-permeable Silastic tubing at 110 cc/min resulting in NO delivery to the culture medium. For O_2^- and NO/O_2^- experiments, 1 ml each of hypoxanthine, catalase, and XOD stock solutions was added to the 100 ml of culture media at the beginning of each experiment.

The culture plate containing the βTC3 cells was secured to the bottom of the Teflon container. High glucose DMEM without serum (25 ml) was added to the container and the cells were incubated for 5 min to capture the initial insulin burst following the increase in glucose concentration (Burr et al., 1977). The culture media was then removed to minimize the buildup of insulin and 100 ml of fresh high-glucose DMEM without serum was added. Sterile air containing 5% CO_2 was continuously purged through the Teflon container head space at 200 sccm. Stirring speed was 10 rpm to minimize cell detachment from the culture plate. NO, O_2^-, or both were delivered to the culture media as described below. The absence of NO and O_2^- delivery was used as the control. All experiments were maintained in an incubator at 37 °C.

The experiments consisted of five sets of control, NO, O_2^-, and NO/O_2^- delivery. Four culture dishes containing the pancreatic βTC3 cells were used for every set of experiments. Two culture dishes were exposed to two treatments in the morning and other two culture dishes to the remaining two treatments in the afternoon. The experiments were randomized to eliminate the experimental bias. For the NO/O_2^- experiments, NO and O_2^- delivery rates were the same as the experiments of NO or O_2^- alone. Aqueous samples (1-1.5 ml) were collected every 30 minutes resulting in a total liquid removal of approximately 10% of the initial volume. However, the effect of the liquid removal on the predicted NO concentration is less than 3%. At the end of four hours, the experiment was terminated. Samples were frozen immediately after collection. The samples were later assayed for NO_2^-, insulin, and lactate dehydrogenase (LDH).

4.2.4 NO delivery

A gas mixture of NO/N_2 at a NO gas partial pressure of 6.9 cmHg was perfused through the gas-permeable Silastic tubing at 110 cc/min resulting in NO delivery to the culture medium. At steady state, the maximum delivery rate of NO (S_{NO}) into the solution is

$$S_{NO} = \left(\frac{\pi dL}{\delta}\right)\alpha D_{NO}\Delta P_{NO} \tag{4.1}$$

where d, L and δ are the average diameter, length, and thickness of the Silastic tubing, respectively (Tamir et al., 1993). The permeability of NO through the Silastic (αD_{NO}) is the product of the diffusivity (D_{NO}) and solubility (α) of NO in the Silastic. The value of αD_{NO} is 5 x 10^{-12} mol $cm^{-1}s^{-1}cmHg^{-1}$ at 37 °C, which is approximately twice the reported value in order to account for the effect of heating the Silastic during autoclaving (Lewis et al., 1992). The difference between the partial pressure of NO in the Silastic tubing and the culture medium is ΔP_{NO}. Thus, for this study the maximum ΔP_{NO} is 6.9 cmHg, corresponding to an S_{NO} value of 2.3 μM/min for 100 ml of solution. Of the NO that is delivered, NO will either react in solution or transport out of solution into the head-space. Since the major reaction products of NO are NO_2^- and NO_3^-, the sum of the rate of formation of these products quantifies the rate at which NO is delivered into the solution and reacts. If desired, the Silastic tubing size or NO partial pressure may be adjusted to vary S_{NO}. In addition, other gases can also be predictably delivered to assess the gas exposure effects on cell function or viability.

4.2.5 O_2^- delivery

An enzymatic method, based on the reaction of hypoxanthine with XOD, was used for the generation of O_2^-. Catalase was added to scavenge hydrogen peroxide, which is generated by the dismutation of O_2^-. For O_2^- and NO/O_2^- experiments, 1 ml each of hypoxanthine, catalase, and XOD stock solutions was added to the 100 ml of culture media at the beginning of each experiment. Therefore, the final concentrations of hypoxanthine, catalase, and XOD were 0.25 mM, 100 U/ml, and 1.5 mU/ml, respectively.

A commonly used spectrophotometric assay based on the rapid reduction of ferricytochrome C (Fe^{3+}) to ferrocytochrome C (Fe^{2+}) by O_2^- was used to measure the O_2^- generation rate prior to the experiments. Hypoxanthine, catalase, and XOD were added to a cuvette to obtain the same final concentrations as in the experiments. A 0.1 M PBS solution (pH 7.4) was used as the medium. The increase in absorbance was continuously measured at 550 nm using a spectrophotometer (UV-1601, Shimadzu, Columbia, Maryland). The molar extinction coefficient (ε_{550}) for the cytochrome C assay was determined to be 18.5 $mM^{-1}cm^{-1}$, which agrees with the previously reported value of 19.5 $mM^{-1}cm^{-1}$ (kelm et al., 1997). The O_2^- generation rate (S_{O2}-) utilized for this study was 0.4 μM/min at 37 °C and was constantly maintained over four hours. In DMEM culture medium, a similar O_2^- generation rate was observed.

4.2.6 Nitrite, insulin, and LDH measurements

The NO_2^- concentration in the aqueous samples was measured using the chemiluminescence method described in Section 3.2.5. Aqueous samples were drawn using a gas-tight syringe (Hamilton Company, Reno, NV) and 0.05 or 0.1ml was injected into 10 ml of NO_2^- reducing solution contained in a glass vial.

The insulin concentration in the aqueous samples was measured using a Coat-A-Count radioimmunoassay kit (DPC, Los Angeles, CA) with rat insulin prepared in DMEM as the standard. Cell viability was assessed using a CYTOTOX-96 kit (Promega, Madison, WI) to measure LDH, which is released by cells upon lysis.

4.2.7 Model predictions of NO, O_2^-, and $ONOO^-$ concentrations

The experimental NO_2^- formation rate, O_2^- delivery rate, and reaction kinetics were utilized to estimate the NO, O_2^-, and/or $ONOO^-$ steady state concentrations within the experimental system. The major reactions in the experimental system are,

$$2NO + O_2 \xrightarrow{k_2} 2NO_2 \tag{4.2}$$

$$NO_2 + NO \underset{k_{-3}}{\overset{k_3}{\rightleftarrows}} N_2O_3 \tag{4.3}$$

$$N_2O_3 + H_2O \xrightarrow{k_4} 2NO_2^- + 2H^+ \tag{4.4}$$

$$NO + O_2^- \xrightarrow{k_5} ONOO^- \rightleftarrows ONOOH \tag{4.5}$$

$$ONOOH \xrightarrow{k_6} NO_3^- + H^+ \quad (4.6)$$

$$ONOOH \xrightarrow{k_7} NO_2^- + \frac{1}{2}O_2 + H^+ \quad (4.7)$$

$$ONOO^-(ONOOH) + NO \xrightarrow{k_8} NO_2 + NO_2^- \quad (4.8)$$

$$HO_2 + O_2^- + H_2O \xrightarrow{k_9} O_2 + H_2O_2 + OH^- \quad (4.9)$$

$$ONOO^- + CO_2 + H_2O \xrightarrow{k_{10}} NO_3^- + CO_3^{2-} + 2H^+ \quad (4.10)$$

Equations 4.2-4.4 represent the oxidation of NO in the presence of molecular O_2, with the overall rate of NO oxidation controlled by Equation 4.2 (Lewis and Deen, 1994). The final product of these reactions is NO_2^-. Equation 4.5 represents the rapid reaction of NO with O_2^- (Huie and Padmaja, 1993). Equations 4.6 and 4.7 represent the decomposition of ONOOH that is in rapid equilibrium with the unprotonated form ($ONOO^-$) to NO_3^- and NO_2^- (Koppenol et al., 1992; Pfeiffer et al., 1997). Equation 4.8 represents an additional mechanism for NO_2^- formation via the reaction of NO with peroxynitrite (Pfeiffer et al., 1997). However, the reactive form of peroxynitrite has not been identified and will be considered as total peroxynitrite (PER). Recent studies have shown that nitrous anhydride (N_2O_3), rather than NO, may be the reactive species with peroxynitrite although this potential reaction does not affect the predictions described below (Goldstein et al., 1999). Equation 4.9 represents the degradation of O_2^- to H_2O_2 and Equation 4.10 represents the CO_2-catalyzed conversion of $ONOO^-$ to NO_3^- (Denicola et al., 1996; Imlay and Fridovich, 1991).

For a well stirred system, the material balance for each species is

$$\frac{dC_i}{dt} = S_i + R_i \tag{4.11}$$

where R_i is the net rate of formation of species *i* based upon the reaction kinetics of Equations 4.2-4.10 (see Chen et al. 1998 for derivations of R_i) and S_i is the delivery rate of species *i*. The derivations for R_i assume that species except NO_2^- and NO_3^- are at steady state ($dC_i/dt \approx 0$). The mass balance equations for NO_2^-, O_2^-, total peroxynitrite (sum of $ONOO^-$ and ONOOH balances), and NO_3^- are

$$\frac{dC_{NO_2^-}}{dt} = 4k_2 C_{NO}^2 C_{O_2} + 3k_8 C_{NO} C_{PER} + k_7 C_{ONOOH} \tag{4.12}$$

$$\frac{dC_{O_2^-}}{dt} = 0 = S_{O_2^-} - k_5 C_{NO} C_{O_2^-} - k_9 C_{HO_2} C_{O_2^-} \tag{4.13}$$

$$\frac{dC_{PER}}{dt} = 0 = \begin{aligned} & k_5 C_{NO} C_{O_2^-} - (k_6 + k_7) C_{ONOOH} \\ & - k_8 C_{NO} C_{PER} - k_{10} C_{ONOO^-} C_{CO_2} \end{aligned} \tag{4.14}$$

$$\frac{dC_{NO_3^-}}{dt} = k_6 C_{ONOOH} + k_{10} C_{ONOO^-} C_{CO_2} \tag{4.15}$$

where k_2=2.4 x 10^6 $M^{-2}s^{-1}$, k_5=6.7 x 10^9 $M^{-1}s^{-1}$, k_6=3.1 s^{-1}, k_7=1.4 s^{-1}, k_8=9.1x 10^4 $M^{-1}s^{-1}$, k_9=8.0 x 10^7 $M^{-1}s^{-1}$, and k_{10}=5.8 x 10^4 $M^{-1}s^{-1}$ at 37 °C (Chen et al., 1998; Radi, 1998). Assuming rapid equilibrium for $ONOO^-$/ONOOH and O_2^-/HO_2 at pH 7.7

$$\frac{C_{PER}}{C_{ONOO^-}} = 1.11, \qquad \frac{C_{ONOOH}}{C_{ONOO^-}} = 0.11, \qquad \frac{C_{HO_2}}{C_{O_2^-}} = 0.0013 \tag{4.16}$$

based on equilibrium constants (pK) of 6.75 and 4.8 for peroxynitrite and superoxide, respectively (Chen et al., 1998; Fridovich, 1978). The relationships in Equation 4.16 were substituted into Equations 4.12-4.15 such that all peroxynitrite and superoxide concentrations were in terms of $ONOO^-$ and O_2^- concentrations, respectively. For all experiments, the O_2 concentration was assumed to remain at the saturated value of 210 μM at 37 °C (Lange, 1967). The aqueous CO_2 concentration was assumed to be 1.1 mM, based on 5% CO_2 (38 mmHg) and the CO_2 solubility in blood plasma of 3.0×10^{-5} M $mmHg^{-1}$ (Davenport, 1974). From experimental measurements of NO_2^- formation ($dC_{NO_2^-}/dt$) and knowledge of $S_{O_2^-}$, the concentrations of NO, O_2^-, and $ONOO^-$ are predictable from Equations 4.12-4.14.

4.2.8 Statistical analysis

Data are presented as mean ± standard deviation unless otherwise noted. The significance of differences between means was evaluated by a two-tailed Student's unpaired *t*-test. A *P* value of <0.05 was considered significant. Formation rates of NO_2^- and insulin were calculated from regression of average data.

4.3 Results and Discussion

4.3.1 Predicted NO, O_2^-, and $ONOO^-$ concentrations

The NO_2^- concentrations with time for the NO and NO/O_2^- experiments are shown in Figure 4.2. It is evident that the NO_2^- increase with time is linear for both experiments. The NO_2^- formation rates are 0.96 ± 0.05 μM/min (n=5 culture dishes) and 0.74 ± 0.09 μM/min (n=5 culture dishes) for the NO and NO/O_2^- experiments, respectively. For the NO experiments, the rate at which NO enters the solution and reacts is 42% of S_{NO}. The theoretical limit of 100% is not achieved due to the loss of NO into the gas head space and the reduced transport rate of NO as a result of boundary layer effects adjacent to the tubing wall. The ratio of NO delivery to O_2^- delivery is approximately 2.4, which is similar to the ratio secreted by activated macrophages (Lewis et al., 1995). The NO_2^- formation rate is reduced by 0.22 μM/min for experiments with NO/O_2^-, which is likely a result of NO_3^- formation as described later. An enzymatic assay (Cayman Chemical Co., Ann Arbor, MI) was utilized to measure the NO_3^- formation rate (due to the reaction of NO with O_2^-) during the NO/O_2^- experiments. However, the culture medium significantly reduced the sensitivity of the assay such that NO_3^- could not be measured. There was not any NO_2^- formation during the control and O_2^- experiments.

For all experiments involving the delivery of NO, the constant rate of NO_2^- formation ($dC_{NO_2^-}/dt$) is indicative of steady state concentrations of NO, O_2^-, and $ONOO^-$. As shown in Equation 4.12, the concentrations on the right hand side (including

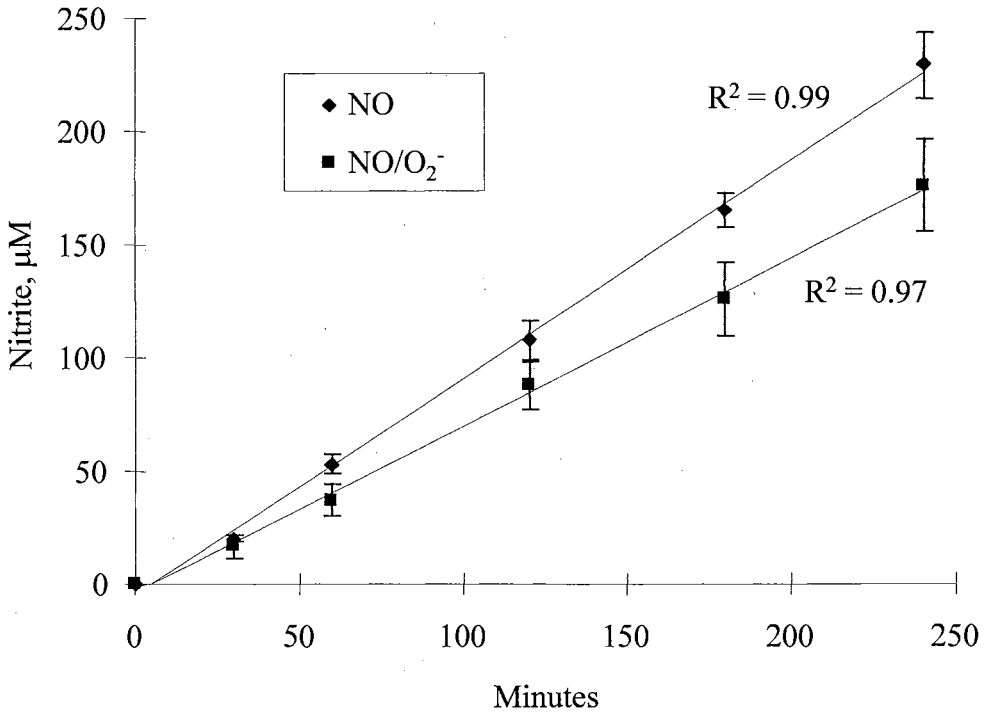

Figure 4.2. Nitrite concentration following NO and NO/ O_2^- delivery, at 37 °C (n=5 culture dishes). The lines (with R^2) represent the best fit. The NO_2^- formation rates are 0.96 ± 0.05 µM/min (n=5 culture dishes) and 0.74 ± 0.09 µM/min (mean ± sd, n=5 culture dishes) for the NO and NO/O_2^- experiments, respectively.

NO and forms of peroxynitrite) must be constant for $dC_{NO_2^-}/dt$ to be constant. Thus, dC_{PER}/dt is zero and similar reasoning demonstrates that O_2^- is at steady state according to Equation 4.14.

For the NO experiments in the absence of O_2^- delivery (C_{ONOOH}, $C_{PER} = 0$), where the NO_2^- formation rate was 0.96 μM/min, the predicted aqueous NO concentration from Equation 4.12 is 2.8 μM. For a NO solubility of 23.3 μM/cmHg, the corresponding aqueous partial pressure of NO is 0.12 cmHg (Lange, 1967). Thus, ΔP_{NO} in Equation 4.1 is approximately equal to only the NO gas partial pressure of 6.9 cmHg as previously assumed. For the O_2^- experiments in the absence of NO delivery ($C_{NO} = 0$), the O_2^- concentration predicted from Equation 4.13 is 0.25 μM . At this O_2^- concentration, the presence of H_2O_2 should be minimal since H_2O_2 was generated at a rate of $k_9 C_{HO_2} C_{O_2^-} = 0.4\ \mu$M/min (see Equation 4.9), but was scavenged by catalase at a rate of 10^5 μM/min (product specification states one unit decomposes 1.0 μmole/min H_2O_2).

For the NO/O_2^- experiments, where the NO_2^- generation rate was 0.74 μM/min and the O_2^- generation rate ($S_{O_2^-}$) was 0.4 μM/min, the simultaneous solution of Equations 4.12-4.14 and 4.16 yields estimated NO, O_2^-, and $ONOO^-$ steady state concentrations of 2.5 μM, 0.4 pM, and 0.1 nM, respectively. According to Equation 4.15, based on C_{ONOO^-} =0.1 nM and C_{ONOOH} =0.011 nM, the estimated NO_3^- formation rate is 0.38 μM/min. Thus, the estimated total NO_2^- and NO_3^- formation rate is 1.12 μM/min, which is similar to the NO delivery rate of 0.96 μM/min observed in the absence of O_2^- delivery.

The estimated NO_3^- formation rate of 0.38 μM/min is larger than the measured difference in the NO_2^- formation rates following NO and NO/O_2^- delivery (0.22 μM/min).

However, the estimated rate is within a factor of two, without using any adjustable parameters. Since $ONOO^-$ is known to react with numerous species in biological solutions (Radi, 1998), the small discrepancy may be a result of excluded reactions in the model. Nevertheless, the general agreement demonstrates that the model and kinetics are useful for predicting concentrations for species of interest.

Due to the detachment of cells from the culture dishes, a low stirring speed was maintained which might lead to a non-mixed solution. The maximum NO delivery rate of 2.3 μM/min would give a NO concentration of 4.4 μM in the system for a well-mixed system with no boundary layer effect as compared to 2.8 μM for the low stirred experimental system. Thus, the effects of the low stirring speed on predicted NO concentration is small. In addition, the potential exists for the O_2 concentration to be less than saturated due to the low stirring rate and the O_2 consumption by the cells. For a 33% reduction in the O_2 concentration (210 μM to 140 μM), the predicted concentrations would change as follows. For NO delivery, the predicted NO concentration would change from 2.8 to 3.4 μM. For O_2^- delivery, the predicted O_2^- concentration would not be affected. For the simultaneous delivery of NO and O_2^-, the NO and O_2^- predicted concentrations would change from 2.5 μM and 0.40 nM to 3.0 μM and 0.33 nM, respectively. The predicted $ONOO^-$ concentration would not be affected. Thus, the effects of the O_2 concentration on the predicted concentrations is small due to the squared dependence of NO on the NO reaction with O_2 and the rapid reaction of NO with O_2^- relative to NO reacting with O_2.

4.3.2 NO Effects on pancreatic cells

Figure 4.3 shows the insulin concentration versus time in the presence and absence of NO exposure for a 4 h period. The insulin secretion rates over the last 3 h are 0.35 ± 0.12 and 0.26 ± 0.12 $\mu U\ ml^{-1}\ min^{-1}$ (n=5 culture dishes) for control and NO experiments, respectively. A t-test (95% confidence interval) on the insulin secretion rates showed that NO (at 2.8 μM) does not have a significant effect on the insulin secretion rate over the experimental time. The LDH concentrations for both cases (control and NO) were also very low and similar (data not shown), demonstrating that NO does not have any significant effect on the viability of the cells.

To assess longer term NO effects, one experiment was conducted in the presence of NO for 24 h. The insulin secretion rate was linear over a majority of the 24 h. As shown in Figure 4.4, the insulin secretion rate in the presence of NO is 0.24 ± 0.02 (mean ± std. error) $\mu U\ ml^{-1}\ min^{-1}$, similar to the 4 h experiments. Since the insulin secretion rate did not significantly change over the entire experiment, NO does not appear to have any significant effect on the insulin secretion rate for at least 24 h.

4.3.3 *O_2^- and NO/O_2^- effects on pancreatic cells*

Figure 4.5 shows the insulin concentration versus time for the O_2^- and the NO/O_2^- experiments. The insulin secretion rates between 30 and 240 minutes are 1.5 ± 0.1 (R^2 = 0.96) and 1.7 ± 0.1 (R^2 = 0.99) $\mu U\ ml^{-1}\ min^{-1}$ (n=5 culture dishes) for the O_2^- and NO/O_2^-

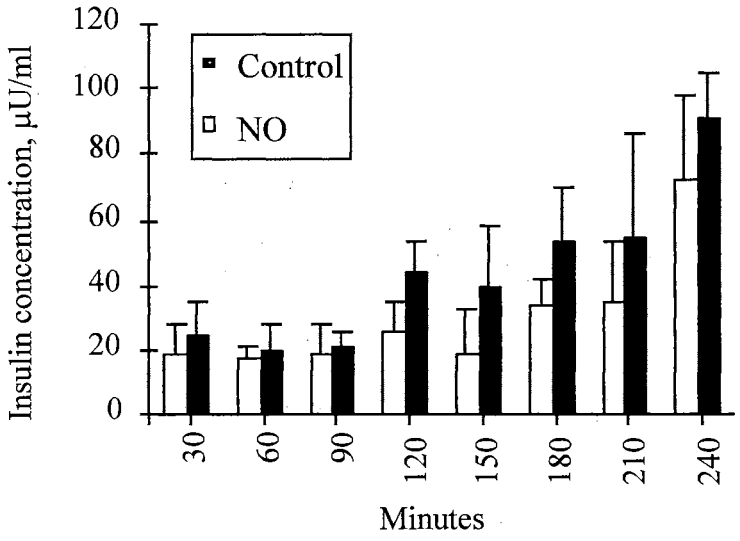

Figure 4.3. Insulin concentration in the presence and absence (control) of NO delivery, at 37 °C (n=5 culture dishes). The insulin secretion rates over the last 3 h are 0.35 ± 0.12 and 0.26 ± 0.12 μU ml^{-1} min^{-1} (mean ± sd) for control and NO experiments, respectively. The predicted NO concentration is 2.8 μM for NO delivery experiments. Experiments were randomized to eliminate experimental bias.

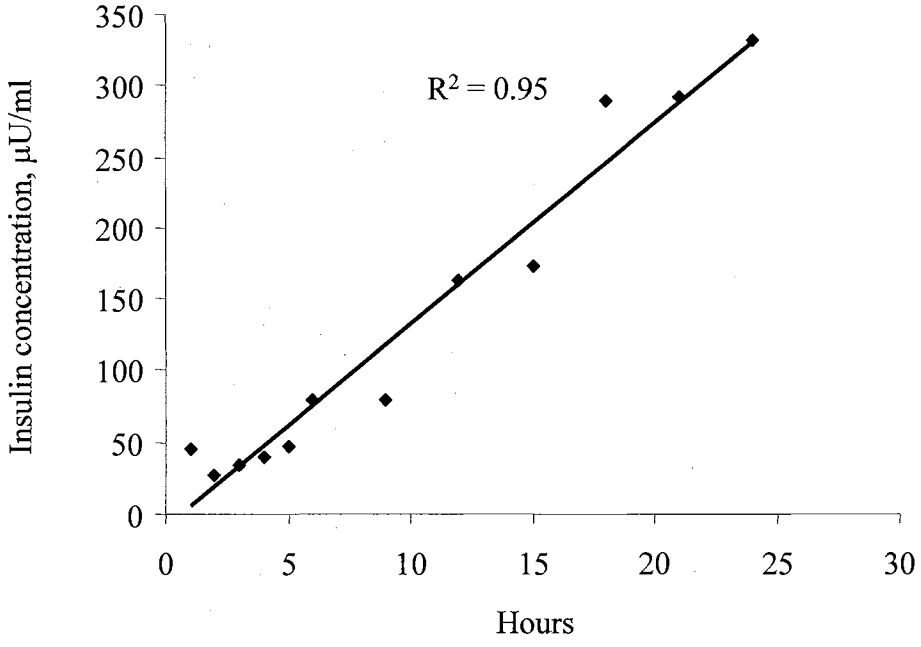

Figure 4.4. Insulin concentration for 24 hour experiment, in the presence of NO delivery at 37 °C. The insulin secretion rate in the presence of NO is 0.24 ± 0.02 (mean ± std. error) μU ml^{-1} min^{-1}, similar to the 4 h experiments in the presence of NO. The predicted NO concentration is 2.8 μM for NO delivery experiments.

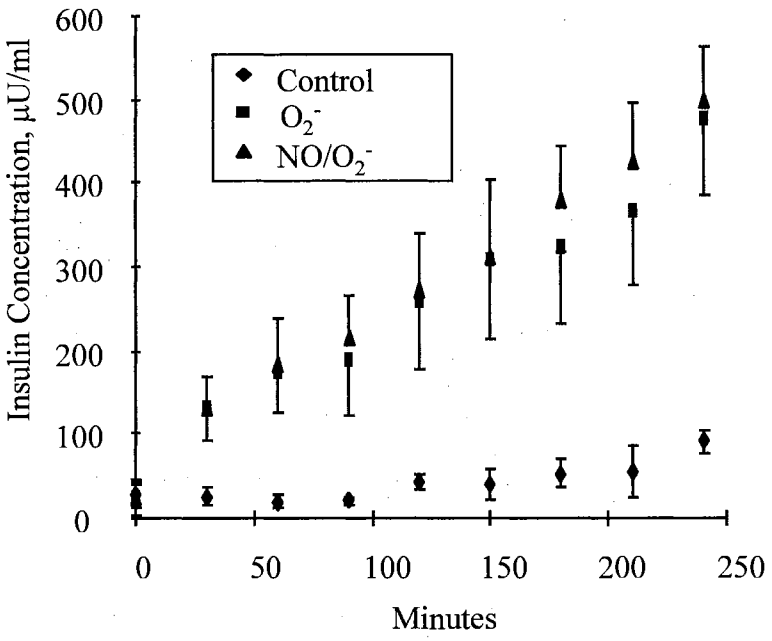

Figure 4.5. Insulin concentration following O_2^- and NO/O_2^- delivery, at 37 °C (n=5 culture dishes). NO/O_2^- delivery achieved $ONOO^-$ delivery at the concentration of 0.1 nM . The insulin secretion rates between 30 and 240 minutes are 1.5 ± 0.1 (R^2 = 0.96) and 1.7 ± 0.1 (R^2 = 0.99) μU ml^{-1} min^{-1} for the O_2^- and NO/O_2^- experiments, respectively. NO and O_2^- delivery rates were 0.96 and 0.4 μM/min, respectively. The control is in the absence of NO and O_2^- delivery. Experiments were randomized to eliminate experimental bias.

experiments, respectively. The insulin secretion rates are linear over the entire duration of the experiment. It is notable that there is no significant difference between the O_2^- experiments in the presence and absence of NO, again demonstrating that NO (predicted at 2.5 μM) does not appear to have an effect on the insulin secretion rate over 4 h.

Although the insulin secretion rates were similar for both sets of experiments, they were significantly higher than the control. Hence, experiments were performed to assess the discrepancy. Experiments showed that XOD and catalase together (in the absence of hypoxanthine and thus O_2^- generation) resulted in an insulin secretion rate of 1.4 ± 0.1 ($R^2 = 0.95$) μU ml^{-1} min^{-1}, similar to that of the O_2^- and NO/O_2^- experiments. Thus, XOD and catalase increase the insulin secretion rate compared to control, although the mechanism for the increased release rate has not been studied further. However, since the insulin secretion rate is similar in the presence and absence of O_2^- generation (with XOD and catalase present in both experiments), O_2^- (at 0.4 pM) and $ONOO^-$ (at 0.1 nM) do not appear to affect the insulin secretion rate over 4 h. The temporal LDH concentrations were low and similar to controls in all of the experiments (O_2^-, NO/O_2^-, and XOD+catalase) indicating that these compounds do not have any significant effect on the viability of the cells.

4.4 Conclusions

The present study indicates that NO at a concentration as high as 2.8 μM does not significantly affect the insulin secretion rate and viability of βTC3 cells for 24 h. Furthermore, O_2^- and $ONOO^-$ at concentrations as high as 0.25 μM and 0.1 nM, (see

Figure 4.5) respectively, do not significantly affect the function of βTC3 cells over 4 h. The concentrations of NO, O_2^- and $ONOO^-$ obtained in this study were obtained from model predictions involving no adjustable parameters. All of the transport and reaction (kinetic) parameters were obtained from independent experimental measurements or literature data. In addition, this study demonstrated a viable method for delivering controlled rates of NO and O_2^- to a cell system with the ability to predict the steady state concentrations of NO, O_2^-, and $ONOO^-$. The experimental system eliminated the potential inhomogeneity, concentration build up, and diffusional problems associated with delivering NO via NO-releasing compounds to tissue culture plates.

Although short term effects of NO, O_2^-, and $ONOO^-$ were evaluated, it cannot be excluded that prolonged exposure of NO, O_2^- and $ONOO^-$ at the studied concentrations may affect the insulin secretion rate and viability of βTC3 cells. For long term studies, serum should be added since glucose-induced insulin secretion of several pancreatic cell lines depends upon serum in long term studies (Sekine et al., 1997). At least for NO, the NO concentration in this study is similar to the reported *in vitro* NO concentration of 1.1 μM near the vicinity of macrophages (Chen et al., 1998). The possibility also exists that higher concentrations than those studied may affect the function of pancreatic cells *in vivo* due to absence of one of the main NO reactions with hemoglobin in tissues as compared to the blood.

Chapter 5. Cellular NO Delivery

5.1 Introduction

Immune cells (cells of the immune system), such as macrophages and lymphocytes, release cytokines and free radicals, including NO and O_2^-, which can also react to form products such as $ONOO^-$. Thus, cellular delivery of NO from generating cells to target cells can occur. In addition, cytokines released by immune cells can stimulate the generation of NO within many cells, such as pancreatic cells (Kaneto et al., 1995).

The infiltration of pancreatic cells by immune cells, such as macrophages and lymphocytes, has been attributed as an inciting cause leading to autoimmune destruction and the onset of IDDM (see Section 4.1). The impact of free radicals (NO, O_2^-, and $ONOO^-$) on β cells include change in insulin generation and secretion ability, DNA damage, and apoptosis/necrosis (Delaney et al., 1993; Hadjivassiliou et al., 1998; Kaneto et al., 1995; Mauricio and Mandrup-Poulsen, 1998). Studies have reported contradictory effects of free radicals on the function of pancreatic cells, such as lowered insulin secretion of human and rat islets in the presence of NO donors SIN-1 and GSNO (Eizirik et al., 1996), no effects on insulin secretion of RINm5f cells in the presence of SNAP (Green et al., 1994), and increased insulin secretion of RINm5f cells in the presence of SIN-1 (Green et al., 1994). Most of these studies did not report the concentrations of free radicals to which the pancreatic cells were exposed. However, as reported in Chapter 4, NO, O_2^-, and $ONOO^-$ at concentrations of 2.8 μM, 0.25 μM, and 0.1 nM, respectively, do

not affect the insulin secretion rates of βTC3 pancreatic cells attached to culture plates over short times.

The implantation of encapsulated pancreatic islets or beta cells (one type of bioartificial pancreas) in diabetic patients is a promising treatment for IDDM (Reach, 1993). Several important factors required for a successful implantation of encapsulated cells include the source (i.e. animal or human) of cells or islets, the type of encapsulation material, the design geometry and the location of the implantation. *In vivo*, encapsulated islets achieved temporary normoglycemia in both chemically induced and spontaneous diabetic rodents (O'Shea and Sun, 1986; Fan et al., 1990), dogs (Soon-Shiong et al., 1992) and monkeys (Sun et al., 1996). However, the efficacy of the implants varied from a few weeks to many months. Fibrotic growth and infiltration of immune cells were observed in some diabetic rats that had temporary resolution of their diabetes when treated with encapsulated islets (Fan et al., 1990).

Encapsulation, which is designed to prevent rejection of the pancreatic cells by impeding the transport of host immune cells and large immunological molecules to the pancreatic cells, typically prohibits the transport of molecules greater than ~60 kDa (Sambanis et al., 1994). Thus, important small molecules, such as glucose and insulin, transport rather freely. Although large immune-generated molecules are hindered from transporting through the encapsulation matrix, cytokines and free radicals are not transport hindered. Thus, cytokines and free radicals generated by activated immune cells may be contributing to the failure of implantation (Kaufman et al., 1990; Wiegand et al., 1993).

Unfortunately, information on the free radical profiles within an encapsulated cell matrix is lacking. Previous mathematical models of encapsulated cell matrices assessed oxygen, glucose, and/or insulin dynamics in both vascular and non-vascular pancreatic systems (Morvan and Jaffrin, 1989; Tziampazis and Sambanis, 1995). The models revealed the importance of several design parameters, including cell loading and matrix diameter. Models were used to assess diffusion and reaction of cellular NO in biological systems (Lancaster, 1994; Vaughn et al, 1998; Wood and Garthwaite, 1994), but cellular NO delivery models have not been applied to encapsulated cells systems. Chen et al. (1998) developed a model coupling reaction and diffusion of NO and O_2^- for a suspension of beads covered by a monolayer of macrophages. The model focused only on predicting concentrations in the fluid surrounding the beads, thus the concentration of free radicals inside the bead was not known.

In view of the potential effects of free radicals generated by immune cells on the failure of encapsulated pancreatic cell systems, a steady state mathematical model predicting free radical concentrations based on reaction and diffusion has been developed for an encapsulated pancreatic cell matrix. The model results provide quantitative concentration ranges for NO, O_2^-, and $ONOO^-$ which could be used for studies assessing NO and O_2^- effects on pancreatic cells or islets. In addition, the results provide important insights into the design of encapsulated pancreatic cell systems.

5.2 Mathematical Model

5.2.1 Model geometry and governing equations

The encapsulated pancreatic cell matrix is modeled as a sphere with radius R as shown in Figure 5.1. Pancreatic cells in the matrix are represented in the model by a homogeneously distributed O_2 consumption rate. A uniform distribution of macrophages at the surface (characterized as a thin layer compared to the matrix radius although shown enlarged for graphical reasons) provides a flux of NO and O_2^- into the matrix to represent the free radical contributions of immune cells (i.e. cellular delivery of NO) attached to the surface. In reality, NO and O_2^- released by immune cells can also transport into the bulk solution and macrophage coverage is not necessarily homogeneous over the surface (Wallgren et al., 1995). However, the model is useful to estimate the effects of various parameters (i.e. matrix diameter) on the free radical concentration profiles within the matrix.

The steady-state continuity equation for any species *i* within the sphere is,

$$\frac{D_i}{r^2}\frac{\partial}{\partial r}\left(r^2\frac{\partial C_i}{\partial r}\right)+R_i=0 \qquad (5.1)$$

where *r* is the radial distance from the center, C_i is the spatial concentration, and D_i is the diffusivity of species *i* within the matrix. The net rate of formation of species *i* (R_i) is the sum of the individual reaction rates for each reaction in which the species is involved.

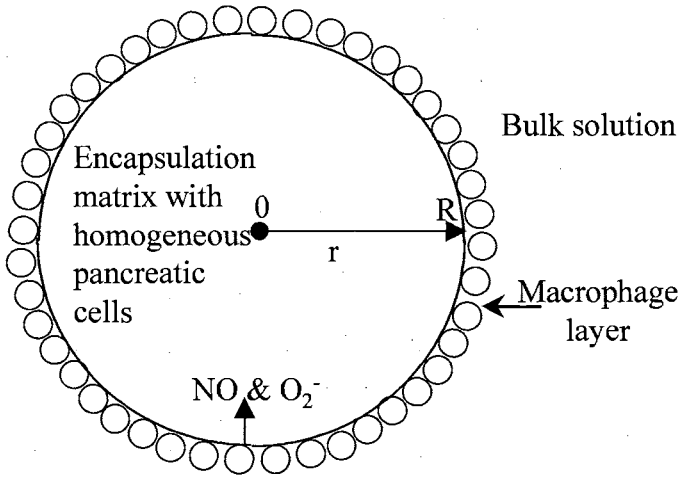

Figure 5.1. Model geometry. A layer of macrophages (shown enlarged, typical macrophage thickness ~10-20 μm) surrounds a spherical matrix of encapsulated pancreatic cells. The uniform layer of macrophages provides a flux of NO and O_2^- into the matrix. The matrix radius is R.

The net rate of formation for each species is described below. The four species of interest include NO, O_2^-, O_2, and total peroxynitrite (PER). PER is denoted as the sum of $ONOO^-$ and ONOOH since it is not known which of these two molecules affects pancreatic cells.

The major reactions in which these species are involved are,

$$2NO + O_2 \xrightarrow{k_2} 2NO_2 \tag{5.2}$$

$$NO_2 + NO \underset{k_{-3}}{\overset{k_3}{\rightleftarrows}} N_2O_3 \tag{5.3}$$

$$N_2O_3 + H_2O \xrightarrow{k_4} 2NO_2^- + 2H^+ \tag{5.4}$$

$$NO + O_2^- \xrightarrow{k_5} ONOO^- \rightleftarrows ONOOH \tag{5.5}$$

$$ONOOH \xrightarrow{k_6} NO_3^- + H^+ \tag{5.6}$$

$$ONOOH \xrightarrow{k_7} NO_2^- + \frac{1}{2}O_2 + H^+ \tag{5.7}$$

$$ONOO^-(ONOOH) + NO \xrightarrow{k_8} NO_2 + NO_2^- \tag{5.8}$$

$$HO_2 + O_2^- + H_2O \xrightarrow{k_9} O_2 + H_2O_2 + OH^- \tag{5.9}$$

$$ONOO^- + CO_2 + H_2O \xrightarrow{k_{10}} NO_3^- + CO_3^{2-} + 2H^+ \tag{5.10}$$

where k_i is the rate constant for reaction i. The oxidation of NO in the presence of O_2 is represented by Equations 5.2-5.4 with the rate of oxidation controlled by Equation 5.2 (Lewis et al., 1994). Nitrous anhydride (N_2O_3) is an intermediate product of NO oxidation yielding NO_2^- as a final product. However, in the presence of O_2^-, NO also

reacts with O_2^- to form $ONOO^-$ (Huie and Padmaja, 1993) as shown in Equation 5.5. ONOOH is assumed to be in rapid equilibrium with the unprotonated form $ONOO^-$. Equation 5.6-5.7 represents the decomposition of ONOOH to form NO_2^- and NO_3^- (Koppenol et al., 1992; Pfeiffer et al., 1997). Nitrite formation can also occur via Equation 5.8 with NO reacting with $ONOO^-$ or ONOOH (Pfeiffer et al., 1997). The degradation of O_2^- to hydrogen peroxide (H_2O_2) is represented by Equation 5.9 (Winterbourn et al., 1994) and CO_2 catalyzed conversion of $ONOO^-$ to NO_3^- is shown in Equation 5.10 (Uppu et al., 1996).

Assuming the pseudo-steady state nature of NO_2 and N_2O_3 and rapid equilibrium for $ONOO^-$/ONOOH and O_2^-/HO_2, the net rates of formation at pH 7.4 for NO, O_2^-, PER, and O_2 are:

$$R_{NO} = -4k_2 C_{NO}^2 C_{O_2} - 3k_8 C_{NO} C_{PER} - k_7 C_{ONOOH} \tag{5.11}$$

$$R_{O_2^-} = -k_5 C_{NO} C_{O_2^-} - k_9 C_{HO_2} C_{O_2^-} \tag{5.12}$$

$$\begin{aligned} R_{PER} = \; & k_5 C_{NO} C_{O_2^-} - (k_6 + k_7) C_{ONOOH} \\ & - k_8 C_{NO} C_{PER} - k_{10} C_{ONOO^-} C_{CO_2} \end{aligned} \tag{5.13}$$

$$R_{O_2} = -4k_2 C_{NO}^2 C_{O_2} - v \tag{5.14}$$

where $(C_{PER}/C_{ONOO^-}) = 1.22$, $(C_{ONOOH}/C_{ONOO^-}) = 0.22$, and $(C_{HO_2}/C_{O_2^-}) = 0.0025$ (Chen et al., 1998; Kavdia et al., 2000).

In addition to the reaction of O_2 with NO, the cellular uptake of O_2 by pancreatic cells is represented as v. Inclusion of v is important in view of hypoxic conditions that

can occur within the encapsulated matrix. Monod's model for ν, which depends on the dissolved O_2 concentration (C_{O_2}), is

$$\nu = \frac{\nu_{\max} C_{O_2}}{k_m + C_{O_2}} \tag{5.15}$$

where k_m and ν_{max} are the half-maximum oxygen uptake concentration and the maximum cellular oxygen uptake rate, respectively.

5.2.2 Boundary conditions

Since Equation 5.1 is a second order differential equation, two boundary conditions are required for each species; one at the surface and the other at the center of the matrix. At the surface, the boundary conditions for NO and O_2^- are

$$\frac{dC_i}{dr}\Big|_{r=R} = \frac{N_i}{D_i}, \qquad i=NO \text{ and } O_2^- \tag{5.16}$$

where N_i is the molar flux of species *i*. The surface boundary condition for PER is based on the generation of $ONOO^-$ from NO and O_2^- and is represented by equating the rate of $ONOO^-$ formation at the surface with the PER flux at the surface according to

$$\frac{dC_{PER}}{dr}\Big|_{r=R} = \frac{hk_5}{D_{PER}} C_{NO,S} C_{O_2^-,S} \tag{5.17}$$

where $C_{NO,S}$ and $C_{O_2^-,S}$ are the concentrations of NO and O_2^- at the surface, respectively, and h is the length of a single grid in which the entire radius is divided to solve Equation 5.1 (see Section 5.2.4). For O_2, the bulk concentration of O_2 ($C_{O_2,bulk}$) is the surface boundary condition. Due to the symmetry of the matrix, the boundary condition at the center for all species is

$$\frac{dC_i}{dr}\Big|_{r=0} = 0 \qquad i=NO,\ O_2^-,\ PER \text{ and } O_2 \tag{5.18}$$

5.2.3 Model parameters

All fixed model parameters are shown in Table 5.1. The diffusivity of each species in alginate is used in the model since alginate is a commonly used encapsulation matrix. The ratio of the effective diffusivity in the alginate to the diffusivity in water does not depend on the molecular size (Crank, 1975; Westrin and Axelsson, 1991). Therefore, based on the average ratio of glucose and insulin diffusivities in alginate as compared to water (44 and 48 %, respectively, see Tziampazis and Sambanis, 1995), the species diffusivity in the alginate is assumed to be 46 % of the reported diffusivity in water at 37 °C for NO, O_2^-, PER, and O_2 (Chen et al., 1998; Tziampazis and Sambanis, 1995).

The half maximum oxygen uptake concentration (k_m) is assumed to be 0.01 mM as the oxygen uptake rate does not depend on the dissolved O_2 concentration as low as 0.015

TABLE 5.1

Fixed parameters at 37°C and pH 7.4

Constant	Value	Reference
k_2	2.4×10^6 $M^{-2}s^{-1}$	Lewis and Deen (1994)
k_5	6.7×10^9 $M^{-1}s^{-1}$	Huie and Padmaja (1993)
k_6	3.1 s^{-1}	Chen et al. (1998)
k_7	1.4 s^{-1}	Chen et al. (1998)
k_8	9.1×10^4 $M^{-1}s^{-1}$	Pfeiffer et al. (1997)
k_9	8.0×10^7 $M^{-1}s^{-1}$	Imlay and Fridovich (1991)
k_{10}	5.8×10^4 $M^{-1}s^{-1}$	Radi, R (1998)
D_{NO}	2.3×10^{-5} cm^2/s	Chen et al. (1998)
$D_{O_2^-}$	1.3×10^{-5} cm^2/s	Chen et al. (1998)
D_{PER}	1.2×10^{-5} cm^2/s	Chen et al. (1998)
D_{O_2}	1.4×10^{-5} cm^2/s	Tziampazis & Sambanis (1995)
k_m	0.01 mM	Refer to text
ν_{max}	1.1 μM/s	Refer to text

mM (Miller et al., 1987). The maximum cellular O_2 uptake rate (v_{max}) of 1.1 μM/s is calculated based on the cellular O_2 consumption data for a typical cell density of 3.3 x 10^7 cells/ml in alginate and a maximum cellular O_2 uptake rate of 2.0 μmol/10^9 cells/min (Wohlpart et al., 1990).

The adjustable parameters (with base-case values shown) are presented in Table 5.2. The base-case radius is 250 μm based on the average values of 200-300 μm utilized for encapsulated islets restoring normoglycemia (Krestow et al., 1991). The base-case values of the NO and O_2^- fluxes are obtained from experimental data for activated macrophages (Lewis et al., 1995). The flux of NO is 3.1 x 10^{-8} mol/s/m^2 based on a release rate of 6.0 pmol/s/10^6 cells, viable cell count of 0.83 x 10^6 cells/ml, number of beads of 1.43 x 10^3 beads/ml, and bead radius of 95 μm. The O_2^- flux is assumed to be half of the NO flux (Lewis et al., 1995).

A typical arterial dissolved oxygen concentration of 100 μM is used as the base-case bulk O_2 concentration ($C_{O_2,bulk}$) (Tziampazis and Sambanis, 1995). A uniform CO_2 concentration of 1.14 mM in the matrix is assumed based on the CO_2 solubility of 3.01 x 10^{-5} M/mmHg and a CO_2 partial pressure of 38 mm Hg in blood plasma.

5.2.4 Numerical solution

The system of second-order differential equations was transformed to a system of first-order differential equations. This system of first-order differential equations was solved using a relaxation method by converting to finite-difference equations (Press et al.,

TABLE 5.2

Adjustable parameters

Parameter	Base-case Value	Reference
R	250 μm	Refer to text
N_{NO} at r=R	3.1×10^{-8} mol s^{-1} m^{-2}	Lewis et al. (1995)
$N_{O_2^-}$ at r=R	1.5×10^{-8} mol s^{-1} m^{-2}	Lewis et al. (1995)
O_2^-/NO flux ratio	0.5	Lewis et al. (1995)
$C_{O_2,bulk}$	100 μM	Tziampazis & Sambanis (1995)
C_{CO_2} in matrix	1.14 mM	Davenport (1974)

1986). The radius of the bead was divided into 5000 equal grids for the numerical analysis. The high number of the grids was necessitated by the very fast reaction of O_2^- with NO. The model was initialized by assuming the surface concentrations of NO and O_2^- as zero, which resulted in a zero flux of PER at the surface. The calculated surface concentrations of NO and O_2^- were then used for subsequent iterations to quantify the PER flux at the surface (see Equation 5.17). The iterations were repeated until the PER flux at the surface did not change significantly.

5.3 Results

5.3.1 Base-case

In order to predict the concentration profiles of free radicals inside the matrix, a base-case was simulated. As shown in Table 5.2, the parameter values for the base-case are: R=250 μm, N_{NO}=3.1 x 10^{-8} mol/s/m^2, $N_{O_2^-}$=1.5 x 10^{-8} mol/s/m^2, $C_{O_2,bulk}$=100 μM, and C_{CO_2} (throughout the matrix)=1.14 mM. The computed concentration profiles of NO, PER, and O_2 are shown for the base-case (case #1) in Figures 5.2-5.4, respectively. For all figures, the concentrations are normalized with the respective surface concentrations. The maximum concentrations of NO, PER and O_2 were at the surface and are 13.5, 0.125, and 100 μM, respectively, as shown in Table 5.3. In addition, the fraction of outer radius to the total radius (f_r=1-(r/R)) in which PER ≥ 0.1 nM is shown in Table 5.3. The significance of 0.1 nM is that quantitative studies of PER between 0.1 nM

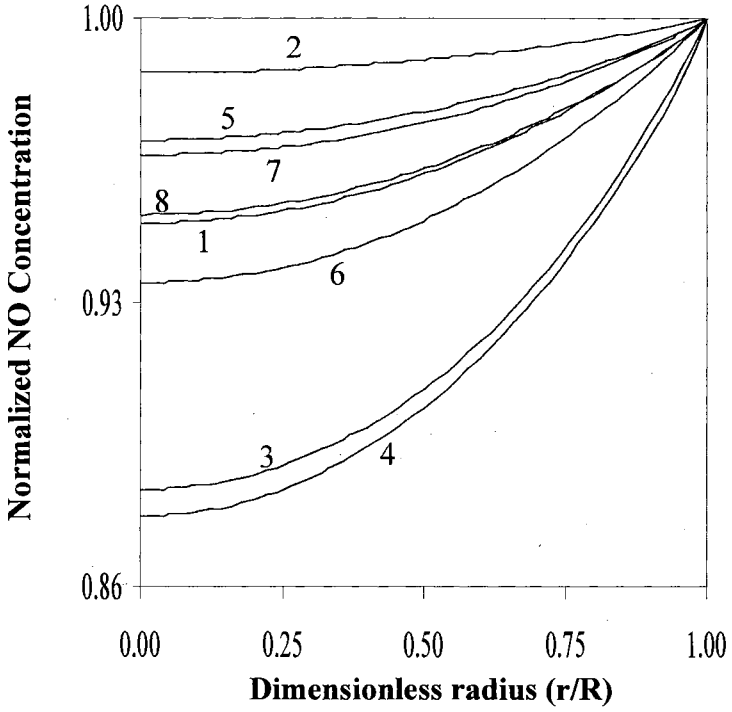

Figure 5.2. Normalized NO concentration profiles. The normalized NO concentrations are the NO concentrations divided by the surface concentrations of NO (see Table 5.3). Numbers correspond to the individual cases shown in Table 5.3 on page 87. The center of the matrix is r/R=0 and the surface of the matrix is r/R= 1.

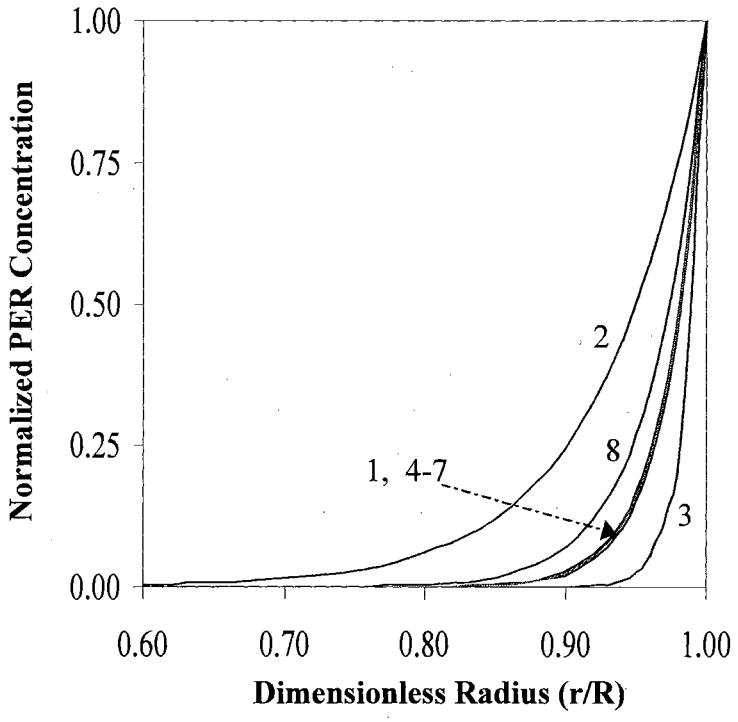

Figure 5.3. Normalized PER concentration profiles. The normalized PER concentrations are the PER concentrations divided by the surface concentrations of PER (see Table 5.3). Numbers correspond to the individual cases shown in Table 5.3 on page 87. The center of the matrix is r/R=0 and the surface of the matrix is r/R= 1.

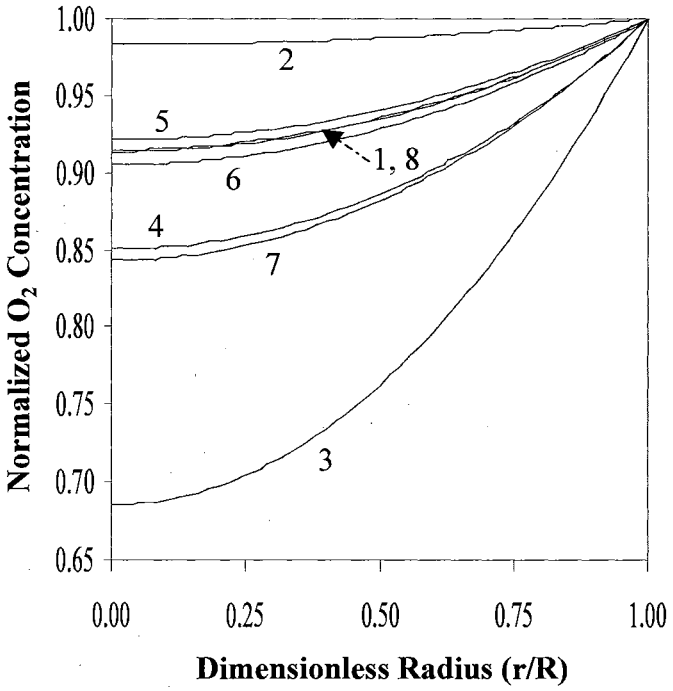

Figure 5.4. Normalized O_2 concentration profiles. The normalized O_2 concentrations are the O_2 concentrations divided by the surface concentrations of O_2 (see Table 5.3). Numbers correspond to the individual cases shown in Table 5.3 on page 87. The center of the matrix is r/R=0 and the surface of the matrix is r/R= 1.

TABLE 5.3

Surface concentrations of species

Case	Variable Parameter	C_{NO}, μM	C_{PER}, μM	$C_{O_2^-}$, nM	$f_r^{\#}$
1	Base-case*	13.5	0.125	1.44	0.196
2	R=100 μm	20.3	0.109	1.17	0.510
3	R=500 μm	10.4	0.151	1.64	0.100
4	NO flux=10x	37.3	1.440	8.64	0.250
5	O_2^-/NO flux ratio=0.8	7.69	0.186	3.05	0.208
6	O_2^-/NO flux ratio=0.2	18.0	0.052	0.50	0.172
7	$C_{O_2,bulk}$=50 μM	18.6	0.130	1.22	0.196
8	C_{CO_2}=0.57 mM	12.7	0.170	1.48	0.280

* Base-case parameter values are given in Table 5.2.

Fraction of outer radius relative to total radius (f_r=1-(r/R)) in which PER ≥ 0.1 nM.

and 200 μM to assess the effects of PER on pancreatic cells have not been reported. The PER concentration of 0.1 nM is reported to have no effects on pancreatic cell function for short times (see Chapter 4 or Kavdia et al., 2000) and concentrations above 200 μM are reported to cause DNA damage to pancreatic cells (Delaney et al., 1996).

While the NO concentration slightly decreased throughout the matrix, the PER concentration dropped rapidly becoming less than 0.1 nM at $r/R \leq 0.80$. The O_2 concentration differed by 8.7 % between the surface and the center. The primary consumption of O_2 was due to cellular uptake and not from the reaction with NO. This is confirmed since the O_2 concentration profile agreed with the O_2 profile calculated by Tziampazis and Sambanis (1995). Because of the diffusion controlled reaction of O_2^- with NO, the concentration of O_2^- rapidly decreased within 2 μm from the surface.

In order to estimate the effects of various parameters on the concentration profiles of the free radicals inside the matrix, all the subsequent results are compared to the base-case. Table 5.3 shows the adjusted parameters and the resulting surface concentrations predicted from the model for NO, PER, and O_2^-. For all simulations, the O_2^- dimensionless concentration profiles were similar with only a variation in the surface concentration.

5.3.2 Effect of matrix radius

One of the important design considerations for encapsulated cells due to the O_2 requirement by the pancreatic cells and the limited volume for implantation is the radius. The effects of size on the free radical profiles are shown for a 100 μm (case #2) and a 500

μm (case #3) radius matrix in Figures 5.2-5.4, for NO, PER and O_2, respectively. For the 100 μm radius matrix, the normalized NO concentration profile differed from the base-case with a higher NO concentration (see Table 5.3) throughout the matrix as shown in Figure 5.2. In addition, the PER concentration decreased slowly into the bead as shown in Figure 5.3. However, the maximum PER concentration was 0.109 μM at the surface, which was lower than the base-case. The PER concentration was less than 0.1 nM at r/R $\leq$ 0.49 (f_r=0.51, Table 5.3). As expected, the O_2 concentration (98.3 μM at the center) did not change much due to the small matrix volume.

For the 500 μm radius matrix, the normalized NO, PER, and O_2 concentration profiles were more steep as compared to the base-case (see Figures 5.2-5.4) due to greater diffusion distances. However, while the NO concentration (see Table 5.3) was lower throughout the matrix, the maximum PER concentration (0.151 μM) was higher at the surface of the matrix, as compared to the base-case. The PER concentration was less than 0.1 nM at r/R $\leq$ 0.90 (f_r=0.10, Table 5.3). The O_2 concentration of 68.6 μM at the matrix center was lower than the base-case due to the larger matrix volume.

5.3.3 Effect of NO flux

The release rate of NO by macrophages depends on the type and concentration of cytokines to which the macrophages are stimulated (Steuher and Marletta, 1987). In addition, multiple layers of macrophages can possibly form at sites of immunological action. One of the effects of these circumstances would be the increase in the NO and O_2^-

fluxes. Therefore, the increased NO flux was simulated by increasing the fluxes of NO and O_2^- to ten times the base-case. As reported in Table 5.3, the surface concentration of NO increased by three times to 37.3 μM (case #4). The PER and O_2^- surface concentrations also increased by 11.5x and 6x, respectively. The normalized NO concentration profile (case #4) was steep as compared to the base-case as shown in Figure 5.2 as a result of the increased reaction of NO with O_2^-. However, the normalized PER concentration profile (case #4) was similar to the base-case as shown in Figure 5.3. The PER concentration was less than 0.1 nM at $r/R \leq 0.75$ (f_r=0.25, Table 5.3). The normalized O_2 concentration profile was slightly different from the base-case (case #4, Figure 5.4) because of a higher O_2 consumption from reaction with NO. The O_2 concentration at the center of the matrix decreased by 15.0 % relative to the surface concentration as compared to 8.7 % for the base-case.

5.3.4 Effect of O_2^-/NO release ratio

The macrophage release ratio of O_2^- to NO depends on the level of L-arginine, dissolved oxygen, and oxidative burst (Chen et al., 1998). The base-case ratio of 0.5 was based on the experimental data provided by Lewis et al. (1995). For the simulation, the effect of the O_2^- to NO flux ratio on the free radical profiles was evaluated and are shown in Figures 5.2-5.4. Because of the very fast reaction of NO with O_2^-, the higher ratio (case #5), which increased the surface O_2^- concentration, favored the formation of PER and lowered the overall concentration of NO. Lowering the ratio (case #6) decreased the available O_2^- for reaction, thus, decreased the surface PER concentration but increased

the surface NO concentration, as reported in Table 5.3. As compared to the base-case, the normalized NO concentration profile did not decrease as much for case #5 due to less NO available for the O_2 reaction. However, the profile decreased more for case #6 due to a higher NO concentration that reacts with O_2. The change in ratio had negligible effect on the PER and O_2 normalized concentration profiles in the matrix as compared to the base-case (see #5 and #6 in Figures 3 and 4).

5.3.5 Effect of CO_2 and O_2 concentration

The surface O_2 concentration for the base-case was based on the typical average arterial dissolved O_2 concentration of 100 μM (Tziampazis and Sambanis, 1995). However, encapsulated cells are often placed in the interstitial region, where the dissolved O_2 concentration is even lower than 50 μM because of the low blood circulation (Tziampazis and Sambanis, 1995). Thus, the effects of lower dissolved O_2 concentration on free radical profiles were also assessed. The normalized PER concentration profile and surface concentration (case #7, Figure 5.3) were similar to the base-case. The surface NO concentration increased by 37 % as shown in Table 5.3 and the NO profile did not drop as rapidly (case #7, Figure 5.2) as compared to the base-case. These trends are a result of the decreased reaction of NO with O_2 due to the lower O_2 concentration. However, the increased NO concentration reduced the O_2^- surface concentration by 15 % due to the increase reaction of NO with O_2^-. The normalized O_2 concentration profile (case #7, Figure 5.4) decreased more rapidly due to the higher decomposition rate, as shown in Figure 5.4. The concentration of O_2 at the center of the

bead was reduced to 84 % of the surface concentration as compared to 91 % for the base-case.

In addition to the study of a lower surface O_2 concentration, a lower surface CO_2 concentration was studied for the same reason of lower diffusional rates in the interstitial spaces. For this purpose, the surface CO_2 concentration was decreased to half the value of the CO_2 concentration of 1.14 mM in blood plasma. The NO and O_2 normalized concentration profiles and surface concentrations (case #8) were similar to the base-case, as shown in Figures 5.2 and 5.3, respectively, and Table 5.3. However, the surface concentration of PER increased by 36 % since the primary decomposition of PER occurs through its reaction with CO_2 and less CO_2 was available for reaction.

5.4 Discussion

Based on the cellular delivery of free radicals including NO, O_2^-, and $ONOO^-$, the free radicals spatial profiles in an encapsulated pancreatic cell matrix for several adjustable parameters are presented in this chapter. The immune response is one possible cause of the dysfunction of implanted islets and cells since macrophages in the vicinity of many failed encapsulated cell matrices have been observed (O'Shea and Sun 1986; Wiegand et al. 1993). Activated macrophages and other immunological cells release many species including NO, O_2^-, and/or cytokines (Lewis et al., 1995) which can diffuse through an encapsulation matrix.

The effects of NO on pancreatic islets or cells have been studied with both chemical and physical delivery via NO donor compounds and diffusion of gaseous NO,

respectively (Cunningham et al., 1994; Eizirik et al., 1996; Kavdia et al., 2000). Cunningham et al. (1994) reported that rat islets of Langerhans had a significantly lower insulin secretion rate after 30 min exposure to NO donor compounds, such as SIN-1 (3-morpholinosydnonimine), SNAP (S-nitroso-N-penicillamine), or GSNO (S-nitrosoglutathione) at concentrations of 100, 500, and 300 μM, respectively. For acute exposure to the NO donor compounds, human pancreatic islets are less sensitive than rat pancreatic islets to SIN-1, sodium nitroprusside, GSNO and other NO donor compounds. However, differences in long-term effects of NO donors have not been observed (Eizirik et al., 1996).

All of the mentioned studies have reported extracellular NO_2^- and NO_3^- temporal concentrations instead of NO concentration values to which islets were exposed. Therefore, using the reported NO_2^- concentration values, an approximate NO concentration range for the previously mentioned studies was obtained from the NO reaction O_2 assuming all of the delivered NO was converted to NO_2^-. Since the NO_2^- formation rate is $R_{NO_2^-} = 4k_2 C_{NO}^2 C_{O_2}$, and reported $R_{NO_2^-}$ values ranged between 0.5-11 μM/min, the estimated NO exposure levels are 2-10 μM for C_{O_2}=210 μM (saturated value at 37 °C) and k_2=2.4 x 10^6 $M^{-2}s^{-1}$ (Kavdia et al., 2000). However, this range of NO concentrations is approximate because of the different release mechanisms, varying NO release rates, and generation of other species, such as O_2^-, by some NO donor compounds. In addition, the solutions were not always stirred and non-steady state NO concentrations would occur. Using the constant physical delivery of gaseous NO and constant O_2^- generation by hypoxanthine/xanthine oxidase, we reported in Chapter 4 that the NO, O_2^- and PER concentrations of 2.8 μM, 0.25 μM, and 0.1 nM, respectively, had

no effect on the insulin secretion rates of pancreatic βTC3 cells for short times. Numerous other studies with conflicting opinions (see Section 5.1) have been reported in the literature, the possibility of NO concentrations as high as 10-40 μM as modeled in this study necessitates the need for further studies assessing the effects of NO on pancreatic cell function.

Wiegand et al. (1993) reported that a small number of activated macrophages (30,000-60,000) in suspension can destroy alginate encapsulated rat islets. Furthermore, coencapsulation with autologous erythrocytes (NO antagonist) eliminated the effect of macrophages on the lysis of islets. Our model predictions demonstrate that a small number of macrophages attached to the surface (2,500-10,000 for the base-case and assumed macrophage radius of 5-10 μm) results in NO and PER concentrations that may be damaging to encapsulated islets or cells. Obviously, experimental studies are necessary to assess the higher predicted free radical concentration effects on pancreatic cell function.

In vitro, $ONOO^-$ is implicated in human and rat pancreatic islet cell dysfunction and death at concentrations of 0.2 mM and higher (Delaney et al., 1996). However, *in vivo* a very large number of activated macrophages and other immunological cells would be required to produce such a high concentration of $ONOO^-$. In addition, superoxide dismutase (SOD) has a very high activity in human islets and will scavenge O_2^-, thus preventing formation of $ONOO^-$ within cells (Welsh et al., 1995). In this study, we predicted some pancreatic cells (especially near the surface of matrix) could be exposed to PER concentrations as high as 0.1-1.5 μM. Therefore, a more realistic exposure

concentration of $ONOO^-$ for *in vitro* experimental studies is of the order of μM and not mM range.

In addition to information about the concentration of free radicals, knowledge of diffusion distance of the free radicals in the encapsulated cell matrix is very useful for design of a matrix. As shown in the Figures 5.2-5.4, the concentration profiles of the free radicals and O_2 are affected most by matrix radius. At steady state, the spatial concentration of NO was generally constant over the entire matrix, thus raising the possibility of incorporating NO scavengers in the matrix formulation if NO is found to affect the pancreatic cell function. Although PER rapidly decomposed, the diffusion distance at which PER was greater than 0.1 nM (see Table 5.3) was significant, in some instances up to 51 % of the radius. Thus, the matrix radius may not only be important for O_2 considerations but also for PER exposure. We reported in Chapter 4 that insulin secretion rate of βTC3 cells is not affected by 0.1 nM PER. If concentrations of PER higher than 0.1 nM affect pancreatic cells over short or long time, the fractional volume of an encapsulated pancreatic matrix potentially affected is 0.88, 0.49, and 0.27 for 100, 250, and 500 μm radius, respectively (based on the outer radius from Table 5.3). The PER exposure has a serious implication on the size of a viable encapsulated pancreatic matrix since more pancreatic cells in a small radius matrix could be potentially damaged (fractional volume affected is 0.88 for 100 μm radius matrix). On the contrary, a larger matrix (radius > 800 μm) deprives the matrix center of O_2. The islets, which are usually found in the periphery of implanted beads (De Vos et al., 1999), would be susceptible to PER exposure for all radius matrix. However, further experimental studies are necessary

to determine if a PER concentration greater than 0.1 nM is damaging to pancreatic cell function.

Another salient feature of the presented model is the O_2^- concentration profile, which diminishes to zero within 2 μm of the matrix surface due to the high reactivity of O_2^- with NO. Thus, direct O_2^- effects on pancreatic cell function seem unlikely. However, the small changes in surface O_2^- concentration affects the surface NO and PER concentration significantly (see Table 5.3).

Finally, the presented model assumes a single layer of macrophages surrounding the implantation. The model was used to estimate free radical concentrations within the matrix. However, the infiltration by macrophages and fibroblasts on transplanted encapsulated cell systems varies markedly *in vivo* in terms of number, types, and spatial distribution (Wallgren et al., 1995). Nevertheless, the results here in presented demonstrate that the potential exists for free radical damage and also demonstrates that some exposure studies may be insufficient as regards to concentrations for assessing free radical effects on pancreatic cell function. Also, care must be taken in assuming that encapsulated cell systems are completely protected from immunological action, since potential for NO and PER exposure to the cells in a matrix exists.

5.5 Conclusions

The model presented in this chapter is a simplified model for the simulation of an immune response on an encapsulated pancreatic cell matrix. The model helps in assessing the validity of results obtained in experiments assessing the effects of NO and

other free radicals on pancreatic cell function from a possible *in vivo* viewpoint. In addition, the model provides a quantitative analysis of the matrix radius and other parameter effects on free radical profiles within the matrix. The importance of the matrix radius on free radical profiles, especially PER, is established.

Chapter 6. Cellular NO Delivery: An Extended Model

6.1 Introduction

There is a need to evaluate cellular NO delivery effects on biological systems *in vitro* because of the difference in the exposure concentrations of free radicals between the existing studies and for an *in vivo* situation (see Section 5.4). The concentrations of NO during *in vitro* experiments should be quantified to establish whether the concentrations are physiological or pharmacological. Laurent et al. (1996) modeled the spatial and temporal NO concentrations in a petri dish or micro-well containing NO-generating cells attached to the bottom. The model was a simplified representation of a possible *in vitro* study as it considered only NO diffusion and autoxidation. Recently, Chen et al. (1998) modeled an experimental system of macrophages attached to microcarrier beads suspended in a stirred system. The reaction-diffusion model incorporated a wide range of NO reactions in biological systems, thus the model was more comprehensive than that reported by Laurent et al. (1996). The model of Chen et al. (1998) predicted NO and other related species concentrations in the fluid surrounding but not inside the beads.

This chapter describes a model for an *in vitro* experimental system of encapsulated cells in a stirred suspension which are exposed to cellular NO delivery via macrophages attached to the encapsulation surface. The model is an extension of the model described in Chapter 5 and incorporates the analysis for the fluid surrounding the matrix as described by Chen et al. (1998). The model predicts NO and other related product

concentration profiles in the encapsulated matrix and in the surrounding fluid for a future *in vitro* experimental study involving encapsulated pancreatic cells. The validation of the model will be performed by comparing bulk fluid model predictions with experimental data, although this is beyond the scope of the thesis objectives.

6.2 Model development

6.2.1 Modeled system

Insulin-secreting cells are normally encapsulated within a semipermeable matrix to act as a bioartificial pancreas. One of the possible *in vitro* experimental scenarios to study the function of a bioartificial pancreas is a suspension of these encapsulated cells in a well-stirred system. To study the effect of immune attack on the encapsulated cells, macrophages can be attached to surface of the encapsulated matrix. A well-stirred system containing 250 μm radius microencapsulated pancreatic cells in suspension is modeled to predict matrix and surrounding fluid concentrations of free radicals (NO, O_2^-, and PER) and O_2. The insulin-secreting cells in the encapsulated matrix are represented in the model by a homogeneous O_2 consumption rate. Macrophages, attached to the outer surface of the matrix, are represented in the model by a constant NO and O_2^- flux at the surface. As shown in Figure 6.1, the complete system is divided into three regions: the matrix region of radius R, which contains the insulin-secreting cells; the stagnant-film

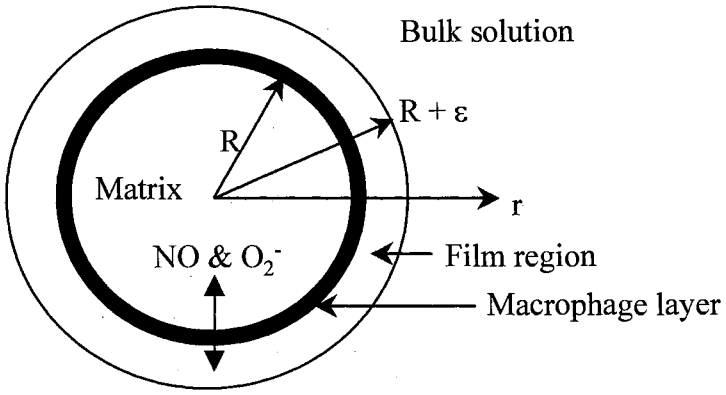

Figure 6.1. Model geometry. A single matrix of radius R=250 μm and its surrounding film region of thickness ε=58 μm are shown. The matrix contains homogeneously distributed pancreatic cells. At the matrix-film interface, macrophages produce NO and O_2^-; a fraction of total NO and O_2^- generated by macrophages is assumed to diffuse into the matrix and the remaining portion is assumed to diffuse into the stagnant-film region.

region of thickness ε, which represents the boundary layer surrounding the matrix; and the bulk solution region, which is a well-mixed region. A fraction of total NO and O_2^- generated by attached macrophages is assumed to diffuse into the matrix and the remaining portion is assumed to diffuse into the stagnant-film region.

6.2.2 Model assumptions

The following assumptions and approximations are made for the simulation of the model:

- Insulin-secreting cells are distributed homogeneously in the matrix.
- Concentrations of free radicals and O_2 are dependent only on the radial position.
- The diffusivity of all species in the bulk and film regions is the same as the diffusivity in water at 37 °C and for the matrix region it is 46 % of the diffusivity in water at 37 °C (see Section 5.2.2).
- Insulin and other macromolecules will not affect the spatial concentrations of species of interest. Hence, the transport and reaction of insulin and other macromolecules is not considered.
- The typical thickness of a macrophage is 5-10 μm, which is relatively thin compared to the matrix and film regions. Therefore, for all numerical purposes, the macrophage layer is ignored.

- NO and O_2^- reacts to form $ONOO^-$, which is in rapid equilibrium with its protonated form of peroxynitrous acid (ONOOH). The sum of $ONOO^-$ and ONOOH is represented as total peroxynitrite (PER).
- The O_2 concentration is assumed constant in the film and is the saturated value of 185.0 μM at 37 °C (Schmidt et al., 1997).

6.2.3 Model equations

The main species of interest are NO, O_2^-, PER, and O_2 for the matrix region, and are NO, O_2^-, and PER for the film and the bulk regions. The conservation equation for the species of interest is a balance between diffusion and reaction. For the matrix and the film region, the steady-state conservation equation is written as

$$\frac{D_i}{r^2}\frac{\partial}{\partial r}\left(r^2\frac{\partial C_i}{\partial r}\right)+R_i=0 \qquad (6.1)$$

where C_i is the spatial concentration and D_i is the diffusion coefficient for each species *i*. The radial position is represented by r. The net formation rate of species *i* (R_i) is the sum of the individual reaction rates for each reaction in which the species is involved. The major reactions in which the species are involved are given in Section 5.2.1. The net rates of formation for NO, O_2^-, PER, and O_2 are given by Equations 5.11-5.14, respectively.

For the bulk region, the balance equations for the main species consists of the mass transfer from the stagnant-film region, formation by reaction in the bulk, and physical losses (significant only for NO) from the system. Therefore, the pseudo steady state conservation equation for species *i* is

$$-4\pi\rho(R+\varepsilon)^2 D_i \frac{dC_i}{dr}\Big|_{r=R+\varepsilon} + R_{i,bs} - L_{i,bs} = 0 \tag{6.2}$$

where R is the bead radius, ρ is the bead density (# of the beads/volume of bulk solution), ε is the thickness of the stagnant-film region, and $R_{i,bs}$ is the net rate of formation of species *i* in bulk solution. L_i represents the removal rate of species i from the system.

6.2.4 Boundary conditions

For the matrix region, the boundary conditions for NO, O_2^-, PER, and O_2, due to symmetry at the center of the matrix and continuity at the surface of the matrix, are

$$\frac{dC_i}{dr}\Big|_{r=0} = 0 \tag{6.3}$$

$$C_i\Big|_{r=R,bead} = C_i\Big|_{r=R,film} \tag{6.4}$$

For the film region, the NO and O_2^- surface boundary conditions (at r=R), based on the total flux of NO and O_2^- (N_i) generated from the attached macrophages, are

$$\frac{dC_i}{dr}\Big|_{r=R} = \frac{fN_i}{D_i} \qquad i=NO \text{ and } O_2^- \qquad (6.5)$$

where f is the fraction of total NO and O_2^- flux (N_i) entering the film region. The surface boundary condition for PER is based on the generation of $ONOO^-$ from NO and O_2^- and is represented by equating the rate of $ONOO^-$ formation at the surface as

$$\frac{dC_{PER}}{dr}\Big|_{r=R} = \frac{h}{D_{PER}} k_5 C_{NO,r=R} C_{O_2^-,r=R} \qquad (6.6)$$

where h is the height of a single grid. The other boundary condition for the film is that the concentration at the film-bulk interface is equal such that

$$C_i\Big|_{r=R+\varepsilon} = C_{i,bulk} \qquad i=NO,\ O_2^-,\ and\ PER \qquad (6.7)$$

6.2.5 Numerical solution

The system of second order differential equations for the matrix and film region was transformed to a system of ordinary differential equations, which was then solved using a finite-difference method (Press et al., 1972). The system of non-algebraic equations for the bulk solution was solved using a globally convergent iteration scheme (Press et al., 1972). Main program and subroutines used for simulation are presented in Appendix 3.

The complete system of equations was solved by initially guessing the bulk concentration ($C_{i,bs}$) of species and specifying the total NO flux (N_i) at the matrix-film interface. The fraction (f) of the total NO flux, which entered the film region was also assumed. The O_2^- flux into the film region was considered to be half of the NO flux into the film region as reported by Lewis et al. (1995) and the PER flux was assumed zero. Using the fluxes at the film-matrix interface and the assumed bulk concentrations, the film region equations (Equation 6.1) were solved to obtain the species concentrations at the film-matrix interface (used as boundary conditions for the matrix region). While solving the film region, the PER flux entering the film region was calculated from Equation 6.6 with the latest available concentrations of NO and O_2^- at the film-matrix interface. Following the film region solution, the matrix region equations (Equation 6.1) were solved. The fluxes at the surface of the matrix and at the film-bulk interface were calculated. Using the fluxes at the film-bulk interface, the bulk solution model (Equation 6.2) was then solved to calculate bulk concentrations ($C_{i,bs}$). The process was repeated until the bulk concentrations did not appreciably change. After convergence of the bulk concentrations were obtained, the NO flux at the matrix-film interface was calculated and divided by the total NO flux to obtain a new guess for f. The entire model was again solved until convergence of f was also obtained.

6.2.6 Parameter values

All the required rate constants, the O_2 consumption parameters and the diffusivity values are given in Table 5.1. The thickness of the film-region (ε) was estimated from a mass transfer correlation (Asai et al., 1988), which is

$$Sh = 2 + \frac{d}{\varepsilon} = \left[2^{5.8} + \left\{ 0.61 \left(\phi^{1/3} d^{4/3} / \nu \right)^{0.58} Sc^{1/3} \right\}^{5.8} \right]^{1/5.8} \tag{6.8}$$

where d (=0.500 cm) is the diameter of matrix, ϕ (=30 cm^2s^{-1}) is proportional to the rate of input of mechanical energy, ν (=6.94 x 10^{-3} cm^2s^{-1}) is the kinematic viscosity, and Sc (=ν/D_{NO}) is the Schmidt number for NO. Except for d, all parameters for the estimation of the Sherwood number (Sh) were obtained from Chen et al. (1998). Based on the calculated Sh of 10.65, ε is 58 μm.

The parameters obtained from the attached macrophage experiments of Lewis et al. (1995) included a total NO flux of 3.1 x 10^{-8} $mols^{-1}m^{-2}$ (see Section 5.2.3), a O_2^- flux to NO flux ratio entering the film region of 0.5, a bead density (ρ) of 1.43 x 10^3 beads/ml, and an L_{NO} of 7.5 x 10^{-4} s^{-1}. The C_{CO_2} was assumed to be 1.14 mM (see Section 5.2.3).

6.3 Results

6.3.1 Preliminary predictions of concentration profiles

The normalized concentration profiles of NO, PER and O_2 are shown in Figure 6.2. The NO, PER and O_2 concentrations were normalized with the respective surface concentration values (at r/R=1) of 2.07, 0.065, and 185 μM. The NO and O_2 concentrations decreased slightly but gradually in the matrix region. At the matrix center, the NO and O_2 concentrations were 98.4 and 95.7 %, respectively. In the film region, the NO concentration decreased more rapidly than the matrix region. At the film-bulk interface (r/R=1.23), the NO concentration reduced to 96.5 % of the surface value. The PER concentration declined rapidly to almost zero (<0.1% of the surface value) in the matrix region at r/R=0.8. In the film region the decrease in the PER concentration was also rapid but entire film region was exposed to at least 0.1 % of the surface PER concentration. The O_2^- concentration was 1.35 nM at the surface and reduced to zero within 2 μm of the matrix-surface in both the matrix and the film regions. In addition to the concentration profiles, the model prediction for f was 0.54.

6.4 Discussion

The preliminary validation of this model was performed with the replication of the data presented by Chen et al. (1998) for a similar system of macrophages attached to

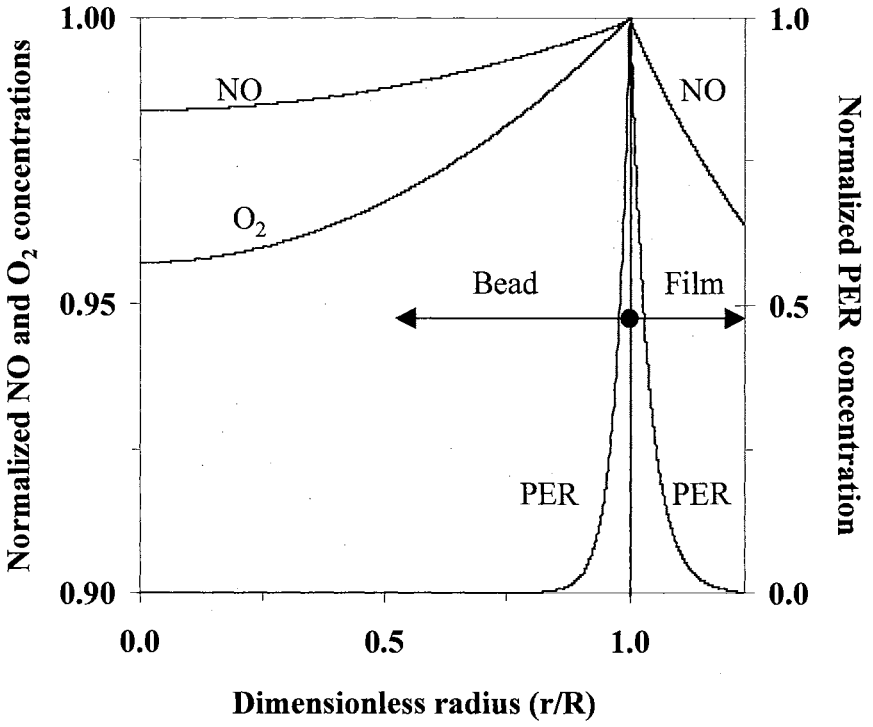

Figure 6.2. Normalized concentration profiles. The NO, PER and O_2 concentrations are normalized (i.e. concentration/concentration at r/R=1) with the respective concentrations at r/R=1, which are 2.09, 0.042, and 185 μM, respectively. The center of the matrix is r/R=0 and the surface of matrix is at r/R=1. The film region is between $1 \leq r/R \leq 1.23$.

microcarrier bead. The complete validation of model predictions for encapsulated pancreatic cells will be performed in the future as described below.

The spatial concentrations of end-products, mainly H_2O_2, NO_2^-, and NO_3^-, can be calculated from the algebraic equations of rate of formations in various regions. The end-products build-up in the system with time. The observed increase in the average concentration ($C_{i,avg}$) of end-products in the matrix region can be calculated from

$$\frac{dC_{i,avg,bead}}{dt} = \frac{3}{R^3}\int_0^R r^2 R_{i,bead}\,dr - \frac{3}{R} D_i \frac{dC_i}{dr}\Big|_{r=R} \tag{6.9}$$

The term $D_i(dC_i/dr)$ on the right hand side of Equation 6.9 represents the flux (F_i) of the end-product leaving the matrix into the film region. This value will not be available. Therefore, neglecting F_i results in predictions of the maximum rate of build up of the end-products in the matrix.

For the film and the bulk region, the increase in concentration of the end-product *i* is

$$\frac{dC_{i,avg,bs}}{dt} = 4\pi\rho \int_R^{R+\varepsilon} r^2 R_{i,sf}\,dr + R_{i,bs} + 4\pi R^2 \rho F_i \tag{6.10}$$

The total matrix volume is negligible compared to the bulk volume. Thus, a large change in the matrix region concentration will have a negligible effect on the bulk solution concentration, which means the third term on the right side will have a negligible effect on the bulk concentrations and can be ignored.

For the validation purpose, the predicted concentrations of NO_2^- and NO_3^- in the matrix region will be compared with the measured concentrations of a homogenized matrix solution from the experimental study. In the bulk solution, the experimental concentrations will be compared with the predicted concentrations of NO_2^-, NO_3^-, and NO.

In conclusion, the presented model provided initial estimates of *in situ* concentrations of NO and other species related to the cellular delivery of NO for the experimental scenario. This is a necessary first step for assessing the effects of immune cells on the encapsulated pancreatic cells.

Chapter 7. Conclusions and Future Studies

7.1 Conclusions

The overall objective of this thesis was completed with the quantitative modeling of NO concentrations in several biological systems arising from the chemical, physical or cellular delivery of NO. For the chemical NO delivery method, the spatial and temporal NO concentrations were predicted for the stagnant biological system. It was shown that the spatial and temporal distribution of NO can be significantly different for different NO donors. In addition, controlled and constant delivery of NO through the chemical methods is difficult. Therefore, the interpretation of NO effects would be complex.

For the physical NO delivery, a delivery device was designed to deliver constant NO to a flowing solution. The NO delivery rate by the delivery device was also predictable. Also, a stirred experimental system (non-flowing solution) was designed to deliver constant physical NO with or without O_2^- to pancreatic cells βTC3 attached to culture plates at the bottom of the system. The results showed that NO, O_2^-, and $ONOO^-$ at concentrations of 2.8 μM, 0.25 μM, and 0.1 nM, respectively, do not affect the insulin secretion rates of βTC3 cells over short times.

The cellular NO delivery was modeled for a possible *in vivo* scenario of a spherical matrix of target cells (containing pancreatic cells) surrounded by activated macrophages (generating NO and O_2^-). The model predictions of NO, O_2^-, and total peroxynitrite (PER) concentrations to which these pancreatic cells were potentially exposed were in the

range of 10-40 μM, 0.5-9 nM, and 0.1-1.5 μM, respectively for a 100 to 500 μm radius matrix.

Therefore in this thesis, the application of fundamental engineering principles in conjunction with chemical, physical, and cellular NO delivery methods demonstrated that the quantitative modeling of NO concentration is possible. The model predicted concentrations were obtained only from the transport and reaction kinetic parameters. Because the NO and other free radicals concentration could vary in a system, the importance of knowledge of the actual NO concentrations in order to effectively estimate the effects of NO on various biological systems was established. Also, the developed models eliminates the need for the complex measurement of NO in biological systems.

7.2 Future studies

Following are the some of the studies which can be performed:

- In Chapter 4, the effects of NO, O_2^-, and $ONOO^-$ on pancreatic cells were studied for concentrations of 2.8 μM, 0.25 μM, and 0.1 nM, respectively, for short time periods. However, *in vivo* the concentrations range of NO, O_2^-, and $ONOO^-$ are in the range of 10-40 μM, 0.5-9 nM, and 0.1-1.5 μM, respectively, (see Chapter 5) which are higher than what were studied. Thus, a study can be performed utilizing the experimental system described in Chapter 4 for studying the effects of higher free radicals concentrations on the pancreatic cells.

- There is a need for studies in which target cell matrix would be exposed to cellular delivery of NO. The model described in Chapter 6 can be utilized to study the effects of cellular NO delivery on target cells such as pancreatic cells.

Bibliography

Asai, S., Konishi, Y., and Sasaki, Y. 1988. Mass transfer between fine particles and liquids in agitated vessels. J. Chem. Eng. Jpn. 21:107-112.

Beckman, J. S., Beckman, T. W., Chen, J., Marshall, P. A., and Freeman, B. A. 1990. Apparent hydroxyl radical production by peroxynitrite: implications for endothelial injury from nitric oxide and superoxide. Proc. Natl. Acad. Sci. 87:1620-1624.

Burr, I. M., Kanazawa, Y., Marliss, E. B., and Lambert, A. E. 1971. Biphasic insulin release from perifused cultured fetal rat pancreas. Diabetes. 20:592-597.

Campbell, I. L., Iscaro, A., and Harrison, L. C. 1988. Interferon gamma and tumor necrosis factor alpha: cytotoxicity to murine islets of Langerhans. J. Immunol. 141:1325-1329.

Chen, B., Keshive, M., and Deen, W.M. 1998. Diffusion and reaction of nitric oxide in suspension cell cultures. Biophysical J. 75:745-754.

Colton, C.K. and Lowrie, E.G. 1981. Hemodialysis: Physical principles and technical considerations. In The Kidney (Brenner, B.M. and Rector, Jr., F.C., Eds.) 2nd Ed., Saunders, Philadelphia, pp:2460-2464.

Corbett, J. A. and McDaniel M. L. 1992. Does nitric oxide mediate autoimmune destruction of beta cells? Possible therapeutic interventions in IDDM. Diabetes. 41:897-903, 1992.

Cox, R. D. 1980. Determination of nitrate and nitrite at the parts per billion level by chemiluminiscence. Anal. Chem. 50:332-335.

Crank, J. 1975. The Mathematics of Diffusion. 2nd ed. Clarendon Press, Oxford, UK.

Cunningham, J. M., Mabley, J. G., Delaney, C. A., and Green, I. C. 1994. The effects of nitric oxide donors on insulin secretion, cyclic GMP and cyclic AMP in rat islets of Langerhans and the insulin-secreting cell lines HIT-T15 and RINm5F. Mol. Cell. Endocrinol. 102:23-29.

Davenport, H.W. 1974. The ABC of Acid-Base Chemistry. 6th ed. University of Chicago Press, Chicago, pp:41.

Davis, H. R., and Parkinson, G. V. 1971. Mass transfer from small capillaries with wall resistance in the laminar flow regime. Appl. Sci. Res. 22:20-30.

De Vos, P., Van Straaten, J. F. M., Nieuwenhuizen, A. G., de Groot, M., Ploeg, R. J., De Haan, B. J., and Schilfgaarde, R. V. 1999. Why do microencapsulated islet grafts fail in the absence of fibrotic overgrowth. Diabetes. 48:1381-1388.

Delaney, C. A., Tyrberg, B., Bouwens, L., Vaghef, H., Hellman, B., and Eizirik, D. L. 1996. Sensitivity of human pancreatic islets to peroxynitrite-induced cell dysfunction and death. FEBS Lett. 394(3):300-306.

Denicola, A., Freeman, B. A., Trujillo, M., and Radi, R.. 1996. Peroxynitrite reaction with carbon dioxide/bicarbonate: kinetics and influence on peroxynitrite mediated oxidations. Arch. Biochem. Biophys. 333:49-58.

Efrat, S., Linde, S., Kofod, H., Spector, D., Delannoy, M., Grant, S., Hanahan, D., and Baekkeskov, S. 1988. Beta-cell lines derived from transgenic mice expressing a hybrid insulin gene-oncogene. Proc. Natl. Acad. Sci. 85:9037-9041.

Eizirik, D. L., Delaney, C. A., Green, M. H. L., Cunningham, J. M., Thorpe, J. R., Pipeleers, D. G., Hellerstorm, C., and Green, I. C. 1996. Nitric oxide donors decrease the function and survival of human pancreatic islets. Mol. Cell. Endocrinol. 118:71-83.

Fan, M. Y., Lum, Z. P., Fu, X. W., Levesque, L., Tai, I. T., and Sun, A. M. 1990. Reversal of diabetes in BB rats by transplantation of encapsulated pancreatic islets. Diabetes. 39: 519-522.

Feelisch, M., and Stamler, J. S. 1996. Methods in Nitric Oxide Research. John Wiley and Sons, New York, pp:71-115.

Fridovich, I. 1978. The biology of oxygen radicals. Science. 201:875-880.

Furchgott, R. F. 1988. Studies on relaxation of rabbit aorta by sodium nitrite: the basis for the proposal that the acid-activatable inhibitory factor from retractor penis is inorganic nitrite and the endothelium-derived relaxing factor is nitric oxide. In Vasodilation: Vascular Smooth Muscle, Peptides, Autonomic Nerves and Endothelium. Raven Press: New York, pp. 401-414.

Garthwaite, J. Charles, S. L. and Chess-Williams, R. 1988. Endothelium-derived relaxing factor release on activation of NMDA receptors suggests role as intercellular messenger in brain. *Nature*. 336:385-388.

Gepts W., and Lecompte, P. M. 1981. The pancreatic islets in diabetes. Am. J. Med. 70:105-115.

Goldstein, S., Czapski, G., Lind, J., and Merenyi, G. 1999. Effect of NO on the decomposition of peroxynitrite: Reaction of N_2O_3 with $ONOO^-$. Chem. Res. Toxicol. 12:132-136.

Green, I. C, Cunningham, J. M., Delaney, C. A., Elphick, M. R., Mabley, J. G., and Green, M. H. L. 1994. Effects of cytokines and nitric oxide donors on insulin secretion, cyclic GMP and DNA damage: relation to nitric oxide production. Biochem. Soc. Trans. 22:30-37.

Hadjivassiliou, V., Green, M. H., James, R. F., Swift, S. M., Clayton, H. A., and Green, I. C. 1998. Insulin secretion, DNA damage, and apoptosis in human and rat islets of Langerhans following exposure to nitric oxide, peroxynitrite, and cytokines. Nitric Oxide. 2(6): 429-441.

Homer, K. and Wanstall, J. 1998. In vitro comparison of two NONOates (novel nitric oxide donors) on rat pulmonary arteries. Eur. J. Pharmacol. 356:49-57.

Huie, R. E. and Padmaja, S. 1993. The reaction of NO with superoxide. Free Rad. Res. Comm. 18:195-199.

Ignarro, L. J., Byrns, R. E., and Wood, K. S. 1988. Biochemical and pharmacological properties of endothelium-derived relaxing factor and its similarity to nitric oxide radical. In Vasodilation: Vascular Smooth Muscle, Peptides, Autonomic Nerves and Endothelium. Raven Press: New York, pp. 427-436.

Imlay, J. A. and Fridovich, I. 1991. Assay of metabolic superoxide production in Escherichia coli. J. Biol. Chem. 266:6957-6965.

Imlay, J. A., and Fridovich, I. 1991. Assay of metabolic superoxide production in Escherichia coli. J. Biol. Chem. 266:6957-6965.

Janjic, D. and Asfari, M. 1992. Effects of cytokines on rat insulinoma INS-1 cells. J. Endocrinol. 132:67-76.

Kaneto, H., Fujii, J., Seo, H. G., Suzuki, K., Matsuoka, T., Nakamura, M., Tatsumi, H., Yamasaki, Y., Kamada, T., and Taniguchi, N. 1995. Apoptotic cell death triggered by nitric oxide in pancreatic beta-cells. Diabetes. 44(7): 733-738.

Kappus, H. 1987. A survey id chemicals inducing lipid peroxidation in biological systems. Chem. Phys. Lipids. 45:105-115.

Kaufman, D. B., Jeffrey, P. L., Rabe, F. L., Dunn, D. L., Bach, F. H., and Sutherland, D. E. R. 1990. Differential roles of Mac-1+ cells, and CD4+ and CD8+ T lymphocytes in primary nonfunction and classic rejection of islet allografts. J. Exp. Med. 172: 291-302.

Kavdia, M., Stanfield, J., and Lewis, R. S. 2000. Nitric oxide, superoxide, and peroxynitrite effects on the insulin secretion and viability of βTC3 cells. Ann. Biomed. Eng. 28:102-109.

Kavdia, M., Nagarajan, S., and Lewis, R.S. 1998. Novel devices for the predictable delivery of nitric oxide to aqueous solutions. Chem. Res. Toxicol. 11(11):1346-1351.

Keefer, L. K. 1998. Nitric oxide-releasing compounds: from basic research to promising drugs. Modern Drug Discovery. Nov./Dec.:20-30.

Keefer, L. K., Nims, R. W., Davies, K.M., and Wink, D. A. 1996. NONOates as nitric oxide donors: convenient nitric oxide dosage forms. Methods in Enzymol. 268:281-293.

Kelm, M., Dahmann, R., Wink, D., and Feelisch, M.. 1997. The nitric oxide/superoxide assay. J. Biol. Chem. 272:9922-9932.

Kolb, H. and Kolb-Bachofen, V. 1992. Type I (insulin dependent) diabetes mellitus and nitric oxide. Diabetologia. 35:796-797.

Koppenol, W. H., Moreno, J. J., Pryor, W. A., Ischiropoulos, H., and Beckman, J. S. 1992. Peroxynitrite: a cloaked oxidant from superoxide and nitric oxide. Chem. Res. Toxicol. 5:834-842.

Krestow, M., Lum, Z. P., Tai, I. T., and Sun, A. 1991. Xenotransplantation of microencapsulated fetal rat islets. Transplantation 51: 651-655.

Kroncke, K. D., Brenner, H. H., Rodriguez, M. L., Etzkorn, K., Noack, E. A., Kolb, H., and Kolb-Bachofen, V. 1993. Pancreatic islet cells are highly susceptible towards the cytotoxic effects of chemically generated nitric oxide. Biochim. Biophys. Acta. 1182: 221-229.

Lancaster, J. R. Jr. 1992. Nitric oxide in cells. *Am. Scientist.* 80:248-260.

Lancaster, J. R. Jr. 1994. Simulation of the diffusion and reaction of endogenously produced nitric oxide. Proc. Natl. Acad. Sci. U.S.A. 91(17): 8137-8141.

Lancaster, J. R. Jr. 1996. Nitric Oxide: Principles and Actions. Academic Press. San Diego, CA.

Lange, N. A. 1967. Lange's Handbook of Chemistry. rev 10^{th} ed., McGraw Hill, New York, pp:1101.

Laurent, M., Lepoivre, M., and Tenu, J. P. 1996. Kinetic modelling of the nitric oxide gradient generated in vivo by adherent cells expressing inducible nitric oxide synthase. Biochem. J. 314:109-113.

Lewis, R. S., and Deen, W. M. 1994. Kinetics of the reaction of nitric oxide with oxygen in aqueous solutions. Chem. Res. Toxicol. 7:568-574.

Lewis, R. S., Deen, W. M., Tannenbaum, S. R., and Wishnok, J. S. 1992. Membrane mass spectrometer inlet for quantitation of nitric oxide. Biol. Mass Spectrom. 22:45-52.

Lewis, R. S., Tamir, S., Tannenbaum, S. R., and Deen, W. M. 1995. Kinetic analysis of the fate of nitric oxide synthesize by macrophage in vitro. J. Biol. Chem. 270:29350-29355.

Loskove, J. A., and Frishman, W. H. 1995. Nitric oxide donors in the treatment of cardiovascular and pulmonary diseases. Am. Heart J. 129:604-613.

Lum, Z. P., Krestow, M., Tai, I. T., Vacek, I., and Sun, A. M. 1992. Xenografts of rat islets into diabetic mice. Transplantation. 53: 1180-1183.

Mandrup-Poulsen, T., Bendtzen, K., Dinarello, C. K., and Nerup, J. 1987. Human tumor necrosis factor potentiates interleukin-1 mediated rate of pancreatic β-cell cytotoxicity. J. Immunol. 139:4077-4082.

Mandrup-Poulsen, T., Helquist, S., Wogensen, L. D., Molvig, J., Pociot, F., Johannesen, J., and Nerup, J. 1990. Cytokines and free radicals as effector molecules in the destruction of pancreatic beta cells. Curr. Top. Microbiol. Immunol. 164:169-193.

Maragos, C. M., Morley, D., Wink, D. A., Dunams, T. M., Saavedra, J.E., Holms, A., Bove, A. A., Isaac, L., Hrabie, J. A., and Keefer, L. K. 1991. Complexes of nitric oxide with nucleophiles as agents for the controlled biological release of nitric oxide. Vasorelaxant effects. J. Med. Chem. 34:3242-3247.

Mauricio, D., and Mandrup-Poulsen, T. 1998. Apoptosis and the pathogenesis of IDDM: a question of life and death. Diabetes. 47(10): 1537-1543.

Melgaard, D. K., and Sincovec, R. F. 1981. General software for two-dimensional nonlinear partial differential equations. ACM Trans. Math. Software. 7(1):1076-135.

Miller, W. M., Wilke, C. R., and Blanch, H. W. 1987. Effects of dissolved oxygen concentration on hybridoma growth and metabolism in continuous culture. J. Cell. Physiol. 132:524-530.

Moncada, S., Palmer, R. M. J., and. Higgs, E. A. 1991. Nitric oxide: Physiology, pathophysiology and pharmacology. Pharmacol. Rev. 43:109-142.

Morvan, D., and Jaffrin, M. Y. 1989. Unsteady diffusion mass transfer in a microencapsulated islet of Langerhans for a bioartificial pancreas. Int. J. Heat Mass Transfer. 32: 995-999.

O'Shea, G. M., and Sun A. M. 1986. Encapsulation of rat islets of Langerhans prolongs xenograft survival in diabetic mice. Diabetes. 35(8): 943-946.

Padmaja, S., Squadrito, G. L., and Pryor, W. A. 1998. Inactivation of glutathione peroxidase by peroxynitrite. Arch. Biochem. Biophys. 349:1-6.

Patel, R. P., McAndrew, J., Sellak, H., White, C. R., Jo, H., Freeman, B. A., Darley-Usmar, V. M. 1999. Biological aspects of reactive nitrogen species. Biochim. Biophys. Acta. 1411:385-400.

Pfeiffer, S., A., Gorren, C. F., Schmidt, K., Werner, E. R.., Hansert, B., Bohle, D. S., and Mayer, B. 1997. Metabolic fate of peroxynitrite in aqueous solution. J. Biol. Chem. 272:3465-3470.

Press, W. H., Teukolsky, S. A., Vetterling, W. T., and Flannery, B. P. 1972. Numerical Recipes in Fortran. Cambridge University Press, Cambridge, 745-777.

Pukel, C., Baquerizo, H., and Rabinovitch, A. 1988. Destruction of rat islet cell monolayers by cytokines: synergistic interactions of interferon-γ, tumor necrosis factor, lymphotoxin, and interleukin-1. Diabetes. 37:133-136.

Radi, R. 1998. Peroxynitrite reactions and diffusion in biology. Chem. Res. Toxicol. 11:720-721.

Radomski, M. W., Palmer, R. M. J., and Moncada, S. 1987. Endogenous nitric oxide inhibits human platelet adhesion to vascular endothelium. Lancet. 2:1057-1058.

Ramamurthi, A., and Lewis, R. S. 1997. Measurement and modeling of nitric oxide release rates for nitric oxide donors. Chem. Res. Toxicol. 10:408-413.

Reach, G. 1993. Bioartificial pancreas. Diabetic Med. 10: 105-109.

Robb, W. L. 1968. Thin silicone membranes-their permeation properties and some applications. Ann. N. Y. Acad. Sci. 146:119-137.

Sambanis, A., Papas, K. K., Flanders, P. C., Long, R. C., Kang, H., and Constantinidis, I. 1994. Toward the development of a bioartificial pancreas: immunoisolation and NMR monitoring of mouse insulinomas. Cytotechnology. 15:351-363.

Schmidt, K., Desch, W., Klatt, P., Kukovetz, W. R., and Mayer, B. 1997. Release of nitric oxide from donors with known half-life: a mathematical model for calculating nitric oxide concentrations in aerobic solutions. Naunyn Schmiedebergs Arch. Pharmacol. 355(4):457-462.

Sekine, N., Fasolato, C., Pralong, W. F., Theler, J., and Wollheim, C. B. 1997. Glucose-induced insulin secretion in INS-1 cells depends on factors present in fetal calf serum and rat islet-conditioned medium. Diabetes. 46:1424-1433.

Soon-Shiong, P., Feldman, E., Nelson, R., Komtebedde, J., Smidsrod, O., Skjak-Braek, G., Espevik, T., Heintz, R., and Lee, M. 1992. Successful reversal of spontaneous diabetes in dogs by intraperitoneal microencapsulated islets. Transplantation. 54(5):769-774.

Stamler, J. S., Jaraki, O., Osborne, J., Simon, D. I., Keaney, J., Vita, J., Singel, D., Valeri, C. R., and Loscalzo, J. 1992. Nitric oxide circulates in mammalian plasma primarily as an S-nitroso adduct of serum albumin. Proc. Natl. Acad. Sci. USA 89:7674-7677.

Stuehr, D. J., and Marletta, M. A. 1987. Induction of nitrite/nitrate synthesis in murine macrophages by BCG infection, lymphokines, or interferons-γ. J. Immunol. 139:518-525.

Sun, Y., Ma, X., Zhou, D., Vacek, I., and Sun, A. M. 1996. Normalization of diabetes in spontaneously diabetic cynomologus monkeys by xenografts of microencapsulated porcine islets without immunosuppression. J. Clin. Invest. 98(6):1417-1422.

Tamir, S., Lewis, R. S., Walker, T. R., Deen, W. M., Wishnok, J. S., and Tannenbaum, S. R. 1993. The influence of delivery rate on the chemistry and biological effects of nitric oxide. Chem. Res. Toxicol. 6:895-899.

Tannenbaum, S. R., Tamir, S., Walker, T. R., and Wishnok, J. S. 1993. DNA damage and cytotoxicity by nitric oxide. In Nitrosamines and Related N-Nitroso Compounds. American Chemical Society. Washington D.C. pp 120-135.

Tziampazis, E. and Sambanis, A. 1995. Tissue engineering of a bioartificial pancreas: Modeling the cell environment and device function. Biotechnol. Prog. 11:115-126.

Uppu, R. M., Squadrito, G. L., and Pryor, W. A. 1996. Acceleration of peroxynitrite oxidations by carbon dioxide. Arch. Biochem. Biophys. 327(2): 335-343.

Vaughn, M. W., Kuo, L., and Liao, J. C. 1998. Estimation of nitric oxide production and reaction rates in tissue by use of a mathematical model. Am. J. Physiol. 274(6 Pt 2): H2163-2176.

Wallgren, A. C., Karlsson-Parra, A., and Korsgren, O. 1995. The main infiltrating cell in xenograft rejection is a $CD4^+$ macrophage and not a T lymphocyte. Transplantation. 60(6): 594-601.

Weinberg, J. B. 1998. Nitricoxide production and nitric oxide syntahse Type 2 expression by human mononuclear phagocytes: a review. *Mol. Med.* 4:557-591.

Welsh, N., Margulis, B., Borg, L. A., Wiklund, H. J., Saldeen, J., Flodstrom, M., Mello, M. A., Andersson, A., Pipeleers, D. G., Hellerstrom, C., and Eizirik, D. L. 1995. Differences in the expression of heat-shock proteins and antioxidant enzymes between human and rodent pancreatic islets: implications for the pathogenesis of insulin-dependent diabetes mellitus. Mol. Med. 1(7): 806-820.

Westrin, B. A., and Axelsson, A. 1991. Diffusion in gels containing immobilized cells: a critical review. Biotenol. Bioeng. 38: 439-454.

Wiegand, F., Kroncke, K. D., and Kolb-Bachofen, V. 1993. Macrophage-generated nitric oxide as cytotoxic factor in destruction of alginate-encapsulated islets. Transplantation. 56(5): 1206-1212.

Wink, D. A., Cook, J. A., Pacelli, R., DeGraff, W., Gamsom, J., Liebmann, J., Krishna, M. C., and Mitchell, J. B. 1996. The effects of various nitric oxide-donor agents on hydrogen peroxide-mediated toxicity: a direct correlation between nitric oxide formation and protection. Arch. Biochem. Biophys. 331(2):241-248.

Winterbourn, C. C., and Metodiewa, D. 1994. Generation of superoxide and tyrosine peroxide as a result of tyrosyl radical scavenging by glutathione. Arch. Biochem. Biophys. 314: 284-290.

Wise, D. L. and Houghton, G. 1968. Diffusion coefficients of neon, krypton, xenon, carbon monoxide, and nitric oxide in water at 10-60 °C. Chem. Eng. Sci. 23:1211-1216.

Wohlpart, D., Kirwan, D., and Gainer, J. 1990. Effects of cell density and glucose and glutamine levels on the respiration rates of hybridoma cells. Biotechnol. Bioeng. 36: 630-635.

Appendix 1. Model for Chemical NO Delivery (Chapter2)

```
! THIS IS THE MAIN PROGRAM FOR THE SOLUTION OF CHEMICAL NO DELIVERY.
! ALGORITHM 565
! MAIN PROGRAM USE THE PDETWO PACKAGE
! PDETWO/PSTEM/GEARB: SOLUTION OF SYSTEMS OF TWO DIMENSIONAL
! NONLINEAR PARTIAL DIFFERENTIAL EQUATIONS
! BY D.K. MELGAARD AND R.F. SINCOVEC
! ACM TRANSACTIONS ON MATHEMATICAL SOFTWARE 7,1 (MARCH 1981)
!
! ****************************************************************

      IMPLICIT REAL (A-H,O-Z)
      REAL  H,S,X,ERR1,DX,Y,TOUT,REALN1,DY,U1,HUSED
      REAL  EXP,R,T0,EPS,ERMAX,ABS,WORK,DL,DLI,DEV
      REAL  U2,U3,ERR2,ERR3,REALN2,REALN3
      INTEGER IX,NPDE,NSTEP,NX,NFE,NODE,MF,NY
      INTEGER  NJE,NQUSED,IY,INDEX,I,IWORK,KODE,IK
      COMMON /GEAR3/ HUSED,NQUSED,NSTEP,NFE,NJE
      COMMON /PROB/ DL,DLI,KODE
      DIMENSION U1(11,10),ERR1(11,10),REALN1(11,10)
      DIMENSION U2(11,31),ERR2(11,31),REALN2(11,31)
      DIMENSION U3(2,51,5),ERR3(2,51,5),REALN3(2,51,5)
      DIMENSION WORK(163952),IWORK(510),X(51),Y(31)
      EQUIVALENCE (U1(1,1),U3(1,1,1)),(ERR1(1,1),ERR3(1,1,1))
EQUIVALENCE (U2(1,1),U3(1,1,1)),(ERR2(1,1),ERR3(1,1,1))
EQUIVALENCE(REALN1(1,1),REALN3(1,1,1)),(REALN2(1,1),REALN3(1,1,1))
!****************************************************************

       OPEN(UNIT=16,FILE ='NO.TXT',STATUS='UNKNOWN')
       OPEN(UNIT=17,FILE ='OXYGEN.TXT',STATUS='UNKNOWN')

      DO 1000 IK=1,2

          KODE = IK
          IF(KODE.EQ.1)  GO TO 100
          IF(KODE.EQ.2)  GO TO 500

100  CONTINUE

!
*********************************************************************
!
! CONSTANT OXYGEN ONE PDE
!
!
*********************************************************************

! DEFINE THE PROBLEM PARAMETERS.
      NX=11
      NY=10
```

```
      NPDE=1
      NODE=NPDE*NX*NY
      MF=22
      INDEX=1
      T0=0.0
      H=0.1E-06
      EPS=0.1E-09
      DX = 1.0/(FLOAT(NX)-1.0)
      DY = 1.0/(FLOAT(NY)-1.0)
      DO 120 IX=1,NX
        Y(IX)=FLOAT(IX)*DY-DY
  120   X(IX)=FLOAT(IX)*DX-DX
      IWORK(1) = NPDE
      IWORK(2) = NX
      IWORK(3) = NY
      IWORK(4) = 5
      IWORK(5) = 4933
      IWORK(6) = 110

!  DEFINE THE INITIAL CONDITION
      DO 160 IY = 1,NY
        DO 160 IX = 1,NX
  160    U1(IX,IY)=0.0

!
!  SET UP THE LOOP FOR CALLING THE INTEGRATOR AT DIFFERENT TOUT VALUES
!
      TOUT=.1
      DO 260 I=1,20
!      WRITE (16,200) TOUT
  200 FORMAT (// 5H TOUT,E15.6)
!
!  CALL THE INTEGRATOR
!
      CALL DRIVEP (NODE,T0,H,U1,TOUT,EPS,MF,INDEX,WORK,IWORK,X,Y)
!
!  CHECK ERROR RETURN
!
      IF (INDEX .NE. 0) GO TO 1000
!
! OUTPUT THE RESULTS
!

  225 FORMAT (E11.4)
           WRITE (16,230) TOUT, (U1(IX,1),IX=1,NX)
  230 FORMAT ((E11.4), 11E11.4)

        TOUT=TOUT+0.1
  260 CONTINUE

!************************** END CONSTANT OXYGEN ************


      GO TO 1000
 500  CONTINUE
!************************************************************
!
```

```
!   NON CONSTANT OXYGEN, COUPLED SYSTEM OF PDE*S
!
!************************************************************

!  DEFINE THE PROBLEM PARAMETERS.  NPDE,NX, AND NY PRIMARILY DETERMINE
!  THE DIMENSIONS FOR THE ARRAYS IN PDETWO AND THE MODIFIED GEARB.
!
      NX=51
      NY=5
      NPDE=2
      NODE=NX*NY*NPDE
      MF=22
      INDEX=1
      T0=0.0
      H=0.1E-06
      EPS=0.1E-06
      DX=1.0/(FLOAT(NX)-1.0)
      DO 520 IX=1,NX
        X(IX)=FLOAT(IX)*DX-DX
  520 CONTINUE

      DY = 1.0/(FLOAT(NY)-1.0)
      DO 525 IY=1,NY
        Y(IY)=FLOAT(IY)*DY-DY
  525   CONTINUE
      IWORK(1) = NPDE
      IWORK(2) = NX
      IWORK(3) = NY
      IWORK(4) = 5
      IWORK(5) = 163952
      IWORK(6) = 510
!
!  DEFINE THE INITIAL CONDITIONS
            DO 560 IY=1,NY
        DO 560 IX=1,NX
          U3(1,IX,IY)=0.
560     U3(2,IX,IY)=185.E-6

      WRITE (16,570) NODE,T0,H,EPS,MF,((U3(1,IX,IY),IX=1,NX),IY=1,NY),&
     &((U3(2,IX,IY),IX=1,NX),IY=1,NY)
  570 FORMAT (6H NODE ,I3,4H T0 ,F9.2,3H H ,E8.1,5H EPS ,E8.1,4H MF
,I2&
     &//19H INITIAL U1 VALUES  / 5(/3H    ,11E11.4)&
     &//19H INITIAL U2 VALUES  / 5(/3H    ,11E11.4))

            WRITE (16,575) T0, (U3(1,IX,1),IX=1,NX)
  575       FORMAT ((E11.4), 51E11.4)
            WRITE (16,585) T0, (U3(2,IX,1),IX=1,NX)
  585       FORMAT ((E11.4), 51E11.4)
!
!  SET UP THE LOOP FOR CALLING THE INTEGRATOR AT DIFFERENT TOUT VALUES
!
      TOUT=.1

      DO 660 I=1,20

!  CALL THE INTEGRATOR
```

```
      CALL DRIVEP (NODE,T0,H,U3,TOUT,EPS,MF,INDEX,WORK,IWORK,X,Y)
!  CHECK ERROR RETURN
!
      IF (INDEX .NE. 0) GO TO 1000
!
!  OUTPUT THE RESULTS
!

            WRITE (16,630) TOUT, (U3(1,IX,1),IX=1,NX)
  630 FORMAT ((E11.4), 51E11.4)
            WRITE (16,635) TOUT, (U3(2,IX,1),IX=1,NX)
  635 FORMAT ((E11.4), 51E11.4)

!     TIME INCREASE

        TOUT=TOUT+.1

  660 CONTINUE
!
!************************** END NON CONSTANT OXYGEN ***************
!
      GO TO 1000

 1000 CONTINUE
            CLOSE(16)
            CLOSE(17)
      STOP
      END

! ***************************************************************
      SUBROUTINE F(T,X,Y,U,UX,UY,DUXX,DUYY,DUDT,NPDE)
!
!  DEFINE THE PDE
!
      REAL  T,U,X,Y,UX,UY,DUXX,DUYY,DUDT,EXP
      REAL RKNO,DEPTH,NOATEI,ENO,RK,COXY
      INTEGER NPDE
      COMMON /PROB/ DL,DLI,KODE
      DIMENSION U(NPDE),UX(NPDE),UY(NPDE),DUXX(NPDE,NPDE),&
     &DUYY(NPDE,NPDE),DUDT(NPDE), ALPHA(NPDE)

            DEPTH=3.E-3
            RK=2.4E6    !2.4E6
            COXY=185E-6

            KNO=1 !1=SPERMINENO; 2=DEA/NO

            IF (KNO.EQ.1) THEN
            RKNO=0.3E-3
            NOATEI=100.E-6
            ENO=1.9
            ENDIF

            IF (KNO.EQ.2) THEN
            RKNO=5.4E-3
            NOATEI=100.E-6
            ENO=1.5
```

```
            ENDIF

          IF(KODE.EQ.1)  GO TO 100
          IF(KODE.EQ.2)  GO TO 300
!
! CONSTANT OXYGEN ONE PDE
!
  100 CONTINUE
              DO 10 I=1,NPDE
              IF (Y.EQ.0.0) THEN
              ALPHA(I)=0.0
              ELSE
              ALPHA(I)=(1.0*UY(I)/Y)
              ENDIF
10      CONTINUE

          DUDT(1)=(DUXX(1,1)/(RKNO*(DEPTH**2)))+(NOATEI*ENO*EXP(-T))&
         &-(4*RK*(U(1)**2)*COXY/RKNO)+ DUYY(1,1) + ALPHA(1)

        GO TO 400
!
!  NON CONSTANT OXYGEN, COUPLED SYSTEM OF PDE*S
!
  300 CONTINUE

          DUDT(1)=(DUXX(1,1)/(RKNO*(DEPTH**2)))+(NOATEI*ENO*EXP(-T))&
         &-(4*RK*(U(1)**2)*U(2)/RKNO)+ DUYY(1,1) + ALPHA(1)
          DUDT(2)=(DUXX(2,2)/(RKNO*(DEPTH**2)))&
         &-(4*RK*(U(1)**2)*U(2)/RKNO)+ DUYY(2,2) + ALPHA(2)


  400 CONTINUE
        RETURN
        END
SUBROUTINE BNDRYH (T,X,Y,U,AH,BH,CH,NPDE)
!
!  DEFINE THE HORIZONTAL BOUNDARY CONDITIONS
!
        REAL  T,U,X,Y,BH,AH,CH
        INTEGER NPDE
        COMMON /PROB/ DL,DLI,KODE
        DIMENSION U(NPDE),AH(NPDE),BH(NPDE),CH(NPDE)
        IF(KODE.EQ.1)  GO TO 100
        IF(KODE.EQ.2)  GO TO 300
!
!  CONSTANT OXYGEN ONE PDE
!
  100 CONTINUE
          AH(1) = 0.0
          BH(1) = 1.0
          CH(1) = 0.0
        GO TO 400
!
!  NON CONSTANT OXYGEN, COUPLED SYSTEM OF PDE*S
!
  300 CONTINUE
  AH(1) = 0.0
```

```
  BH(1) = 1.0
  CH(1) = 0.0
  AH(2) = 0.0
  BH(2) = 1.0
  CH(2) = 0.0

  400 CONTINUE
      RETURN
      END
SUBROUTINE BNDRYV (T,X,Y,U,AV,BV,CV,NPDE)
!
!  DEFINE THE VERTICAL BOUNDARY CONDITIONS
!
      REAL  T,U,X,Y,BV,AV,CV
      INTEGER NPDE
      COMMON /PROB/ DL,DLI,KODE
      DIMENSION U(NPDE),AV(NPDE),BV(NPDE),CV(NPDE)
      IF(KODE.EQ.1)  GO TO 100
      IF(KODE.EQ.2)  GO TO 300
!
!  CONSTANT OXYGEN ONE PDE
!
100   CONTINUE
      IF (X .NE. 0.0) GO TO 110
        AV(1)=0.0
        BV(1)=1.0
        CV(1)=0.0
      GO TO 400
110     CONTINUE
        AV(1) = 1.0
        BV(1) = 0.0
        CV(1) =0.0
      GO TO 400
!
!  NON CONSTANT OXYGEN, COUPLED SYSTEM OF PDE*S
!
  300 CONTINUE
      IF (X .NE. 0.0) GO TO 310
        AV(1)=0.0
        BV(1)=1.0
        CV(1)=0.0
        AV(2) = 0.0
        BV(2) = 1.0
        CV(2) = ((200e-6*u(2))/(.015e-3+u(2)))
      GO TO 400
310   CONTINUE
        AV(1) = 1.0
        BV(1) = 0.0
        CV(1) =0.0
        AV(2) = 1.0
        BV(2) = 0.0
        CV(2) =185.e-6

400   CONTINUE
      RETURN
      END
SUBROUTINE DIFFH (T,X,Y,U,DH,NPDE)
```

```
!
!  DEFINE THE HORIZONTAL DIFFUSION COEFFICIENTS
!
      REAL  T,U,X,Y,DH
      INTEGER NPDE
      COMMON /PROB/ DL,DLI,KODE
      DIMENSION U(NPDE),DH(NPDE,NPDE)
      IF(KODE.EQ.1)  GO TO 100
      IF(KODE.EQ.2)  GO TO 300
!
!  CONSTANT OXYGEN ONE PDE
!
  100 CONTINUE
        DH(1,1) = 5.1e-9
      GO TO 400
!
!  NON CONSTANT OXYGEN, COUPLED SYSTEM OF PDE*S
!
  300 CONTINUE
       DH(1,1)=5.1e-9
       DH(1,2)=0.0
       DH(2,1)=0.0
       DH(2,2)=3.0e-9
  400 CONTINUE
      RETURN
      END
SUBROUTINE DIFFV (T,X,Y,U,DV,NPDE)
!
!  DEFINE THE VERTICAL DIFFUSION COEFFICIENTS
!
      REAL  T,U,X,Y,DV
      INTEGER NPDE
      COMMON /PROB/ DL,DLI,KODE
      DIMENSION U(NPDE),DV(NPDE,NPDE)
      IF(KODE.EQ.1)  GO TO 100
      IF(KODE.EQ.2)  GO TO 300
!
!  CONSTANT OXYGEN ONE PDE
!
  100 CONTINUE
        DV(1,1) = 0
      GO TO 400
!
!  NON CONSTANT OXYGEN, COUPLED SYSTEM OF PDE*S
!
  300 CONTINUE
        DV(1,1)=5.1e-9
        DV(1,2)=0.0
        DV(2,1)=0.0
        DV(2,2)=3.e-9

  400 CONTINUE
      RETURN
      END
```

Appendix 2. Model for Cellular NO Delivery

(Chapter 5)

```
      PROGRAM DRFREERAD
      INTEGER NE,M,NB,NCI,NCJ,NCK,NSI,NSJ,NYJ,NYK
      INTEGER KN,ITCONV
      INTEGER I,ITMAX,K
      INTEGER , ALLOCATABLE :: INDEXV(:)
      INTEGER ITCONV_1
      COMMON /SFRCOM/ RR,H
      COMMON /GEOMETRY/ BEAD_RADIUS
      COMMON /BULKCONC/ CSUPB,CNOB,CPERB

C     THE VALUES IN PAR1 AND PAR2 ARE PARAMETER VALUES OBTINED FROM
C     DEEN'S PAPER.  THESE VALUES ARE SHARED WITH SUBROUTINE DIFEQ5
C     AND FUNCV.
      COMMON /PAR1/ COXY,CCAR,DNO,DSUP,DPER
      COMMON /PAR2/ RK1,RK2,RK3,RKT,RK5,RK6,RK7,RK9,RK10,RK11,FF
C     THE VALUES IN SURFVAL1 ARE SURFACE VALUES OF CONCENTRATIONS
C     AND FLUXES OBTAINES FROM THESE CONCENTRATIONS. THESE VALUES
C     ARE SHARED WITH DIFEQ5 SUBROUTINE.
      COMMON /SURFVAL1/ CNOS,CSUPS,CPERS,FNOS,FSUPS,FPERS
C     OXYGEN CONSTANTS
      COMMON /OXYGEN/DOXY,RKOXY,RKMOXY,COXYB,FOXYS
      DOUBLE PRECISION DOXY,RKOXY,RKMOXY,COXYB,FOXYS
C     ----------------
      PARAMETER (KN=3)
      PARAMETER (M=5001,NCK=M+1,NYK=M)
      DOUBLE PRECISION CBULK(KN),CONC(KN),FNO,FSUP,FPER,CONVN,ERRN(KN)
      DOUBLE PRECISION FNOS,FSUPS,FPERS
      DOUBLE PRECISION CNOS,CSUPS,CPERS
      DOUBLE PRECISION COXY,CCAR,DNO,DSUP,DPER
      DOUBLE PRECISION RK1,RK2,RK3,RKT,RK5,RK6,RK7,RK9,RK10,RK11,FF
      DOUBLE PRECISION CONV,SLOWC
      DOUBLE PRECISION , ALLOCATABLE :: C(:,:,:),S(:,:)
      DOUBLE PRECISION , ALLOCATABLE :: Y(:,:),SCALV(:)
      DOUBLE PRECISION RR(M),H,FRACTION_SUP,FRACTION_DIFF
      DOUBLE PRECISION CSUPB,CNOB,CPERB
      DOUBLE PRECISION BEAD_RADIUS
      DOUBLE PRECISION CAL_FRAC_NO,SUC_DIFF,FLUX_NO
      DOUBLE PRECISION CONCNOS,CONCSUPS
      DOUBLE PRECISION CHECK_PERSUFFLUX,CPERB1


CU    USES SOLVDE
      OPEN(UNIT=15,FILE='BIOPANOUT.CSV',STATUS='UNKNOWN')
      OPEN(UNIT=16,FILE='MESSAGEBIO.TXT',STATUS='UNKNOWN')
C     THE PARAMETER FOR THE MODEL ARE GIVEN BELOW.
      COXY=100.D-6
      CCAR=1.14D-3
      FRACTION_DIFF=0.46E0
      RK1=2.4D+6
```

```
      RK2=1.1D+9
      RK3=1.6D+3
      RK5=6.7D+9
      RK6=3.1D+0
      RK7=1.4D+0
      RK9=8.D+7
      RK10=2.9D+4
      RK11=9.1D+4
      RKT=(0.26D0*(RK6+RK7))+(0.74D0*RK10*CCAR)
      FF=2.51D-3
C     THESE ARE THE PARAMETER FOR OXYGEN CONSUMPTION RATE
      COXYB=COXY
      RKMOXY=0.01E-3
      RKOXY=1.1E-6
C     THESE ARE THE PARAMETER FOR RADIUS AND FILM THICKNESS
      BEAD_RADIUS=250.0D-6
      FLUX_NO=3.1D-8
      FRACTION_SUP=0.5
C     CALCULATION OF FLUXES
C     DCI/DR=-NI/DI
C     FOR NO, DNO=5.1E-9 M2/S AND NNO=3.1E-8 MOL/S/M2
C     DCNO/DR=-3.1E-8/5.1E-9 (MOL/(M4(=1000LITER*M))
C     DCNO/DR= -6.078E-3 (MOLAR/M)=(MOLES/L/M)
C     THE CONVERGENCE PARAMETERS
      ITMAX=200
      ITCONV= 0
      CONV=1.D-7
      CONVN=1.D-2
      SLOWC=5.D-1
      DNO=5.1D-9
      DSUP=2.8D-9
      DPER=2.6D-9
      DOXY=3.0E-9
CCCCCCCCCCCCCCCCCCCCCCCCCCCCCCCCCCCCCCCCCCCCCCCCCCCCCCCCCCCCCCCCCCCCC
C     THIS MODULE WILL SOLVE THE BEAD REGION
      DNO=DNO*FRACTION_DIFF
      DSUP=DSUP*FRACTION_DIFF
      DPER=DPER*FRACTION_DIFF
      DOXY=DOXY*FRACTION_DIFF
      FNOS=0.D+0
      FSUPS=0.D+0
      FPERS=0.D+0
      FOXYS=0.D+0
      H=-BEAD_RADIUS/(M-1)
      CNOB=(FLUX_NO/(DNO*1.D3))
      CSUPB=(FLUX_NO*FRACTION_SUP/(DSUP*1.D3))
      CPERB=CONCNOS*CONCSUPS*RK5*H/(DPER)
      COXYB=COXY
      NE=8
      NB=4
      NCJ=NE-NB+1
      NCI=NE
      NSI=NE
      NSJ=2*NE+1
      NYJ=NE
100   CONTINUE
      ALLOCATE(INDEXV(NE))
```

```
      ALLOCATE(C(NCI,NCJ,NCK), S(NSI,NSJ))
      ALLOCATE(Y(NE,M),SCALV(NE))
      INDEXV(1)=1
      INDEXV(2)=2
      INDEXV(3)=3
      INDEXV(4)=4
      INDEXV(5)=5
      INDEXV(6)=6
      INDEXV(7)=7
      INDEXV(8)=8
C     INITIAL GUESSES
      DO 640 K=1,M
            Y(1,K)=0.1D-2
            Y(2,K)=0.1D-2

            Y(3,K)=0.1D-2
            Y(4,K)=0.1D-4
            Y(5,K)=5.D-6
            Y(6,K)=1.D-7
            Y(7,K)=1.D-10
            Y(8,K)=1.D-2
640    CONTINUE
      SCALV(1)=DMAX1(1.D0,Y(1,M))
      SCALV(2)=DMAX1(1.D0,Y(2,M))
      SCALV(3)=DMAX1(1.D0,Y(3,M))
      SCALV(4)=DMAX1(1.D0,Y(4,M))
      SCALV(5)=DMAX1(1.D-3,Y(5,M))
      SCALV(6)=DMAX1(1.D-3,Y(6,M))
      SCALV(7)=DMAX1(1.D-3,Y(7,M))
      SCALV(8)=DMAX1(1.D-3,Y(8,M))
      DO 645 K=1,M
            RR(K)=BEAD_RADIUS+(K-1)*H
645   CONTINUE
      CALL SOLVDE(ITMAX,CONV,SLOWC,SCALV,INDEXV,NE,NB,M,Y,NYJ,NYK,C,
     *NCI,NCJ,NCK,S,NSI,NSJ)
      IF (ITCONV.GT.ITMAX) THEN
            STOP
      ENDIF
      CONCNOS=DABS(Y(5,1))
      CONCSUPS=DABS(Y(7,1))
      CPERB1=CONCNOS*CONCSUPS*RK5*H/(DPER)
      SUC_DIFF=DABS(1.D0-DABS(DABS(CPERB)/DABS(CPERB1)))
            IF (SUC_DIFF.GT.1.D-2) THEN
      CPERB=DABS(CPERB1)
      DEALLOCATE(INDEXV)
      DEALLOCATE(C,S)
      DEALLOCATE(Y,SCALV)
      GOTO 100
      ENDIF
      DO 650 K=1,M
            WRITE(15,260)K,RR(K),(Y(I,K),I=1,8)
650   CONTINUE
      DEALLOCATE(INDEXV)
      DEALLOCATE(C,S)
      DEALLOCATE(Y,SCALV)
CCCCCCCCCCCCCCCCCCCCCCCCCCCCCCCCCCCCCCCCCCCCCCCCCCCCCCCCCCCCCCCCCC
65    CONTINUE
```

```
C     THE FOLLOWING ARE THE FORMATING STATEMENTS.
260   FORMAT(5X,I4,5X,E11.5,3X,8(E11.5,3X))
      CLOSE(15)
      CLOSE(16)
      END

      SUBROUTINE DIFEQ(K,K1,K2,JSF,IS1,ISF,INDEXV,NE,S,NSI,NSJ,Y,NYJ,
     *NYK)
      INTEGER IS1,ISF,JSF,K,K1,K2,NE,NSI,NSJ,NYJ,NYK,INDEXV(NYJ),M
      DOUBLE PRECISION S(NSI,NSJ),Y(NYJ,NYK)
      COMMON /SFRCOM/ RR,H
      COMMON /GEOMETRY/ BEAD_RADIUS
      DOUBLE PRECISION BEAD_RADIUS
      COMMON /BULKCONC/ CSUPB,CNOB,CPERB
      COMMON /PAR1/ COXY,CCAR,DNO,DSUP,DPER
      COMMON /PAR2/ RK1,RK2,RK3,RKT,RK5,RK6,RK7,RK9,RK10,RK11,FF
      COMMON /SURFVAL1/ CNOS,CSUPS,CPERS,FNOS,FSUPS,FPERS
C     OXYGEN CONSTANTS
      COMMON /OXYGEN/DOXY,RKOXY,RKMOXY,COXYB,FOXYS
      DOUBLE PRECISION DOXY,RKOXY,RKMOXY,COXYB,FOXYS
C     ----------------
      PARAMETER (M=5001)
      DOUBLE PRECISION H,TEMP,TEMP1,TEMP2,TEMP3,TEMP4,TEMP5,TEMP6,TEMP7
      DOUBLE PRECISION RR(M)
      DOUBLE PRECISION FNOS,FSUPS,FPERS
      DOUBLE PRECISION CNOS,CSUPS,CPERS
      DOUBLE PRECISION CNOB,CSUPB,CPERB
      DOUBLE PRECISION RNO,RSUP,RPER,ROXY
      DOUBLE PRECISION COXY,CCAR,DNO,DSUP,DPER
      DOUBLE PRECISION RK1,RK2,RK3,RKT,RK5,RK6,RK7,RK9,RK10,RK11,FF

C     S=AT THE BEAD SURFACE AND B=IN THE BULK


C     FOR BEAD REGION

      IF(K.EQ.K1) THEN

          S(5,8+INDEXV(1))=1.D0
          S(5,8+INDEXV(2))=0.D0
          S(5,8+INDEXV(3))=0.D0
          S(5,8+INDEXV(4))=0.D0
          S(5,8+INDEXV(5))=0.D0
          S(5,8+INDEXV(6))=0.D0
          S(5,8+INDEXV(7))=0.D0
          S(5,8+INDEXV(8))=0.D0
          S(5,JSF)=Y(1,1)-CNOB

          S(6,8+INDEXV(1))=0.D0
          S(6,8+INDEXV(2))=1.D0
          S(6,8+INDEXV(3))=0.D0
          S(6,8+INDEXV(4))=0.D0
          S(6,8+INDEXV(5))=0.D0
          S(6,8+INDEXV(6))=0.D0
          S(6,8+INDEXV(7))=0.D0
          S(6,8+INDEXV(8))=0.D0
```

```
      S(6,JSF)=Y(2,1)-CPERB

      S(7,8+INDEXV(1))=0.D0
      S(7,8+INDEXV(2))=0.D0
      S(7,8+INDEXV(3))=1.D0
      S(7,8+INDEXV(4))=0.D0
      S(7,8+INDEXV(5))=0.D0
      S(7,8+INDEXV(6))=0.D0
      S(7,8+INDEXV(7))=0.D0
      S(7,8+INDEXV(8))=0.D0
      S(7,JSF)=Y(3,1)-CSUPB


      S(8,8+INDEXV(1))=0.D0
      S(8,8+INDEXV(2))=0.D0
      S(8,8+INDEXV(3))=0.D0
      S(8,8+INDEXV(4))=1.D0
      S(8,8+INDEXV(5))=0.D0
      S(8,8+INDEXV(6))=0.D0
      S(8,8+INDEXV(7))=0.D0
      S(8,8+INDEXV(8))=0.D0
      S(8,JSF)=Y(4,1)-COXYB

  ELSE IF(K.GT.K2) THEN

      S(1,8+INDEXV(1))=1.D0
      S(1,8+INDEXV(2))=0.D0
      S(1,8+INDEXV(3))=0.D0
      S(1,8+INDEXV(4))=0.D0
      S(1,8+INDEXV(5))=0.D0
      S(1,8+INDEXV(6))=0.D0
      S(1,8+INDEXV(7))=0.D0
      S(1,8+INDEXV(8))=0.D0
      S(1,JSF)=Y(1,M)-FNOS

      S(2,8+INDEXV(1))=0.D0
      S(2,8+INDEXV(2))=1.D0
      S(2,8+INDEXV(3))=0.D0
      S(2,8+INDEXV(4))=0.D0
      S(2,8+INDEXV(5))=0.D0
      S(2,8+INDEXV(6))=0.D0
      S(2,8+INDEXV(7))=0.D0
      S(2,8+INDEXV(8))=0.D0
      S(2,JSF)=Y(2,M)-FPERS

      S(3,8+INDEXV(1))=0.D0
      S(3,8+INDEXV(2))=0.D0
      S(3,8+INDEXV(3))=1.D0
      S(3,8+INDEXV(4))=0.D0
      S(3,8+INDEXV(5))=0.D0
      S(3,8+INDEXV(6))=0.D0
      S(3,8+INDEXV(7))=0.D0
      S(3,8+INDEXV(8))=0.D0
      S(3,JSF)=Y(3,M)-FSUPS

      S(4,8+INDEXV(1))=0.D0
      S(4,8+INDEXV(2))=0.D0
```

```
            S(4,8+INDEXV(3))=0.D0
            S(4,8+INDEXV(4))=0.D0
            S(4,8+INDEXV(5))=0.D0
            S(4,8+INDEXV(6))=0.D0
            S(4,8+INDEXV(7))=0.D0
            S(4,8+INDEXV(8))=1.D0
            S(4,JSF)=Y(8,M)-FOXYS


          ELSE

          TEMP=1.D0/(RR(K)+RR(K-1))
          TEMP1=((Y(5,K)+Y(5,K-1))/2.D0)
          TEMP3=((Y(6,K)+Y(6,K-1))/2.D0)
          TEMP2=((Y(7,K)+Y(7,K-1))/2.D0)
          TEMP4=-
(H*((4.D0*RK1*TEMP5*TEMP1)+(RK11*TEMP3)+(.5D0*RK5*TEMP2))/D
         *NO)
          TEMP5=((Y(4,K)+Y(4,K-1))/2.D0)
          TEMP6=1/((RKMOXY+TEMP5)**2)
          TEMP7=H*((2.D0*RK1*TEMP1*TEMP1)+(RKMOXY*RKOXY*TEMP6/2))

            S(1,INDEXV(1))=-1.D0+(2.D0*H*TEMP)
            S(1,INDEXV(2))=0.D0
            S(1,INDEXV(3))=0.D0
            S(1,INDEXV(4))=-H*(2.D0*RK1*TEMP1*TEMP1)
            S(1,INDEXV(5))=TEMP4
            S(1,INDEXV(6))=-(H*RK11*TEMP1/DNO)
            S(1,INDEXV(7))=-(.5D0*H*RK5*TEMP1/DNO)
            S(1,INDEXV(8))=0.D0
            S(1,8+INDEXV(1))=1.D0+(2.D0*H*TEMP)
            S(1,8+INDEXV(2))=S(1,INDEXV(2))
            S(1,8+INDEXV(3))=S(1,INDEXV(3))
            S(1,8+INDEXV(4))=S(1,INDEXV(4))
            S(1,8+INDEXV(5))=S(1,INDEXV(5))
            S(1,8+INDEXV(6))=S(1,INDEXV(6))
            S(1,8+INDEXV(7))=S(1,INDEXV(7))
            S(1,8+INDEXV(8))=S(1,INDEXV(8))

            S(2,INDEXV(1))=0.D0
            S(2,INDEXV(2))=-1.D0+(2.D0*H*TEMP)
            S(2,INDEXV(3))=0.D0
            S(2,INDEXV(4))=0.D0
            S(2,INDEXV(5))=.5D0*H*((RK5*TEMP2)-(RK11*TEMP3))/DPER
            S(2,INDEXV(6))=-(H*((.5D0*RKT)+(.5D0*RK11*TEMP1))/DPER)
            S(2,INDEXV(7))=.5D0*H*RK5*TEMP1/DPER
            S(2,INDEXV(8))=0.D0
            S(2,8+INDEXV(1))=S(2,INDEXV(1))
            S(2,8+INDEXV(2))=1.D0+(2.D0*H*TEMP)
            S(2,8+INDEXV(3))=S(2,INDEXV(3))
            S(2,8+INDEXV(4))=S(2,INDEXV(4))
            S(2,8+INDEXV(5))=S(2,INDEXV(5))
            S(2,8+INDEXV(6))=S(2,INDEXV(6))
            S(2,8+INDEXV(7))=S(2,INDEXV(7))
            S(2,8+INDEXV(8))=S(2,INDEXV(8))

            S(3,INDEXV(1))=0.D0
```

```
S(3,INDEXV(2))=0.D0
S(3,INDEXV(3))=-1.D0+(2.D0*H*TEMP)
S(3,INDEXV(4))=0.D0
S(3,INDEXV(5))=-(.5D0*RK5*H*TEMP2/DSUP)
S(3,INDEXV(6))=0.D0
S(3,INDEXV(7))=-(H*((.5D0*RK5*TEMP1)+(RK9*TEMP2*FF))/DSUP)
S(3,INDEXV(8))=0.D0
S(3,8+INDEXV(1))=S(3,INDEXV(1))
S(3,8+INDEXV(2))=S(3,INDEXV(2))
S(3,8+INDEXV(3))=1.D0+(2.D0*H*TEMP)
S(3,8+INDEXV(4))=S(3,INDEXV(4))
S(3,8+INDEXV(5))=S(3,INDEXV(5))
S(3,8+INDEXV(6))=S(3,INDEXV(6))
S(3,8+INDEXV(7))=S(3,INDEXV(7))
S(3,8+INDEXV(8))=S(3,INDEXV(8))

S(4,INDEXV(1))=0.D0
S(4,INDEXV(2))=0.D0
S(4,INDEXV(3))=0.D0
S(4,INDEXV(4))=-1.D0
S(4,INDEXV(5))=0.D0
S(4,INDEXV(6))=0.D0
S(4,INDEXV(7))=0.D0
S(4,INDEXV(8))=-(.5D0*H)
S(4,8+INDEXV(1))=0.D0
S(4,8+INDEXV(2))=0.D0
S(4,8+INDEXV(3))=0.D0
S(4,8+INDEXV(4))=1.D0
S(4,8+INDEXV(5))=0.D0
S(4,8+INDEXV(6))=0.D0
S(4,8+INDEXV(7))=0.D0
S(4,8+INDEXV(8))=-(.5D0*H)


S(5,INDEXV(1))=-(.5D0*H)
S(5,INDEXV(2))=0.D0
S(5,INDEXV(3))=0.D0
S(5,INDEXV(4))=0.D0
S(5,INDEXV(5))=-1.D0
S(5,INDEXV(6))=0.D0
S(5,INDEXV(7))=0.D0
S(5,INDEXV(8))=0.D0
S(5,8+INDEXV(1))=-(.5D0*H)
S(5,8+INDEXV(2))=0.D0
S(5,8+INDEXV(3))=0.D0
S(5,8+INDEXV(4))=0.D0
S(5,8+INDEXV(5))=1.D0
S(5,8+INDEXV(6))=0.D0
S(5,8+INDEXV(7))=0.D0
S(5,8+INDEXV(8))=0.D0

S(6,INDEXV(1))=0.D0
S(6,INDEXV(2))=-(.5D0*H)
S(6,INDEXV(3))=0.D0
S(6,INDEXV(4))=0.D0
S(6,INDEXV(5))=0.D0
S(6,INDEXV(6))=-1.D0
```

```
      S(6,INDEXV(7))=0.D0
      S(6,INDEXV(8))=0.D0
      S(6,8+INDEXV(1))=0.D0
      S(6,8+INDEXV(2))=-(.5D0*H)
      S(6,8+INDEXV(3))=0.D0
      S(6,8+INDEXV(4))=0.D0
      S(6,8+INDEXV(5))=0.D0
      S(6,8+INDEXV(6))=1.D0
      S(6,8+INDEXV(7))=0.D0
      S(6,8+INDEXV(8))=0.D0

      S(7,INDEXV(1))=0.D0
      S(7,INDEXV(2))=0.D0
      S(7,INDEXV(3))=-(.5*H)
      S(7,INDEXV(4))=0.D0
      S(7,INDEXV(5))=0.D0
      S(7,INDEXV(6))=0.D0
      S(7,INDEXV(7))=-1.D0
      S(7,INDEXV(8))=0.D0
      S(7,8+INDEXV(1))=0.D0
      S(7,8+INDEXV(2))=0.D0
      S(7,8+INDEXV(3))=-(.5*H)
      S(7,8+INDEXV(4))=0.D0
      S(7,8+INDEXV(5))=0.D0
      S(7,8+INDEXV(6))=0.D0
      S(7,8+INDEXV(7))=1.D0
      S(7,8+INDEXV(8))=0.D0

      S(8,INDEXV(1))=0.D0
      S(8,INDEXV(2))=0.D0
      S(8,INDEXV(3))=0.D0
      S(8,INDEXV(4))=-(TEMP7/DOXY)
      S(8,INDEXV(5))=-(4.D0*RK1*H*TEMP5*TEMP1/DOXY)
      S(8,INDEXV(6))=0.D0
      S(8,INDEXV(7))=0.D0
      S(8,INDEXV(8))=-1.D0+(2.D0*H*TEMP)
      S(8,8+INDEXV(1))=S(8,INDEXV(1))
      S(8,8+INDEXV(2))=S(8,INDEXV(2))
      S(8,8+INDEXV(3))=S(8,INDEXV(3))
      S(8,8+INDEXV(4))=S(8,INDEXV(4))
      S(8,8+INDEXV(5))=S(8,INDEXV(5))
      S(8,8+INDEXV(6))=S(8,INDEXV(6))
      S(8,8+INDEXV(7))=S(8,INDEXV(7))
      S(8,8+INDEXV(8))=1.D0+(2.D0*H*TEMP)

  RNO=(TEMP1*((4.D0*RK1*TEMP1*TEMP5)+(RK5*TEMP2)+(2.D0*RK11*TEMP3))/
*DNO)

  RSUP=(((RK5*TEMP1*TEMP2)+(FF*RK9*TEMP2*TEMP2))/DSUP)


  RPER=((RK5*TEMP1*TEMP2)-(TEMP3*(RKT+(RK11*TEMP1))))/DPER

  ROXY=((4.D0*RK1*(TEMP1**2)*TEMP5)+(RKOXY*TEMP5)/(RKMOXY+TEMP5))/
*DOXY


  S(1,JSF)=(Y(1,K)-Y(1,K-1))+(H*(((Y(1,K)+Y(1,K-1))*2.D0*TEMP)-RNO))
```

```
      S(2,JSF)=(Y(2,K)-Y(2,K-1))+(H*(((Y(2,K)+Y(2,K-1))*2.D0*TEMP)+RPER)
     *)
      S(3,JSF)=(Y(3,K)-Y(3,K-1))+(H*(((Y(3,K)+Y(3,K-1))*2.D0*TEMP)-RSUP)
     *)
      S(4,JSF)=(Y(4,K)-Y(4,K-1))-(.5D0*H*(Y(8,K)+Y(8,K-1)))
      S(5,JSF)=(Y(5,K)-Y(5,K-1))-(.5D0*H*(Y(1,K)+Y(1,K-1)))
      S(6,JSF)=(Y(6,K)-Y(6,K-1))-(.5D0*H*(Y(2,K)+Y(2,K-1)))
      S(7,JSF)=(Y(7,K)-Y(7,K-1))-(.5D0*H*(Y(3,K)+Y(3,K-1)))
      S(8,JSF)=(Y(8,K)-Y(8,K-1))+(H*(((Y(8,K)+Y(8,K-1))*2.D0*TEMP)-ROXY)
     *)

      ENDIF
      RETURN
      END
      SUBROUTINE BKSUB(NE,NB,JF,K1,K2,C,NCI,NCJ,NCK)
      INTEGER JF,K1,K2,NB,NCI,NCJ,NCK,NE
      DOUBLE PRECISION C(NCI,NCJ,NCK)
      INTEGER I,IM,J,K,KP,NBF
      DOUBLE PRECISION XX
      NBF=NE-NB
      IM=1
      DO 13 K=K2,K1,-1
        IF (K.EQ.K1) IM=NBF+1
        KP=K+1
        DO 12 J=1,NBF
          XX=C(J,JF,KP)
          DO 11 I=IM,NE
            C(I,JF,K)=C(I,JF,K)-C(I,J,K)*XX
11        CONTINUE
12      CONTINUE
13    CONTINUE
      DO 16 K=K1,K2
        KP=K+1
        DO 14 I=1,NB
          C(I,1,K)=C(I+NBF,JF,K)
14      CONTINUE
        DO 15 I=1,NBF
          C(I+NB,1,K)=C(I,JF,KP)
15      CONTINUE
16    CONTINUE
      RETURN
      END
      SUBROUTINE RED(IZ1,IZ2,JZ1,JZ2,JM1,JM2,JMF,IC1,JC1,JCF,KC,C,NCI,
     *NCJ,NCK,S,NSI,NSJ)
      INTEGER IC1,IZ1,IZ2,JC1,JCF,JM1,JM2,JMF,JZ1,JZ2,KC,NCI,NCJ,NCK,
     *NSI,NSJ
      DOUBLE PRECISION C(NCI,NCJ,NCK),S(NSI,NSJ)
      INTEGER I,IC,J,L,LOFF
      DOUBLE PRECISION VX
      LOFF=JC1-JM1
      IC=IC1
      DO 14 J=JZ1,JZ2
        DO 12 L=JM1,JM2
          VX=C(IC,L+LOFF,KC)
          DO 11 I=IZ1,IZ2
            S(I,L)=S(I,L)-S(I,J)*VX
11        CONTINUE
```

```
12      CONTINUE
        VX=C(IC,JCF,KC)
        DO 13 I=IZ1,IZ2
          S(I,JMF)=S(I,JMF)-S(I,J)*VX
13      CONTINUE
        IC=IC+1
14    CONTINUE
      RETURN
      END
      SUBROUTINE PINVS(IE1,IE2,JE1,JSF,JC1,K,C,NCI,NCJ,NCK,S,NSI,NSJ)
      INTEGER IE1,IE2,JC1,JE1,JSF,K,NCI,NCJ,NCK,NSI,NSJ,NMAX
      DOUBLE PRECISION C(NCI,NCJ,NCK),S(NSI,NSJ)
      PARAMETER (NMAX=10)
      INTEGER I,ICOFF,ID,IPIV,IROW,J,JCOFF,JE2,JP,JPIV,JS1,INDXR(NMAX)
      DOUBLE PRECISION BIG,DUM,PIV,PIVINV,PSCL(NMAX)
      JE2=JE1+IE2-IE1
      JS1=JE2+1
      DO 12 I=IE1,IE2
        BIG=0.D0
        DO 11 J=JE1,JE2
          IF(DABS(S(I,J)).GT.BIG) BIG=DABS(S(I,J))
11      CONTINUE
        IF(BIG.EQ.0.D0) PAUSE 'SINGULAR MATRIX, ROW ALL 0 IN PINVS'
        PSCL(I)=1./BIG
        INDXR(I)=0
12    CONTINUE
      DO 18 ID=IE1,IE2
        PIV=0.
        DO 14 I=IE1,IE2
          IF(INDXR(I).EQ.0) THEN
            BIG=0.D0
            DO 13 J=JE1,JE2
              IF(DABS(S(I,J)).GT.BIG) THEN
                JP=J
                BIG=DABS(S(I,J))
              ENDIF
13          CONTINUE
            IF(BIG*PSCL(I).GT.PIV) THEN
              IPIV=I
              JPIV=JP
              PIV=BIG*PSCL(I)
            ENDIF
          ENDIF
14      CONTINUE
        IF(S(IPIV,JPIV).EQ.0.) PAUSE 'SINGULAR MATRIX IN PINVS'
        INDXR(IPIV)=JPIV
        PIVINV=1.D0/S(IPIV,JPIV)
        DO 15 J=JE1,JSF
          S(IPIV,J)=S(IPIV,J)*PIVINV
15      CONTINUE
        S(IPIV,JPIV)=1.
        DO 17 I=IE1,IE2
          IF(INDXR(I).NE.JPIV) THEN
            IF(S(I,JPIV).NE.0.) THEN
              DUM=S(I,JPIV)
              DO 16 J=JE1,JSF
                S(I,J)=S(I,J)-DUM*S(IPIV,J)
```

```
16            CONTINUE
              S(I,JPIV)=0.D0
            ENDIF
          ENDIF
17      CONTINUE
18    CONTINUE
      JCOFF=JC1-JS1
      ICOFF=IE1-JE1
      DO 21 I=IE1,IE2
        IROW=INDXR(I)+ICOFF
        DO 19 J=JS1,JSF
          C(IROW,J+JCOFF,K)=S(I,J)
19      CONTINUE
21    CONTINUE
      RETURN
      END
      SUBROUTINE SOLVDE(ITMAX,CONV,SLOWC,SCALV,INDEXV,NE,NB,M,Y,NYJ,
     * NYK,C,NCI,NCJ,NCK,S,NSI,NSJ)
      INTEGER ITMAX,M,NB,NCI,NCJ,NCK,NE,NSI,NSJ,NYJ,NYK,INDEXV(NYJ)
      INTEGER NMAX
      DOUBLE PRECISION CONV,SLOWC
      DOUBLE PRECISION C(NCI,NCJ,NCK),S(NSI,NSJ),SCALV(NYJ),Y(NYJ,NYK)
      PARAMETER (NMAX=20)
CU    USES BKSUB,DIFEQ,PINVS,RED
      INTEGER IC1,IC2,IC3,IC4,IT,J,J1,J2,J3,J4,J5,J6,J7,J8,J9,JC1,JCF,
     *JV,K,K1,K2,KM,KP,NVARS,KMAX(NMAX)
      DOUBLE PRECISION ERR,ERRJ,FAC,VMAX,VZ,ERMAX(NMAX)
      K1=1
      K2=M
      NVARS=NE*M
      J1=1
      J2=NB
      J3=NB+1
      J4=NE
      J5=J4+J1
      J6=J4+J2
      J7=J4+J3
      J8=J4+J4
      J9=J8+J1
      IC1=1
      IC2=NE-NB
      IC3=IC2+1
      IC4=NE
      JC1=1
      JCF=IC3
      DO 16 IT=1,ITMAX
        K=K1
        CALL DIFEQ(K,K1,K2,J9,IC3,IC4,INDEXV,NE,S,NSI,NSJ,Y,NYJ,NYK)
        CALL PINVS(IC3,IC4,J5,J9,JC1,K1,C,NCI,NCJ,NCK,S,NSI,NSJ)
        DO 11 K=K1+1,K2
          KP=K-1
          CALL DIFEQ(K,K1,K2,J9,IC1,IC4,INDEXV,NE,S,NSI,NSJ,Y,NYJ,NYK)
          CALL RED(IC1,IC4,J1,J2,J3,J4,J9,IC3,JC1,JCF,KP,C,NCI,NCJ,NCK,
     *S,NSI,NSJ)
          CALL PINVS(IC1,IC4,J3,J9,JC1,K,C,NCI,NCJ,NCK,S,NSI,NSJ)
11      CONTINUE
        K=K2+1
```

```
        CALL DIFEQ(K,K1,K2,J9,IC1,IC2,INDEXV,NE,S,NSI,NSJ,Y,NYJ,NYK)
        CALL RED(IC1,IC2,J5,J6,J7,J8,J9,IC3,JC1,JCF,K2,C,NCI,NCJ,NCK,S,
     *NSI,NSJ)
        CALL PINVS(IC1,IC2,J7,J9,JCF,K2+1,C,NCI,NCJ,NCK,S,NSI,NSJ)
        CALL BKSUB(NE,NB,JCF,K1,K2,C,NCI,NCJ,NCK)
        ERR=0.D+0
        DO 13 J=1,NE
          JV=INDEXV(J)
          ERRJ=0.D+0
          KM=0
          VMAX=0.D+0
          DO 12 K=K1,K2
            VZ=DABS(C(JV,1,K))
            IF(VZ.GT.VMAX) THEN
               VMAX=VZ
               KM=K
            ENDIF
            ERRJ=ERRJ+VZ
12        CONTINUE
          ERR=ERR+ERRJ/SCALV(J)
          ERMAX(J)=C(JV,1,KM)/SCALV(J)
          KMAX(J)=KM
13      CONTINUE
        ERR=ERR/NVARS
        FAC=SLOWC/DMAX1(SLOWC,ERR)
        DO 15 J=1,NE
          JV=INDEXV(J)
          DO 14 K=K1,K2
            Y(J,K)=Y(J,K)-(FAC*C(JV,1,K))
14        CONTINUE
15      CONTINUE

C     THE FOLLOWING STATEMENT IS TO CORRECT FOR A ZERO
      DO 1001 J=1,3
      DO 1002 K=K1,K2
      IF (ABS(Y(J,K)).LT.1.D-15) THEN
      Y(J,K)=0.D0
      ENDIF
1002  CONTINUE
1001  CONTINUE
      DO 1003 J=1,NE
            DO 1004 K=K1,K2
      IF (ABS(Y(J,K)).LT.1.D-20) THEN
      Y(J,K)=0.D0
      ENDIF

1004  CONTINUE
1003  CONTINUE
        WRITE(16,100) IT,ERR,FAC
        IF(ERR.LT.CONV) RETURN
16    CONTINUE
      PAUSE 'ITMAX EXCEEDED IN SOLVDE'
100   FORMAT('SOLVDE',1X,I4,10X,2(E12.6,5X))
      RETURN
      END
```

Appendix 3. Extended Model for Cellular NO Delivery

(Chapter 6)

```
      PROGRAM DRPHDKAV1
      INTEGER NE,M,NB,NCI,NCJ,NCK,NSI,NSJ,NYJ,NYK
      INTEGER KN,ITCONV,KCHANGE
      INTEGER I,ITMAX,K
      INTEGER , ALLOCATABLE :: INDEXV(:)
      INTEGER ITCONV_1
      COMMON /SFRCOM/ RR,H
      COMMON /GEOMETRY/ BEAD_RADIUS
      COMMON /BULKCONC/ CSUPB,CNOB,CPERB
      COMMON /BULKFLUX/ FNO,FSUP,FPER,BEAD_DENSITY,HEADLOSS_NO,FILM_RAD
      COMMON /CODECH/ KCHANGE
C     THE VALUES IN PAR1 AND PAR2 ARE PARAMETER VALUES OBTINED FROM
C     DEEN'S PAPER.  THESE VALUES ARE SHARED WITH SUBROUTINE DIFEQ5
C     AND FUNCV.
      COMMON /PAR1/ COXY,CCAR,DNO,DSUP,DPER
      COMMON /PAR2/ RK1,RK2,RK3,RKT,RK5,RK6,RK7,RK9,RK10,RK11,FF
C     THE VALUES IN SURFVAL1 ARE SURFACE VALUES OF CONCENTRATIONS
C     AND FLUXES OBTAINES FROM THESE CONCENTRATIONS. THESE VALUES
C     ARE SHARED WITH DIFEQ5 SUBROUTINE.
      COMMON /SURFVAL1/ CNOS,CSUPS,CPERS,FNOS,FSUPS,FPERS
C     OXYGEN CONSTANTS
      COMMON /OXYGEN/DOXY,RKOXY,RKMOXY,COXYB,FOXYS
      DOUBLE PRECISION DOXY,RKOXY,RKMOXY,COXYB,FOXYS
C     ----------------

      LOGICAL CHECK
      PARAMETER (KN=3)
      PARAMETER (M=501,NCK=M+1,NYK=M)

      DOUBLE PRECISION CBULK(KN),CONC(KN),FNO,FSUP,FPER,CONVN,ERRN(KN)
      DOUBLE PRECISION FNOS,FSUPS,FPERS
      DOUBLE PRECISION CNOS,CSUPS,CPERS
      DOUBLE PRECISION COXY,CCAR,DNO,DSUP,DPER
      DOUBLE PRECISION RK1,RK2,RK3,RKT,RK5,RK6,RK7,RK9,RK10,RK11,FF
      DOUBLE PRECISION CONV,SLOWC
      DOUBLE PRECISION , ALLOCATABLE :: C(:,:,:),S(:,:)
      DOUBLE PRECISION , ALLOCATABLE :: Y(:,:),SCALV(:),B(:,:),BB(:,:)
      DOUBLE PRECISION RR(M),RRF(M),RRB(M),H,FRACTION_SUP,FRACTION_DIFF
      DOUBLE PRECISION CSUPB,CNOB,CPERB
      DOUBLE PRECISION FILM_RAD
      DOUBLE PRECISION FRACTION_FILM,BEAD_RADIUS,FILM_THICKNESS
      DOUBLE PRECISION CAL_FRAC_NO,SUC_DIFF,FLUX_NO,CHECKFLUXNO
      DOUBLE PRECISION BEAD_DENSITY,HEADLOSS_NO,CONCNOS,CONCSUPS
      DOUBLE PRECISION CHECK_NOBEADCONC,CHECK_PERBEADCONC
      DOUBLE PRECISION CHECK_SUPBEADCONC,CHECK_OXYBEADCONC
      DOUBLE PRECISION
CHECK_NOSUFCONC,CHECK_PERSUFCONC,CHECK_SUPSUFCONC
```

```
CU    USES SOLVDE,NEWT

      OPEN(UNIT=15,FILE='BIOPANOUT.CSV',STATUS='UNKNOWN')
      OPEN(UNIT=16,FILE='MESSAGEBIO.TXT',STATUS='UNKNOWN')
C     THE PARAMETER FOR THE MODEL ARE GIVEN BELOW.

      COXY=185.D-6
      CCAR=1.14D-3
      FRACTION_DIFF=0.46E0
      RK1=2.4D+6
      RK2=1.1D+9
      RK3=1.6D+3
      RK5=6.7D+9
      RK6=3.1D+0
      RK7=1.4D+0
      RK9=8.D+7
      RK10=2.9D+4
      RK11=9.1D+4
      RKT=(0.26D0*(RK6+RK7))+(0.74D0*RK10*CCAR)
      FF=2.51D-3
C     THESE ARE THE PARAMETER FOR OXYGEN CONSUMPTION RATE
      COXYB=COXY
      RKMOXY=0.01E-3
      RKOXY=1.1E-6
C     THESE ARE THE PARAMETER FOR  RADIUS AND FILM THICKNESS
      BEAD_RADIUS=250.0D-6
      FILM_THICKNESS=58.D-6
      FLUX_NO=3.1D-8
      FRACTION_SUP=0.5
C     BEAD DENSITY IN BEADS/ML, HEADLOSS IN S-1
      BEAD_DENSITY=(1.43E+3)/1.0
      HEADLOSS_NO=7.5E-4
      FILM_RAD=(BEAD_RADIUS+FILM_THICKNESS)
C     CALCULATION OF FLUXES
C     DCI/DR=-NI/DI
C     FOR NO, DNO=5.1E-9 M2/S AND NNO=3.1E-8 MOL/S/M2
C     DCNO/DR=-3.1E-8/5.1E-9 (MOL/(M4(=1000LITER*M))
C     DCNO/DR= -6.078E-3 (MOLAR/M)=(MOLES/L/M)
      FRACTION_FILM=0.5D0
C     INITIAL GUESSES
      CSUPB=0.1D-9
      CPERB=0.2D-7
      CNOB=0.02D-4
      CBULK(1)=CNOB
      CBULK(2)=CSUPB
      CBULK(3)=CPERB
C     THE CONVERGENCE PARAMETERS
      ITMAX=200
      ITCONV= 0
      ITCONV_1=0
      CONV=1.D-7
      CONVN=1.D-3
      SLOWC=5.D-1

100   CONTINUE
```

```
      DNO=5.1D-9
      DSUP=2.8D-9
      DPER=2.6D-9
      DOXY=3.0E-9
      KCHANGE=1
      NE=6
      NB=3
      NCJ=NE-NB+1
      NCI=NE
      NSI=NE
      NSJ=2*NE+1
      NYJ=NE
      ALLOCATE(INDEXV(NE))
      ALLOCATE(C(NCI,NCJ,NCK), S(NSI,NSJ))
      ALLOCATE(Y(NE,M),SCALV(NE))
      INDEXV(1)=1
      INDEXV(2)=2
      INDEXV(3)=3
      INDEXV(4)=4
      INDEXV(5)=5
      INDEXV(6)=6

      DO 10 K=1,M

            Y(1,K)=0.1D-2
            Y(2,K)=0.1D-2
            Y(3,K)=0.1D-2
            Y(4,K)=0.5D-6
            Y(5,K)=1.D-9
            Y(6,K)=1.D-9

10    CONTINUE

      SCALV(1)=DMAX1(1.D0,Y(1,M))
      SCALV(2)=DMAX1(1.D0,Y(2,M))
      SCALV(3)=DMAX1(1.D0,Y(3,M))
      SCALV(4)=DMAX1(1.D-3,Y(4,M))
      SCALV(5)=DMAX1(1.D-3,Y(5,M))
      SCALV(6)=DMAX1(1.D-3,Y(6,M))

      FNOS=-(FLUX_NO*FRACTION_FILM/(DNO*1.D3))
      FSUPS=-(FLUX_NO*FRACTION_FILM*FRACTION_SUP/(DSUP*1.D3))
      FPERS=-CONCNOS*CONCSUPS*RK5*BEAD_RADIUS/(DPER*1*500)
      CHECKFLUXNO=(FLUX_NO/(DNO*1.D3))
      H=FILM_THICKNESS/(M-1)
      DO 15 K=1,M
            RR(K)=BEAD_RADIUS+(K-1)*H
15    CONTINUE

      CALL SOLVDE(ITMAX,CONV,SLOWC,SCALV,INDEXV,NE,NB,M,Y,NYJ,NYK,C,
     *NCI,NCJ,NCK,S,NSI,NSJ)

      DEALLOCATE(C, S)
C     SPECIFYING THE FLUXES TO THE BULK TO GET THE BULK CONCENTRATION
C     FROM THE NEWT ROUTINE

      FNO=Y(1,M)
```

```
      FSUP=Y(2,M)
      FPER=Y(3,M)
      CONC(1)=(Y(4,M))
      CONC(2)=(Y(5,M))
      CONC(3)=(Y(6,M))

      CONCNOS=DABS(Y(4,1))
      CONCSUPS=DABS(Y(5,1))

      CALL NEWT(CONC,KN,CHECK)

      DO 20 K=1,KN

            ERRN(K)=DABS(1.D0-DABS(CBULK(K)/CONC(K)))
            CBULK(K)=DABS(CONC(K))
            WRITE(16,220)K, CONC(K), ERRN(K)

20    CONTINUE

C     CONVERGENCE CHECK TO ESTIMATE THE DIFFERENCE BETWEEN
C     ASSUMED BULK CONCENTRATION AND CALCULATED BULK CONC.

      ITCONV=ITCONV+1
      WRITE(16,210) ITCONV

C     TO NOT LET THE PROGRAM GO IN A LOOP

      IF (ITCONV.GT.ITMAX) THEN
            STOP
      ENDIF

      DO 25 K=1,KN
            IF (ERRN(K).GT.CONVN) THEN
                  CNOB=DABS(CBULK(1))
                  CSUPB=DABS(CBULK(2))
                  CPERB=DABS(CBULK(3))
                  DEALLOCATE(Y,SCALV,INDEXV)
            GOTO 100
            ENDIF
25    CONTINUE
      ITCONV=0
C     THE FOLLOWING MODULE SAVES THE SOLUTION FOR PRINTING IN THE END.
C     IN ADDITION, THIS WILL INTERCHANGE THE VALUES OF SUPEROXIDE AND
C     PEROXYNITRITE. IN THE PRINTOUT.
      ALLOCATE(B(NE,M))
      DO 30 K=1,M
            B(1,K)=Y(1,K)
            B(2,K)=Y(3,K)
            B(3,K)=Y(2,K)
            B(4,K)=Y(4,K)/Y(4,1)
            B(5,K)=Y(6,K)/Y(6,1)
            B(6,K)=Y(5,K)/Y(5,1)
30    CONTINUE
      CHECK_NOSUFCONC=Y(4,1)
      CHECK_PERSUFCONC=Y(6,1)
      CHECK_SUPSUFCONC=Y(5,1)
      DO 35 K=1,M
```

```
            RRF(K)=RR(K)/BEAD_RADIUS

35      CONTINUE
C-------------------------------------------------------------

C       THIS MODULE WILL SOLVE THE BEAD REGION

        FNOS=0.D+0
        FSUPS=0.D+0
        FPERS=0.D+0
        FOXYS=0.D+0
        CNOB=Y(4,1)
        CSUPB=Y(5,1)
        CPERB=Y(6,1)
        COXYB=COXY

        DEALLOCATE(Y,SCALV,INDEXV)
        DNO=DNO*FRACTION_DIFF
        DSUP=DSUP*FRACTION_DIFF
        DPER=DPER*FRACTION_DIFF
        DOXY=DOXY*FRACTION_DIFF
        KCHANGE=0
        NE=8
        NB=4
        NCJ=NE-NB+1
        NCI=NE
        NSI=NE
        NSJ=2*NE+1
        NYJ=NE
        H=BEAD_RADIUS/(M-1)
        ALLOCATE(INDEXV(NE))
        ALLOCATE(C(NCI,NCJ,NCK), S(NSI,NSJ))
        ALLOCATE(Y(NE,M),SCALV(NE))

        INDEXV(1)=1
        INDEXV(2)=2
        INDEXV(3)=3
        INDEXV(4)=4
        INDEXV(5)=5
        INDEXV(6)=6
        INDEXV(7)=7
        INDEXV(8)=8

        DO 40 K=1,M

              Y(1,K)=0.1D-2
              Y(2,K)=0.1D-2
              Y(3,K)=0.1D-2
              Y(4,K)=0.1D-2
              Y(5,K)=5.D-5
              Y(6,K)=1.D-8
              Y(7,K)=1.D-8
              Y(8,K)=1.D-8

40      CONTINUE
```

```
      SCALV(1)=DMAX1(1.D0,Y(1,M))
      SCALV(2)=DMAX1(1.D0,Y(2,M))
      SCALV(3)=DMAX1(1.D0,Y(3,M))
      SCALV(4)=DMAX1(1.D0,Y(4,M))
      SCALV(5)=DMAX1(1.D-3,Y(5,M))
      SCALV(6)=DMAX1(1.D-3,Y(6,M))
      SCALV(7)=DMAX1(1.D-3,Y(7,M))
      SCALV(8)=DMAX1(1.D-3,Y(8,M))

      DO 45 K=1,M

            RR(K)=0.D0+(K-1)*H

45    CONTINUE

      CALL SOLVDE(ITMAX,CONV,SLOWC,SCALV,INDEXV,NE,NB,M,Y,NYJ,NYK,C,
     *NCI,NCJ,NCK,S,NSI,NSJ)
            ITCONV_1=ITCONV_1+1
      WRITE(16,215) ITCONV_1

C     TO NOT LET THE PROGRAM GO IN ALOOP

      IF (ITCONV_1.GT.ITMAX) THEN

            STOP

      ENDIF

      CAL_FRAC_NO=1.D0-DABS(Y(1,M)/CHECKFLUXNO)
      SUC_DIFF=DABS(1.D0-DABS(FRACTION_FILM/CAL_FRAC_NO))
      WRITE(16,250) CAL_FRAC_NO
      IF (SUC_DIFF.GT.1.D-3) THEN
      FRACTION_FILM=DABS(CAL_FRAC_NO)

      DEALLOCATE(C, S)
      DEALLOCATE(Y,SCALV,INDEXV)
      DEALLOCATE(B)
      GOTO 100
      ENDIF

      WRITE(15,250) BEAD_RADIUS,CAL_FRAC_NO
      ALLOCATE(BB(NE,M))
      DO 46 K=1,M
            BB(1,K)=Y(1,K)
            BB(2,K)=Y(2,K)
            BB(3,K)=Y(3,K)
            BB(4,K)=Y(5,K)/Y(5,M)
            BB(5,K)=Y(6,K)/Y(6,M)
            BB(6,K)=Y(7,K)/Y(7,M)
            BB(7,K)=Y(8,K)/Y(8,M)
            BB(8,K)=Y(4,K)

46    CONTINUE
      CHECK_NOBEADCONC=Y(5,M)
      CHECK_PERBEADCONC=Y(6,M)
      CHECK_SUPBEADCONC=Y(7,M)
      CHECK_OXYBEADCONC=Y(8,M)
```

```
      WRITE(15,270)
      WRITE(15,310)CHECK_NOBEADCONC,CHECK_PERBEADCONC,CHECK_SUPBEADCONC
     *,CHECK_OXYBEADCONC
      WRITE(15,295)
      WRITE(15,320)CHECK_NOSUFCONC,CHECK_PERSUFCONC,CHECK_SUPSUFCONC

      DO 47 K=1,M

            RRB(K)=RR(K)/BEAD_RADIUS

47    CONTINUE

      WRITE(15,280)

      DO 50 K=1,M

            WRITE(15,260)K,RRB(K),(BB(I,K),I=1,8)

50    CONTINUE

      DO 55 K=1,M

            WRITE(15,240)K,RRF(K),(B(I,K),I=1,6)

55    CONTINUE
      DEALLOCATE(B)
C     THE FOLLOWING ARE THE FORMATING STATEMENTS.
210   FORMAT('ITCONV FOR NEWT=',I4)
215   FORMAT('ITCONV FOR BEAD SOLVEDE =',I4)
220   FORMAT(5X,I4,3X,E15.3,3X,E15.3,15(', ',E15.3))
230   FORMAT(5X,'NOTCONVERGED')
240   FORMAT(5X,I4,5X,E11.5,3X,6(E11.5,3X))
250   FORMAT('BEAD_RADIUS=',E15.3,'FRACTION_FILM=',E15.3)
260   FORMAT(5X,I4,5X,E11.5,3X,8(E11.5,3X))
280   FORMAT(7X,'K',10X,'R',12X,'DCNO/DR',11X,'DCPER/DR',10X,'DCSUP/DR'
     *,10X,'CNO',12X,'CPER',11X,'CSUP',11X,'COXY',11X,'DCOXY/DR')
290   FORMAT(7X,'K',10X,'R', 20X,'DCNO/DR',9X,'DCPER/DR',9X,'DCSUP/DR'
     *,11X,'CNO',14X,'CPER',14X,'CSUP')
270   FORMAT(5X,'THE BEAD REGION')
295   FORMAT(5X,'THE FILM REGION')
310   FORMAT(5X,'NO=',E8.3,'PER=',E8.3,'SUP=',E8.3,'OXY=',E8.3)
320   FORMAT(5X,'NO=',E8.3,'PER=',E8.3,'SUP=',E8.3)
      CLOSE(15)
      CLOSE(16)
      END

      SUBROUTINE DIFEQ(K,K1,K2,JSF,IS1,ISF,INDEXV,NE,S,NSI,NSJ,Y,NYJ,
     *NYK)
      INTEGER IS1,ISF,JSF,K,K1,K2,NE,NSI,NSJ,NYJ,NYK,INDEXV(NYJ),M
      DOUBLE PRECISION S(NSI,NSJ),Y(NYJ,NYK)
      COMMON /SFRCOM/ RR,H
      COMMON /GEOMETRY/ BEAD_RADIUS
      DOUBLE PRECISION BEAD_RADIUS
      COMMON /BULKCONC/ CSUPB,CNOB,CPERB
      COMMON /PAR1/ COXY,CCAR,DNO,DSUP,DPER
      COMMON /PAR2/ RK1,RK2,RK3,RKT,RK5,RK6,RK7,RK9,RK10,RK11,FF
```

```
      COMMON /SURFVAL1/ CNOS,CSUPS,CPERS,FNOS,FSUPS,FPERS
      COMMON /CODECH/ KCHANGE
C     OXYGEN CONSTANTS
      COMMON /OXYGEN/DOXY,RKOXY,RKMOXY,COXYB,FOXYS
      DOUBLE PRECISION DOXY,RKOXY,RKMOXY,COXYB,FOXYS
C     ----------------
      PARAMETER (M=501)
C     INTEGER MM,N
      INTEGER KCHANGE
C     DOUBLE PRECISION H,RR(M),TEMP,TEMP1,TEMP2,TEMP3,TEMP4
      DOUBLE PRECISION H,TEMP,TEMP1,TEMP2,TEMP3,TEMP4,TEMP5,TEMP6,TEMP7
      DOUBLE PRECISION RR(M)
      DOUBLE PRECISION FNOS,FSUPS,FPERS
      DOUBLE PRECISION CNOS,CSUPS,CPERS
      DOUBLE PRECISION CNOB,CSUPB,CPERB
      DOUBLE PRECISION RNO,RSUP,RPER,ROXY
      DOUBLE PRECISION COXY,CCAR,DNO,DSUP,DPER
      DOUBLE PRECISION RK1,RK2,RK3,RKT,RK5,RK6,RK7,RK9,RK10,RK11,FF

C     S=AT THE BEAD SURFACE AND B=IN THE BULK
C     DECIDES BETWEEN FILM OR THE BEAD REGION.
      IF (KCHANGE.EQ.0)THEN
      GO TO 100
      ENDIF

      IF(K.EQ.K1) THEN

          S(4,6+INDEXV(1))=1.D0
          S(4,6+INDEXV(2))=0.D0
          S(4,6+INDEXV(3))=0.D0
          S(4,6+INDEXV(4))=0.D0
          S(4,6+INDEXV(5))=0.D0
          S(4,6+INDEXV(6))=0.D0
          S(4,JSF)=Y(1,1)-FNOS

          S(5,6+INDEXV(1))=0.D0
          S(5,6+INDEXV(2))=1.D0
          S(5,6+INDEXV(3))=0.D0
          S(5,6+INDEXV(4))=0.D0
          S(5,6+INDEXV(5))=0.D0
          S(5,6+INDEXV(6))=0.D0
          S(5,JSF)=Y(2,1)-FSUPS

          S(6,6+INDEXV(1))=0.D0
          S(6,6+INDEXV(2))=0.D0
          S(6,6+INDEXV(3))=1.D0
          S(6,6+INDEXV(4))=0.D0
          S(6,6+INDEXV(5))=0.D0
          S(6,6+INDEXV(6))=0.D0
          S(6,JSF)=Y(3,1)-FPERS

      ELSE IF(K.GT.K2) THEN

          S(1,6+INDEXV(1))=0.D0
          S(1,6+INDEXV(2))=0.D0
          S(1,6+INDEXV(3))=0.D0
          S(1,6+INDEXV(4))=1.D0
```

```
            S(1,6+INDEXV(5))=0.D0
            S(1,6+INDEXV(6))=0.D0
            S(1,JSF)=Y(4,M)-CNOB

            S(2,6+INDEXV(1))=0.D0
            S(2,6+INDEXV(2))=0.D0
            S(2,6+INDEXV(3))=0.D0
            S(2,6+INDEXV(4))=0.D0
            S(2,6+INDEXV(5))=1.D0
            S(2,6+INDEXV(6))=0.D0
            S(2,JSF)=Y(5,M)-CSUPB

            S(3,6+INDEXV(1))=0.D0
            S(3,6+INDEXV(2))=0.D0
            S(3,6+INDEXV(3))=0.D0
            S(3,6+INDEXV(4))=0.D0
            S(3,6+INDEXV(5))=0.D0
            S(3,6+INDEXV(6))=1.D0
            S(3,JSF)=Y(6,M)-CPERB

         ELSE

         TEMP=1.D0/(RR(K)+RR(K-1))
         TEMP1=((Y(4,K)+Y(4,K-1))/2.D0)
         TEMP2=((Y(5,K)+Y(5,K-1))/2.D0)
         TEMP3=((Y(6,K)+Y(6,K-1))/2.D0)
         TEMP4=-
(H*((4.D0*RK1*COXY*TEMP1)+(RK11*TEMP3)+(.5D0*RK5*TEMP2))/DN
        *O)

           S(1,INDEXV(1))=-1.D0+(2.D0*H*TEMP)
           S(1,INDEXV(2))=0.D0
           S(1,INDEXV(3))=0.D0
           S(1,INDEXV(4))=TEMP4
           S(1,INDEXV(5))=-(.5D0*H*RK5*TEMP1/DNO)
           S(1,INDEXV(6))=-(H*RK11*TEMP1/DNO)
           S(1,6+INDEXV(1))=1.D0+(2.D0*H*TEMP)
           S(1,6+INDEXV(2))=S(1,INDEXV(2))
           S(1,6+INDEXV(3))=S(1,INDEXV(3))
           S(1,6+INDEXV(4))=S(1,INDEXV(4))
           S(1,6+INDEXV(5))=S(1,INDEXV(5))
           S(1,6+INDEXV(6))=S(1,INDEXV(6))

           S(2,INDEXV(1))=0.D0
           S(2,INDEXV(2))=-1.D0+(2.D0*H*TEMP)
           S(2,INDEXV(3))=0.D0
           S(2,INDEXV(4))=-(.5D0*RK5*H*TEMP2/DSUP)
           S(2,INDEXV(5))=-(H*((.5D0*RK5*TEMP1)+(RK9*TEMP2*FF))/DSUP)
           S(2,INDEXV(6))=0.D0
           S(2,6+INDEXV(1))=S(2,INDEXV(1))
           S(2,6+INDEXV(2))=1.D0+(2.D0*H*TEMP)
           S(2,6+INDEXV(3))=S(2,INDEXV(3))
           S(2,6+INDEXV(4))=S(2,INDEXV(4))
           S(2,6+INDEXV(5))=S(2,INDEXV(5))
           S(2,6+INDEXV(6))=S(2,INDEXV(6))

           S(3,INDEXV(1))=0.D0
```

```
      S(3,INDEXV(2))=0.D0
      S(3,INDEXV(3))=-1.D0+(2.D0*H*TEMP)
      S(3,INDEXV(4))=.5D0*H*((RK5*TEMP2)-(RK11*TEMP3))/DPER
      S(3,INDEXV(5))=.5D0*H*RK5*TEMP1/DPER
      S(3,INDEXV(6))=-(H*((.5D0*RKT)+(.5D0*RK11*TEMP1))/DPER)
      S(3,6+INDEXV(1))=S(3,INDEXV(1))
      S(3,6+INDEXV(2))=S(3,INDEXV(2))
      S(3,6+INDEXV(3))=1.D0+(2.D0*H*TEMP)
      S(3,6+INDEXV(4))=S(3,INDEXV(4))
      S(3,6+INDEXV(5))=S(3,INDEXV(5))
      S(3,6+INDEXV(6))=S(3,INDEXV(6))

      S(4,INDEXV(1))=-(.5D0*H)
      S(4,INDEXV(2))=0.D0
      S(4,INDEXV(3))=0.D0
      S(4,INDEXV(4))=-1.D0
      S(4,INDEXV(5))=0.D0
      S(4,INDEXV(6))=0.D0
      S(4,6+INDEXV(1))=-(.5D0*H)
      S(4,6+INDEXV(2))=0.D0
      S(4,6+INDEXV(3))=0.D0
      S(4,6+INDEXV(4))=1.D0
      S(4,6+INDEXV(5))=0.D0
      S(4,6+INDEXV(6))=0.D0

      S(5,INDEXV(1))=0.D0
      S(5,INDEXV(2))=-(.5D0*H)
      S(5,INDEXV(3))=0.D0
      S(5,INDEXV(4))=0.D0
      S(5,INDEXV(5))=-1.D0
      S(5,INDEXV(6))=0.D0
      S(5,6+INDEXV(1))=0.D0
      S(5,6+INDEXV(2))=-(.5D0*H)
      S(5,6+INDEXV(3))=0.D0
      S(5,6+INDEXV(4))=0.D0
      S(5,6+INDEXV(5))=1.D0
      S(5,6+INDEXV(6))=0.D0

      S(6,INDEXV(1))=0.D0
      S(6,INDEXV(2))=0.D0
      S(6,INDEXV(3))=-(.5D0*H)
      S(6,INDEXV(4))=0.D0
      S(6,INDEXV(5))=0.D0
      S(6,INDEXV(6))=-1.D0
      S(6,6+INDEXV(1))=0.D0
      S(6,6+INDEXV(2))=0.D0
      S(6,6+INDEXV(3))=-(.5D0*H)
      S(6,6+INDEXV(4))=0.D0
      S(6,6+INDEXV(5))=0.D0
      S(6,6+INDEXV(6))=1.D0

      RNO=(TEMP1*((4.D0*RK1*TEMP1*COXY)+(RK5*TEMP2)+(2.D0*RK11*TEMP3))/
     *DNO)

      RSUP=(((RK5*TEMP1*TEMP2)+(FF*RK9*TEMP2*TEMP2))/DSUP)

      RPER=((RK5*TEMP1*TEMP2)-(TEMP3*(RKT+(RK11*TEMP1))))/DPER
```

```
      S(1,JSF)=(Y(1,K)-Y(1,K-1))+(H*(((Y(1,K)+Y(1,K-1))*2.D0*TEMP)-
RNO))

      S(2,JSF)=(Y(2,K)-Y(2,K-1))+(H*(((Y(2,K)+Y(2,K-1))*2.D0*TEMP)-
RSUP)
     *)
      S(3,JSF)=(Y(3,K)-Y(3,K-1))+(H*(((Y(3,K)+Y(3,K-
1))*2.D0*TEMP)+RPER)
     *)
      S(4,JSF)=(Y(4,K)-Y(4,K-1))-(.5D0*H*(Y(1,K)+Y(1,K-1)))
      S(5,JSF)=(Y(5,K)-Y(5,K-1))-(.5D0*H*(Y(2,K)+Y(2,K-1)))
      S(6,JSF)=(Y(6,K)-Y(6,K-1))-(.5D0*H*(Y(3,K)+Y(3,K-1)))

      ENDIF
      RETURN

100   CONTINUE
C     FOR BEAD REGION

      IF(K.EQ.K1) THEN

          S(5,8+INDEXV(1))=1.D0
          S(5,8+INDEXV(2))=0.D0
          S(5,8+INDEXV(3))=0.D0
          S(5,8+INDEXV(4))=0.D0
          S(5,8+INDEXV(5))=0.D0
          S(5,8+INDEXV(6))=0.D0
          S(5,8+INDEXV(7))=0.D0
          S(5,8+INDEXV(8))=0.D0
          S(5,JSF)=Y(1,1)-FNOS

          S(6,8+INDEXV(1))=0.D0
          S(6,8+INDEXV(2))=1.D0
          S(6,8+INDEXV(3))=0.D0
          S(6,8+INDEXV(4))=0.D0
          S(6,8+INDEXV(5))=0.D0
          S(6,8+INDEXV(6))=0.D0
          S(6,8+INDEXV(7))=0.D0
          S(6,8+INDEXV(8))=0.D0
          S(6,JSF)=Y(2,1)-FPERS

          S(7,8+INDEXV(1))=0.D0
          S(7,8+INDEXV(2))=0.D0
          S(7,8+INDEXV(3))=1.D0
          S(7,8+INDEXV(4))=0.D0
          S(7,8+INDEXV(5))=0.D0
          S(7,8+INDEXV(6))=0.D0
          S(7,8+INDEXV(7))=0.D0
          S(7,8+INDEXV(8))=0.D0
          S(7,JSF)=Y(3,1)-FSUPS

          S(8,8+INDEXV(1))=0.D0
          S(8,8+INDEXV(2))=0.D0
          S(8,8+INDEXV(3))=0.D0
          S(8,8+INDEXV(4))=1.D0
          S(8,8+INDEXV(5))=0.D0
```

```
            S(8,8+INDEXV(6))=0.D0
            S(8,8+INDEXV(7))=0.D0
            S(8,8+INDEXV(8))=0.D0
            S(8,JSF)=Y(4,1)-FOXYS

        ELSE IF(K.GT.K2) THEN

            S(1,8+INDEXV(1))=0.D0
            S(1,8+INDEXV(2))=0.D0
            S(1,8+INDEXV(3))=0.D0
            S(1,8+INDEXV(4))=0.D0
            S(1,8+INDEXV(5))=1.D0
            S(1,8+INDEXV(6))=0.D0
            S(1,8+INDEXV(7))=0.D0
            S(1,8+INDEXV(8))=0.D0
            S(1,JSF)=Y(5,M)-CNOB

            S(2,8+INDEXV(1))=0.D0
            S(2,8+INDEXV(2))=0.D0
            S(2,8+INDEXV(3))=0.D0
            S(2,8+INDEXV(4))=0.D0
            S(2,8+INDEXV(5))=0.D0
            S(2,8+INDEXV(6))=1.D0
            S(2,8+INDEXV(7))=0.D0
            S(2,8+INDEXV(8))=0.D0
            S(2,JSF)=Y(6,M)-CPERB

            S(3,8+INDEXV(1))=0.D0
            S(3,8+INDEXV(2))=0.D0
            S(3,8+INDEXV(3))=0.D0
            S(3,8+INDEXV(4))=0.D0
            S(3,8+INDEXV(5))=0.D0
            S(3,8+INDEXV(6))=0.D0
            S(3,8+INDEXV(7))=1.D0
            S(3,8+INDEXV(8))=0.D0
            S(3,JSF)=Y(7,M)-CSUPB

            S(4,8+INDEXV(1))=0.D0
            S(4,8+INDEXV(2))=0.D0
            S(4,8+INDEXV(3))=0.D0
            S(4,8+INDEXV(4))=0.D0
            S(4,8+INDEXV(5))=0.D0
            S(4,8+INDEXV(6))=0.D0
            S(4,8+INDEXV(7))=0.D0
            S(4,8+INDEXV(8))=1.D0
            S(4,JSF)=Y(8,M)-COXYB

        ELSE

        TEMP=1.D0/(RR(K)+RR(K-1))
        TEMP1=((Y(5,K)+Y(5,K-1))/2.D0)
        TEMP3=((Y(6,K)+Y(6,K-1))/2.D0)
        TEMP2=((Y(7,K)+Y(7,K-1))/2.D0)
        TEMP4=-
(H*((4.D0*RK1*TEMP5*TEMP1)+(RK11*TEMP3)+(.5D0*RK5*TEMP2))/D
      *NO)
        TEMP5=((Y(8,K)+Y(8,K-1))/2.D0)
```

```
TEMP6=1/((RKMOXY+TEMP5)**2)
TEMP7=H*((2.D0*RK1*TEMP1*TEMP1)+(RKMOXY*RKOXY*TEMP6/2))

  S(1,INDEXV(1))=-1.D0+(2.D0*H*TEMP)
  S(1,INDEXV(2))=0.D0
  S(1,INDEXV(3))=0.D0
  S(1,INDEXV(4))=0.D0
  S(1,INDEXV(5))=TEMP4
  S(1,INDEXV(6))=-(H*RK11*TEMP1/DNO)
  S(1,INDEXV(7))=-(.5D0*H*RK5*TEMP1/DNO)
  S(1,INDEXV(8))=-H*(2.D0*RK1*TEMP1*TEMP1)
  S(1,8+INDEXV(1))=1.D0+(2.D0*H*TEMP)
  S(1,8+INDEXV(2))=S(1,INDEXV(2))
  S(1,8+INDEXV(3))=S(1,INDEXV(3))
  S(1,8+INDEXV(4))=S(1,INDEXV(4))
  S(1,8+INDEXV(5))=S(1,INDEXV(5))
  S(1,8+INDEXV(6))=S(1,INDEXV(6))
  S(1,8+INDEXV(7))=S(1,INDEXV(7))
  S(1,8+INDEXV(8))=S(1,INDEXV(8))

  S(2,INDEXV(1))=0.D0
  S(2,INDEXV(2))=-1.D0+(2.D0*H*TEMP)
  S(2,INDEXV(3))=0.D0
  S(2,INDEXV(4))=0.D0
  S(2,INDEXV(5))=.5D0*H*((RK5*TEMP2)-(RK11*TEMP3))/DPER
  S(2,INDEXV(6))=-(H*((.5D0*RKT)+(.5D0*RK11*TEMP1))/DPER)
  S(2,INDEXV(7))=.5D0*H*RK5*TEMP1/DPER
  S(2,INDEXV(8))=0.D0
  S(2,8+INDEXV(1))=S(2,INDEXV(1))
  S(2,8+INDEXV(2))=1.D0+(2.D0*H*TEMP)
  S(2,8+INDEXV(3))=S(2,INDEXV(3))
  S(2,8+INDEXV(4))=S(2,INDEXV(4))
  S(2,8+INDEXV(5))=S(2,INDEXV(5))
  S(2,8+INDEXV(6))=S(2,INDEXV(6))
  S(2,8+INDEXV(7))=S(2,INDEXV(7))
  S(2,8+INDEXV(8))=S(2,INDEXV(8))

  S(3,INDEXV(1))=0.D0
  S(3,INDEXV(2))=0.D0
  S(3,INDEXV(3))=-1.D0+(2.D0*H*TEMP)
  S(3,INDEXV(4))=0.D0
  S(3,INDEXV(5))=-(.5D0*RK5*H*TEMP2/DSUP)
  S(3,INDEXV(6))=0.D0
  S(3,INDEXV(7))=-(H*((.5D0*RK5*TEMP1)+(RK9*TEMP2*FF))/DSUP)
  S(3,INDEXV(8))=0.D0
  S(3,8+INDEXV(1))=S(3,INDEXV(1))
  S(3,8+INDEXV(2))=S(3,INDEXV(2))
  S(3,8+INDEXV(3))=1.D0+(2.D0*H*TEMP)
  S(3,8+INDEXV(4))=S(3,INDEXV(4))
  S(3,8+INDEXV(5))=S(3,INDEXV(5))
  S(3,8+INDEXV(6))=S(3,INDEXV(6))
  S(3,8+INDEXV(7))=S(3,INDEXV(7))
  S(3,8+INDEXV(8))=S(3,INDEXV(8))

  S(4,INDEXV(1))=0.D0
  S(4,INDEXV(2))=0.D0
  S(4,INDEXV(3))=0.D0
```

```
S(4,INDEXV(4))=-1.D0+(2.D0*H*TEMP)
S(4,INDEXV(5))=-(4.D0*RK1*H*TEMP5*TEMP1/DOXY)
S(4,INDEXV(6))=0.D0
S(4,INDEXV(7))=0.D0
S(4,INDEXV(8))=-(TEMP7/DOXY)
S(4,8+INDEXV(1))=S(4,INDEXV(1))
S(4,8+INDEXV(2))=S(4,INDEXV(2))
S(4,8+INDEXV(3))=S(4,INDEXV(3))
S(4,8+INDEXV(4))=1.D0+(2.D0*H*TEMP)
S(4,8+INDEXV(5))=S(4,INDEXV(5))
S(4,8+INDEXV(6))=S(4,INDEXV(6))
S(4,8+INDEXV(7))=S(4,INDEXV(7))
S(4,8+INDEXV(8))=S(4,INDEXV(8))



S(5,INDEXV(1))=-(.5D0*H)
S(5,INDEXV(2))=0.D0
S(5,INDEXV(3))=0.D0
S(5,INDEXV(4))=0.D0
S(5,INDEXV(5))=-1.D0
S(5,INDEXV(6))=0.D0
S(5,INDEXV(7))=0.D0
S(5,INDEXV(8))=0.D0
S(5,8+INDEXV(1))=-(.5D0*H)
S(5,8+INDEXV(2))=0.D0
S(5,8+INDEXV(3))=0.D0
S(5,8+INDEXV(4))=0.D0
S(5,8+INDEXV(5))=1.D0
S(5,8+INDEXV(6))=0.D0
S(5,8+INDEXV(7))=0.D0
S(5,8+INDEXV(8))=0.D0

S(6,INDEXV(1))=0.D0
S(6,INDEXV(2))=-(.5D0*H)
S(6,INDEXV(3))=0.D0
S(6,INDEXV(4))=0.D0
S(6,INDEXV(5))=0.D0
S(6,INDEXV(6))=-1.D0
S(6,INDEXV(7))=0.D0
S(6,INDEXV(8))=0.D0
S(6,8+INDEXV(1))=0.D0
S(6,8+INDEXV(2))=-(.5D0*H)
S(6,8+INDEXV(3))=0.D0
S(6,8+INDEXV(4))=0.D0
S(6,8+INDEXV(5))=0.D0
S(6,8+INDEXV(6))=1.D0
S(6,8+INDEXV(7))=0.D0
S(6,8+INDEXV(8))=0.D0

S(7,INDEXV(1))=0.D0
S(7,INDEXV(2))=0.D0
S(7,INDEXV(3))=-(.5D0*H)
S(7,INDEXV(4))=0.D0
S(7,INDEXV(5))=0.D0
```

```
      S(7,INDEXV(6))=0.D0
      S(7,INDEXV(7))=-1.D0
      S(7,INDEXV(8))=0.D0
      S(7,8+INDEXV(1))=0.D0
      S(7,8+INDEXV(2))=0.D0
      S(7,8+INDEXV(3))=-(.5D0*H)
      S(7,8+INDEXV(4))=0.D0
      S(7,8+INDEXV(5))=0.D0
      S(7,8+INDEXV(6))=0.D0
      S(7,8+INDEXV(7))=1.D0
      S(7,8+INDEXV(8))=0.D0

      S(8,INDEXV(1))=0.D0
      S(8,INDEXV(2))=0.D0
      S(8,INDEXV(3))=0.D0
      S(8,INDEXV(4))=-(.5D0*H)
      S(8,INDEXV(5))=0.D0
      S(8,INDEXV(6))=0.D0
      S(8,INDEXV(7))=0.D0
      S(8,INDEXV(8))=-1.D0
      S(8,8+INDEXV(1))=0.D0
      S(8,8+INDEXV(2))=0.D0
      S(8,8+INDEXV(3))=0.D0
      S(8,8+INDEXV(4))=-(.5D0*H)
      S(8,8+INDEXV(5))=0.D0
      S(8,8+INDEXV(6))=0.D0
      S(8,8+INDEXV(7))=0.D0
      S(8,8+INDEXV(8))=1.D0


      RNO=(TEMP1*((4.D0*RK1*TEMP1*TEMP5)+(RK5*TEMP2)+(2.D0*RK11*TEMP3))/
     *DNO)

      RSUP=(((RK5*TEMP1*TEMP2)+(FF*RK9*TEMP2*TEMP2))/DSUP)

      RPER=((RK5*TEMP1*TEMP2)-(TEMP3*(RKT+(RK11*TEMP1))))/DPER

      ROXY=((4.D0*RK1*(TEMP1**2)*TEMP5)+(RKOXY*TEMP5)/(RKMOXY+TEMP5))/
     *DOXY

      S(1,JSF)=(Y(1,K)-Y(1,K-1))+(H*(((Y(1,K)+Y(1,K-1))*2.D0*TEMP)-RNO))

      S(2,JSF)=(Y(2,K)-Y(2,K-1))+(H*(((Y(2,K)+Y(2,K-1))*2.D0*TEMP)+RPER)
     *)
      S(3,JSF)=(Y(3,K)-Y(3,K-1))+(H*(((Y(3,K)+Y(3,K-1))*2.D0*TEMP)-RSUP)
     *)
      S(4,JSF)=(Y(4,K)-Y(4,K-1))+(H*(((Y(4,K)+Y(4,K-1))*2.D0*TEMP)-ROXY)
     *)
      S(5,JSF)=(Y(5,K)-Y(5,K-1))-(.5D0*H*(Y(1,K)+Y(1,K-1)))
      S(6,JSF)=(Y(6,K)-Y(6,K-1))-(.5D0*H*(Y(2,K)+Y(2,K-1)))
      S(7,JSF)=(Y(7,K)-Y(7,K-1))-(.5D0*H*(Y(3,K)+Y(3,K-1)))
      S(8,JSF)=(Y(8,K)-Y(8,K-1))-(.5D0*H*(Y(4,K)+Y(4,K-1)))

      ENDIF
      RETURN
      END

      SUBROUTINE BKSUB(NE,NB,JF,K1,K2,C,NCI,NCJ,NCK)
      INTEGER JF,K1,K2,NB,NCI,NCJ,NCK,NE
```

```
      DOUBLE PRECISION C(NCI,NCJ,NCK)
      INTEGER I,IM,J,K,KP,NBF
      DOUBLE PRECISION XX
      NBF=NE-NB
      IM=1
      DO 13 K=K2,K1,-1
        IF (K.EQ.K1) IM=NBF+1
        KP=K+1
        DO 12 J=1,NBF
          XX=C(J,JF,KP)
          DO 11 I=IM,NE
            C(I,JF,K)=C(I,JF,K)-C(I,J,K)*XX
11        CONTINUE
12      CONTINUE
13    CONTINUE
      DO 16 K=K1,K2
        KP=K+1
        DO 14 I=1,NB
          C(I,1,K)=C(I+NBF,JF,K)
14      CONTINUE
        DO 15 I=1,NBF
          C(I+NB,1,K)=C(I,JF,KP)
15      CONTINUE
16    CONTINUE
      RETURN
      END

      SUBROUTINE RED(IZ1,IZ2,JZ1,JZ2,JM1,JM2,JMF,IC1,JC1,JCF,KC,C,NCI,
     *NCJ,NCK,S,NSI,NSJ)
      INTEGER IC1,IZ1,IZ2,JC1,JCF,JM1,JM2,JMF,JZ1,JZ2,KC,NCI,NCJ,NCK,
     *NSI,NSJ
      DOUBLE PRECISION C(NCI,NCJ,NCK),S(NSI,NSJ)
      INTEGER I,IC,J,L,LOFF
      DOUBLE PRECISION VX
      LOFF=JC1-JM1
      IC=IC1
      DO 14 J=JZ1,JZ2
        DO 12 L=JM1,JM2
          VX=C(IC,L+LOFF,KC)
          DO 11 I=IZ1,IZ2
            S(I,L)=S(I,L)-S(I,J)*VX
11        CONTINUE
12      CONTINUE
        VX=C(IC,JCF,KC)
        DO 13 I=IZ1,IZ2
          S(I,JMF)=S(I,JMF)-S(I,J)*VX
13      CONTINUE
        IC=IC+1
14    CONTINUE
      RETURN
      END

      SUBROUTINE PINVS(IE1,IE2,JE1,JSF,JC1,K,C,NCI,NCJ,NCK,S,NSI,NSJ)
      INTEGER IE1,IE2,JC1,JE1,JSF,K,NCI,NCJ,NCK,NSI,NSJ,NMAX
      DOUBLE PRECISION C(NCI,NCJ,NCK),S(NSI,NSJ)
      PARAMETER (NMAX=10)
      INTEGER I,ICOFF,ID,IPIV,IROW,J,JCOFF,JE2,JP,JPIV,JS1,INDXR(NMAX)
```

```
      DOUBLE PRECISION BIG,DUM,PIV,PIVINV,PSCL(NMAX)
      JE2=JE1+IE2-IE1
      JS1=JE2+1
      DO 12 I=IE1,IE2
        BIG=0.D0
        DO 11 J=JE1,JE2
          IF(DABS(S(I,J)).GT.BIG) BIG=DABS(S(I,J))
11      CONTINUE
        IF(BIG.EQ.0.D0) PAUSE 'SINGULAR MATRIX, ROW ALL 0 IN PINVS'
        PSCL(I)=1./BIG
        INDXR(I)=0
12    CONTINUE
      DO 18 ID=IE1,IE2
        PIV=0.
        DO 14 I=IE1,IE2
          IF(INDXR(I).EQ.0) THEN
            BIG=0.D0
            DO 13 J=JE1,JE2
              IF(DABS(S(I,J)).GT.BIG) THEN
                JP=J
                BIG=DABS(S(I,J))
              ENDIF
13          CONTINUE
            IF(BIG*PSCL(I).GT.PIV) THEN
              IPIV=I
              JPIV=JP
              PIV=BIG*PSCL(I)
            ENDIF
          ENDIF
14      CONTINUE
        IF(S(IPIV,JPIV).EQ.0.) PAUSE 'SINGULAR MATRIX IN PINVS'
        INDXR(IPIV)=JPIV
        PIVINV=1.D0/S(IPIV,JPIV)
        DO 15 J=JE1,JSF
          S(IPIV,J)=S(IPIV,J)*PIVINV
15      CONTINUE
        S(IPIV,JPIV)=1.
        DO 17 I=IE1,IE2
          IF(INDXR(I).NE.JPIV) THEN
            IF(S(I,JPIV).NE.0.) THEN
              DUM=S(I,JPIV)
              DO 16 J=JE1,JSF
                S(I,J)=S(I,J)-DUM*S(IPIV,J)
16            CONTINUE
              S(I,JPIV)=0.D0
            ENDIF
          ENDIF
17      CONTINUE
18    CONTINUE
      JCOFF=JC1-JS1
      ICOFF=IE1-JE1
      DO 21 I=IE1,IE2
        IROW=INDXR(I)+ICOFF
        DO 19 J=JS1,JSF
          C(IROW,J+JCOFF,K)=S(I,J)
19      CONTINUE
21    CONTINUE
```

```
      RETURN
      END

      SUBROUTINE SOLVDE(ITMAX,CONV,SLOWC,SCALV,INDEXV,NE,NB,M,Y,NYJ,
     * NYK,C,NCI,NCJ,NCK,S,NSI,NSJ)
      INTEGER ITMAX,M,NB,NCI,NCJ,NCK,NE,NSI,NSJ,NYJ,NYK,INDEXV(NYJ)
      INTEGER NMAX
      DOUBLE PRECISION CONV,SLOWC
      DOUBLE PRECISION C(NCI,NCJ,NCK),S(NSI,NSJ),SCALV(NYJ),Y(NYJ,NYK)
      PARAMETER (NMAX=20)
CU    USES BKSUB,DIFEQ,PINVS,RED
      INTEGER IC1,IC2,IC3,IC4,IT,J,J1,J2,J3,J4,J5,J6,J7,J8,J9,JC1,JCF,
     *JV,K,K1,K2,KM,KP,NVARS,KMAX(NMAX)
      DOUBLE PRECISION ERR,ERRJ,FAC,VMAX,VZ,ERMAX(NMAX)
      K1=1
      K2=M
      NVARS=NE*M
      J1=1
      J2=NB
      J3=NB+1
      J4=NE
      J5=J4+J1
      J6=J4+J2
      J7=J4+J3
      J8=J4+J4
      J9=J8+J1
      IC1=1
      IC2=NE-NB
      IC3=IC2+1
      IC4=NE
      JC1=1
      JCF=IC3
      DO 16 IT=1,ITMAX
        K=K1
        CALL DIFEQ(K,K1,K2,J9,IC3,IC4,INDEXV,NE,S,NSI,NSJ,Y,NYJ,NYK)
        CALL PINVS(IC3,IC4,J5,J9,JC1,K1,C,NCI,NCJ,NCK,S,NSI,NSJ)
        DO 11 K=K1+1,K2
          KP=K-1
          CALL DIFEQ(K,K1,K2,J9,IC1,IC4,INDEXV,NE,S,NSI,NSJ,Y,NYJ,NYK)
          CALL RED(IC1,IC4,J1,J2,J3,J4,J9,IC3,JC1,JCF,KP,C,NCI,NCJ,NCK,
     *S,NSI,NSJ)
          CALL PINVS(IC1,IC4,J3,J9,JC1,K,C,NCI,NCJ,NCK,S,NSI,NSJ)
11      CONTINUE
        K=K2+1
        CALL DIFEQ(K,K1,K2,J9,IC1,IC2,INDEXV,NE,S,NSI,NSJ,Y,NYJ,NYK)
        CALL RED(IC1,IC2,J5,J6,J7,J8,J9,IC3,JC1,JCF,K2,C,NCI,NCJ,NCK,S,
     *NSI,NSJ)
        CALL PINVS(IC1,IC2,J7,J9,JCF,K2+1,C,NCI,NCJ,NCK,S,NSI,NSJ)
        CALL BKSUB(NE,NB,JCF,K1,K2,C,NCI,NCJ,NCK)
        ERR=0.D+0
        DO 13 J=1,NE
          JV=INDEXV(J)
          ERRJ=0.D+0
          KM=0
          VMAX=0.D+0
          DO 12 K=K1,K2
            VZ=DABS(C(JV,1,K))
```

```
              IF(VZ.GT.VMAX) THEN
                 VMAX=VZ
                 KM=K
              ENDIF
              ERRJ=ERRJ+VZ
12          CONTINUE
            ERR=ERR+ERRJ/SCALV(J)
            ERMAX(J)=C(JV,1,KM)/SCALV(J)
            KMAX(J)=KM
13        CONTINUE
          ERR=ERR/NVARS
          FAC=SLOWC/DMAX1(SLOWC,ERR)
          DO 15 J=1,NE
            JV=INDEXV(J)
            DO 14 K=K1,K2
              Y(J,K)=Y(J,K)-(FAC*C(JV,1,K))
14          CONTINUE
15        CONTINUE

C       THE FOLLOWING STATEMENT IS TO CORRECT FOR A ZERO
        DO 1001 J=1,3
        DO 1002 K=K1,K2
        IF (ABS(Y(J,K)).LT.1.D-15) THEN
        Y(J,K)=0.D0
        ENDIF
1002    CONTINUE
1001    CONTINUE
        DO 1003 J=1,NE
              DO 1004 K=K1,K2
        IF (ABS(Y(J,K)).LT.1.D-20) THEN
        Y(J,K)=0.D0
        ENDIF

1004    CONTINUE
1003    CONTINUE
          WRITE(16,100) IT,ERR,FAC
          IF(ERR.LT.CONV) RETURN
16      CONTINUE
        PAUSE 'ITMAX EXCEEDED IN SOLVDE'
100     FORMAT('SOLVDE',1X,I4,10X,2(E12.6,5X))
        RETURN
        END

        SUBROUTINE FDJAC(N,X,FVEC,NP,DF)
        INTEGER N,NP,NMAX
        DOUBLE PRECISION DF(NP,NP),FVEC(N),X(N),EPS
        PARAMETER (NMAX=40,EPS=1.D-10)
CU      USES FUNCV
        INTEGER I,J
        DOUBLE PRECISION H,TEMP,F(NMAX)
        DO 12 J=1,N
          TEMP=X(J)
          H=EPS*DABS(TEMP)
          IF(H.EQ.0.)H=EPS
          X(J)=TEMP+H
          H=X(J)-TEMP
          CALL FUNCV(N,X,F)
```

```
        X(J)=TEMP
        DO 11 I=1,N
          DF(I,J)=(F(I)-FVEC(I))/H
11      CONTINUE
12    CONTINUE
      RETURN
      END

      FUNCTION FMIN(X)
      INTEGER N,NP
      DOUBLE PRECISION FMIN,X(*),FVEC
      PARAMETER (NP=40)
      COMMON /NEWTV/ FVEC(NP),N
      SAVE /NEWTV/
CU    USES FUNCV
      INTEGER I
      DOUBLE PRECISION SUM
      CALL FUNCV(N,X,FVEC)
      SUM=0.
      DO 11 I=1,N
        SUM=SUM+FVEC(I)**2
11    CONTINUE
      FMIN=0.5D+0*SUM
      RETURN
      END

      FUNCTION func(x)
      INTEGER n
      double precision func,x(*)
        func=1.e-1
      return
      END

      SUBROUTINE FUNCV(N,X,FVEC)
C     THIS SUBROUTINE STORES THE FUNCTIONS FOR WHICH THE SOLUTION IS
C     REQUIRED.
      PARAMETER (NP=40)
      INTEGER N
      DOUBLE PRECISION FVEC(NP),X(NP)
      COMMON /BULKFLUX/ FNO,FSUP,FPER,BEADD_DENSITY,HEADLOSS_NO,FILM_RA
      COMMON /PAR1/ COXY,CCAR,DNO,DSUP,DPER
      COMMON /PAR2/ RK1,RK2,RK3,RKT,RK5,RK6,RK7,RK9,RK10,RK11,FF
      DOUBLE PRECISION FNO,FSUP,FPER,COXY,CCAR,DNO,DSUP,DPER
      DOUBLE PRECISION RK1,RK2,RK3,RKT,RK5,RK6,RK7,RK9,RK10,RK11
      DOUBLE PRECISION FLNO,FLSUP,FLPER
      DOUBLE PRECISION CONST1,CONC(NP)
      DOUBLE PRECISION BEAD_DENSITY,HEADLOSS_NO,FILM_RAD,FF

      CONST1=(4.0)*(3.1426)*(1.0E+6)*BEAD_DENSITY*((FILM_RAD)**2)
      FLNO=-FNO*DNO
      FLSUP=-FSUP*DSUP
      FLPER=-FPER*DPER
      FVEC(1)=(CONST1*FLNO)+(-X(1)*((4.*RK1*X(1)*COXY)+(RK5*X(2))+(2.*
     *RK11*X(3))))-(HEADLOSS_NO*X(1))
      FVEC(2)=(CONST1*FLSUP)-(RK5*X(1)*X(2))-(RK9*FF*(X(2)**2))
      FVEC(3)=(CONST1*FLPER)+((RK5*X(1)*X(2))-(X(3)*(RKT+(RK11*X(1)))))
      RETURN
```

```
      END

      SUBROUTINE LNSRCH(N,XOLD,FOLD,G,P,X,F,STPMAX,CHECK,FUNC)
      INTEGER N
      LOGICAL CHECK
      DOUBLE PRECISION F,FOLD,STPMAX,G(N),P(N),X(N),XOLD(N),FUNC
      DOUBLE PRECISION ALF,TOLX
      PARAMETER (ALF=1.E-6,TOLX=1.E-55)
      EXTERNAL FUNC
CU    USES FUNC
      INTEGER I
      DOUBLE PRECISION A,ALAM,ALAM2,ALAMIN,B,DISC,F2,FOLD2,RHS1,RHS2
      DOUBLE PRECISION SLOPE,SUM,TEMP,TEST,TMPLAM

      CHECK=.FALSE.
      SUM=0.
      DO 11 I=1,N
        SUM=SUM+P(I)*P(I)
11    CONTINUE
      SUM=SQRT(SUM)
      IF(SUM.GT.STPMAX)THEN
        DO 12 I=1,N
          P(I)=P(I)*STPMAX/SUM
12      CONTINUE
      ENDIF
      SLOPE=0.
      DO 13 I=1,N
        SLOPE=SLOPE+G(I)*P(I)
13    CONTINUE
      TEST=0.
      DO 14 I=1,N
        TEMP=ABS(P(I))/MAX(ABS(XOLD(I)),1.)
        IF(TEMP.GT.TEST)TEST=TEMP
14    CONTINUE
      ALAMIN=TOLX/TEST
      ALAM=1.
1     CONTINUE
        DO 15 I=1,N
          X(I)=XOLD(I)+ALAM*P(I)
15      CONTINUE
        F=FUNC(X)
        IF(ALAM.LT.ALAMIN)THEN
          DO 16 I=1,N
            X(I)=XOLD(I)
16        CONTINUE
          CHECK=.TRUE.
          RETURN
        ELSE IF(F.LE.FOLD+ALF*ALAM*SLOPE)THEN
          RETURN
        ELSE
          IF(ALAM.EQ.1.)THEN
            TMPLAM=-SLOPE/(2.*(F-FOLD-SLOPE))
          ELSE
            RHS1=F-FOLD-ALAM*SLOPE
            RHS2=F2-FOLD2-ALAM2*SLOPE
            A=(RHS1/ALAM**2-RHS2/ALAM2**2)/(ALAM-ALAM2)
            B=(-ALAM2*RHS1/ALAM**2+ALAM*RHS2/ALAM2**2)/(ALAM-ALAM2)
```

```
          IF(A.EQ.0.)THEN
            TMPLAM=-SLOPE/(2.*B)
          ELSE
            DISC=B*B-3.*A*SLOPE
            IF(DISC.LT.0.) PAUSE 'ROUNDOFF PROBLEM IN LNSRCH'
            TMPLAM=(-B+SQRT(DISC))/(3.*A)
          ENDIF
          IF(TMPLAM.GT..5*ALAM)TMPLAM=.5*ALAM
        ENDIF
      ENDIF
      ALAM2=ALAM
      F2=F
      FOLD2=FOLD
      ALAM=MAX(TMPLAM,.1*ALAM)
    GOTO 1
    END

    SUBROUTINE LUBKSB(A,N,NP,INDX,B)
    INTEGER N,NP,INDX(N)
    DOUBLE PRECISION A(NP,NP),B(N),SUM
    INTEGER I,II,J,LL
    II=0
    DO 12 I=1,N
      LL=INDX(I)
      SUM=B(LL)
      B(LL)=B(I)
      IF (II.NE.0)THEN
        DO 11 J=II,I-1
          SUM=SUM-A(I,J)*B(J)
11      CONTINUE
      ELSE IF (SUM.NE.0.) THEN
        II=I
      ENDIF
      B(I)=SUM
12  CONTINUE
    DO 14 I=N,1,-1
      SUM=B(I)
      DO 13 J=I+1,N
        SUM=SUM-A(I,J)*B(J)
13    CONTINUE
      B(I)=SUM/A(I,I)
14  CONTINUE
    RETURN
    END

    SUBROUTINE LUDCMP(A,N,NP,INDX,D)
    INTEGER N,NP,INDX(N),NMAX
    DOUBLE PRECISION A(NP,NP),TINY,D
    PARAMETER (NMAX=500,TINY=1.0E-25)
    INTEGER I,IMAX,J,K
    DOUBLE PRECISION AAMAX,DUM,SUM,VV(NMAX)
    D=1.
    DO 12 I=1,N
      AAMAX=0.
      DO 11 J=1,N
        IF (ABS(A(I,J)).GT.AAMAX) AAMAX=ABS(A(I,J))
11    CONTINUE
```

```
        IF (AAMAX.EQ.0.) PAUSE 'SINGULAR MATRIX IN LUDCMP'
        VV(I)=1./AAMAX
12    CONTINUE
      DO 19 J=1,N
        DO 14 I=1,J-1
          SUM=A(I,J)
          DO 13 K=1,I-1
            SUM=SUM-A(I,K)*A(K,J)
13        CONTINUE
          A(I,J)=SUM
14      CONTINUE
        AAMAX=0.
        DO 16 I=J,N
          SUM=A(I,J)
          DO 15 K=1,J-1
            SUM=SUM-A(I,K)*A(K,J)
15        CONTINUE
          A(I,J)=SUM
          DUM=VV(I)*ABS(SUM)
          IF (DUM.GE.AAMAX) THEN
            IMAX=I
            AAMAX=DUM
          ENDIF
16      CONTINUE
        IF (J.NE.IMAX)THEN
          DO 17 K=1,N
            DUM=A(IMAX,K)
            A(IMAX,K)=A(J,K)
            A(J,K)=DUM
17        CONTINUE
          D=-D
          VV(IMAX)=VV(J)
        ENDIF
        INDX(J)=IMAX
        IF(A(J,J).EQ.0.)A(J,J)=TINY
        IF(J.NE.N)THEN
          DUM=1./A(J,J)
          DO 18 I=J+1,N
            A(I,J)=A(I,J)*DUM
18        CONTINUE
        ENDIF
19    CONTINUE
      RETURN
      END

      SUBROUTINE NEWT(X,N,CHECK)
      INTEGER N,NN,NP,MAXITS
      LOGICAL CHECK
      DOUBLE PRECISION X(N)
      DOUBLE PRECISION FVEC,TOLF,TOLMIN,TOLX,STPMX

      PARAMETER (NP=40,MAXITS=200,TOLF=1.E-15,TOLMIN=1.E-15,TOLX=1E-20,
     *STPMX=100.D+0)
      COMMON /NEWTV/ FVEC(NP),NN
      SAVE /NEWTV/
C     COMMON /CONCENT/ CONC
C     REAL CONC(N)
```

```
CU    USES FDJAC,FMIN,LNSRCH,LUBKSB,LUDCMP
      INTEGER I,ITS,J,INDX(NP)
      DOUBLE PRECISION D,DEN,F,FOLD,STPMAX,SUM,TEMP,TEST,G(NP),P(NP)
      DOUBLE PRECISION XOLD(NP),FMIN
C     REAL D,DEN,F,FOLD,STPMAX,SUM,TEMP,TEST,G(NP),P(NP),XOLD(NP),FMIN
      DOUBLE PRECISION FJAC(NP,NP)
C      REAL D,DEN,F,FOLD,STPMAX,SUM,TEMP,TEST,FJAC(NP,NP),G(NP),P(NP),
C     *XOLD(NP),FMIN

      EXTERNAL FMIN
      NN=N
      F=FMIN(X)
      TEST=0.
      DO 11 I=1,N
        IF(DABS(FVEC(I)).GT.TEST)TEST=DABS(FVEC(I))
11    CONTINUE
      IF(TEST.LT..01*TOLF)THEN
        CHECK=.FALSE.
        RETURN
      ENDIF
      SUM=0.
      DO 12 I=1,N
        SUM=SUM+X(I)**2
12    CONTINUE
      STPMAX=STPMX*DMAX1(SQRT(SUM),FLOAT(N))
      DO 21 ITS=1,MAXITS
        CALL FDJAC(N,X,FVEC,NP,FJAC)
        DO 14 I=1,N
          SUM=0.
          DO 13 J=1,N
            SUM=SUM+FJAC(J,I)*FVEC(J)
13        CONTINUE
          G(I)=SUM
14      CONTINUE
        DO 15 I=1,N
          XOLD(I)=X(I)
15      CONTINUE
        FOLD=F
        DO 16 I=1,N
          P(I)=-FVEC(I)
16      CONTINUE
        CALL LUDCMP(FJAC,N,NP,INDX,D)
        CALL LUBKSB(FJAC,N,NP,INDX,P)
        CALL LNSRCH(N,XOLD,FOLD,G,P,X,F,STPMAX,CHECK,FMIN)
        TEST=0.
        DO 17 I=1,N
          IF(DABS(FVEC(I)).GT.TEST)TEST=DABS(FVEC(I))
17      CONTINUE
        IF(TEST.LT.TOLF)THEN
          CHECK=.FALSE.
          RETURN
        ENDIF
        IF(CHECK)THEN
          TEST=0.
          DEN=DMAX1(F,.5*N)
          DO 18 I=1,N
            TEMP=DABS(G(I))*DMAX1(DABS(X(I)),1.)/DEN
```

```
            IF(TEMP.GT.TEST)TEST=TEMP
18        CONTINUE
          IF(TEST.LT.TOLMIN)THEN
            CHECK=.TRUE.
          ELSE
            CHECK=.FALSE.
          ENDIF
          RETURN
        ENDIF
        TEST=0.
        DO 19 I=1,N
          TEMP=(DABS(X(I)-XOLD(I)))/DMAX1(DABS(X(I)),1.D-9)
          IF(TEMP.GT.TEST)TEST=TEMP
19      CONTINUE
        IF(TEST.LT.TOLX)RETURN
21    CONTINUE
      PAUSE 'MAXITS EXCEEDED IN NEWT'
      END
```

Vita

Mahendra Kavdia

Candidate for the Degree of

Doctor of Philosophy

Thesis: CHEMICAL, PHYSICAL AND CELLULAR DELIVERY OF NITRIC OXIDE

Major Field: Chemical Engineering

Biographical:

Education: Graduated from College of Science, Udaipur, May 1987; received Bachelor of Technology degree in Chemical Engineering from Indian Institute of Technology, Delhi, May 1992; received Master of Technology degree in Chemical Engineering from Indian Institute of Technology, Madras, May 1995. Completed the requirements for the Doctor of Philosophy degree at Oklahoma State University in July, 2000.

Experience: Graduate Research Assistant, Department of Chemical Engineering, Oklahoma State University, August 1996 to August 1998. Teaching Assistant, Department of Chemical Engineering, Oklahoma State University, August 1998 to present.